THERMAL PLANTS

CHARACTERIZING VEGETATION PARAMETERS USING MID TO THERMAL INFRARED HYPERSPECTRAL REMOTE SENSING

Saleem Ullah

Examining committee:

Prof.dr. F.D. van der Meer	University of Twente/ITC
Prof.dr.ing. W. Verhoef	University of Twente/ITC
Prof.dr. T. Udelhoven	Universität Trier
Prof.dr. S. Schmidtlein	Karlsruhe Institute of Technology
Prof.dr. V. Carrere	University of Nantes

ITC dissertation number 229
ITC, P.O. Box 217, 7500 AE Enschede, The Netherlands

ISBN 978-90-6164-357-9
Cover designed by Saleem Ullah
Printed by ITC Printing Department
Copyright © 2013 by Saleem Ullah

UNIVERSITY OF TWENTE.

FACULTY OF GEO-INFORMATION SCIENCE AND EARTH OBSERVATION

THERMAL PLANTS

CHARACTERIZING VEGETATION PARAMETERS USING MID TO THERMAL INFRARED HYPERSPECTRAL REMOTE SENSING

DISSERTATION

to obtain
the degree of doctor at the University of Twente,
on the authority of the Rector Magnificus,
prof.dr. H. Brinksma,
on account of the decision of the graduation committee,
to be publicly defended
on Thursday, July 4, 2013 at 12.45 hrs

by

Saleem Ullah

born on 1st June 1980

in Dir Lower, Pakistan

This thesis is approved by:

Prof.dr. A.K. Skidmore, Promotor	University of Twente
Dr.ir. T.A. Groen, Assistant Promotor	University of Twente
Dr. Martin Schlerf, Assistant Promotor	Centre Research Public Gabriel Lippmann (CRPGL), Luxembourg

Acknowledgements

I express heartfelt gratitude to the Higher Education Commission (HEC) of Pakistan for awarding me MSc and PhD scholarship. Without their financial support this thesis would have not been possible.

Although PhD degree is awarded to one individual but in fact there is always a support and help of many people which make the candidate capable to defend his/her PhD thesis at the end. I seize the opportunity to thank some of them. First, I extend my sincere gratitude to my promotor Prof. Andrew K. Skidmore for motivating, supporting and guiding me throughout my PhD. I had very long discussion with Andrew and I learnt a lot from him. I still remember the initial days when my work was not progressing well and you always encouraged me. I extremely like one sentence "always think and work smartly" I learnt it from Andrew. It has been an honour to do PhD with you Andrew.

I am extending profound thanks to my co-promotors, Dr. Martin Schlerf and Dr. ir. T.A. Groen for their guidance, encouragement and timely feedback. During the research, whenever I got stuck, you people always helped and pull me out of the doldrums. Yours advice and critical reviews were extremely helpful in enhancing the quality of research and without your valuable support this thesis would have been very difficult to accomplish. I felt extremely comfortable and enjoyed working with you through the long journey of my PhD.

I would also like to thank the other staff members of NRS department, ITC student affairs and ITC geoscience laboratory team who helped me during my stay at ITC. I am grateful to Dr. Christoph Hecker, Henk Wilbrink and Boudewijn de Smeth for assisting me with the BRUKER and ASD spectrometer problems. My special thanks go to Mr. Willem Nieuwenhuis for helping me with programing which make my life easy. I would also like to thank Loes Colenbrander, Esther Hondebrink, Marga Koelen, Carla Gerritsen, Theresa van den Boogaard, Bettine Geerdink, Job Duim and Benno Masselink for their excellent service.

Cordial thanks to the PhD community at ITC with whom I always feel at home during my PhD journey in the Netherlands. Few of them are; Abebe Ali, Anas Fauzi, Aidin Niamir, Dr. Abel Ramoelo, Babak Naimi, Dr. Mohammed Aljoufie, Maria Buitrago, Teng Fei, Sam Khosravi, Mitra Shariati, Maitreyi Sur, Khamarrul Azahari Razak, Linlin Li and Nasrullah Zaini. I wish you all success in life.

I am thankful to Pakistani friends at ITC, who gave me wonderful company during my PhD and we shared too many cherishing moments. Dr. Shafique, Amjad, Jehanzeb, Yaseen, Haris, Rehmat, Saad, Dr. Mubashir, Imran, Sumbal, Salma, Sajid and Nayyer you guys were simply remarkable. I will for long remember the warmth discussions on the political scenario of our country, particularly in the tea breaks. On the weekends, the periodic dinner was amazing and good source of relaxation after a tough work. I also enjoyed playing badminton with few of you on the weekend. I am proud of having good friends like you.

Finally with the utter zest, I would like to extend cordial gratitude to my whole family, my grandmother, father, mother, brothers and sister for their limitless love and affections. Yours prayers were always a source of my success and achievement. Last but not the least, I am extending thanks to my wife for supporting and encouraging me during the entire period of my PhD. At the end, thanks to my lovely daughter Alishba, she was always source of amusement after long hours of hard work at ITC.

To my entire family

Table of Contents

List of figures

List of tables

List of Abbreviations

AHS airborne hyperspectral imager

ANOVA analysis of variance

ASD analytical spectral device, Inc.

CWT continuous wavelet transformation

DHR directional-hemispherical reflectance

FOV field of view

FWHM full width half maximum

J-M Jefferies Matusita distance

LAI leaf area index

LWC_d leaf water content (water mass in leaf relative dry weight)

LWC_f leaf water content (water mass in leaf relative fresh weight)

MASI mid-wave infrared airborne spectrographic imager

MCT mercury-cadmium-tellurium detector

MIR mid-wave infrared region of reflectance (2.5-6 μm)

MNDWI mid-wave infrared normalized difference water index

MSDWI mid-wave infrared simple difference water index

MSRWI mid-wave infrared Simple Ratio Water Index

NDVI normalized difference vegetation index

NDWI normalized difference water index

NIR near infrared region of reflectance (0.7-1.1 μm)

PLSR partial least square regression

QDA quadratic discriminant analysis

RMSE root mean square error

$RMSE_{CV}$ root mean square error or cross validation

SAM spectral angle mapper

SAVI soil adjusted vegetation index

SEBASS spatially enhanced broadband array spectrograph system

SMLR stepwise multiple linear regression

SNR signal-to-nose-ratio of a sensor

SR simple ratios

SWIR short-wave infrared region of reflectance (1.1-2.5 μm)

TASI thermal airborne spectrographic imager

TIR thermal infrared region of reflectance (6.0-14.0 μm)

TSAVI transformed soil adjusted vegetation index

Tukey's HSD (honestly significant difference)

VNIR visible- near infrared region of reflectance (0.4-1.1 μm)

WI water index

Chapter 1

Introduction

General Introduction

In this thesis, the potential of mid-wave and thermal infrared spectroscopy is studied in order to identify plant species and estimate leaf water content. This chapter reviews the importance of characterising vegetation parameters using remote sensing. The application of hyperspectral remote sensing to quantify vegetation parameters is discussed and the potential of mid-wave and thermal infrared remote sensing highlighted. Then, the importance of identifying plant species and estimating leaf water content are elaborated. Finally, the research objectives and outline of the thesis are described.

1.1 Remote sensing to characterise vegetation parameters

Vegetation constitutes 65% of the terrestrial land surface and is an important factor influencing the exchange of energy between the earth's surface and the atmosphere (Hansen and Schjoerring 2003; Wang et al. 2006). Knowledge of vegetation parameters (biophysical and biochemical among others) is critical for efficient management schemes in various disciplines like agriculture (e.g. crop yield, productivity, irrigation scheduling), forestry (e.g. timber biomass, growth conditions), ecology (e.g. quality and availability of forage, species diversity) (Asner 1998; Broge and Mortensen 2002; Mutanga and Skidmore 2004b). The traditional methods of measuring vegetation parameters are reliable, however they are labour intensive, time consuming and only practical for areas of limited size (Pu et al. 2003). Remote sensing is recognised as an effective alternative for characterizing vegetation parameters being non-destructive and providing continuous spatial coverage over a large area at repetitive intervals (Curran et al. 2001; Hansen and Schjoerring 2003). Remote sensing is the acquisition of information about an object or phenomena through measuring reflected or emitted electromagnetic radiation by special instruments (called remote sensors) that are not in physical contact with the objects or phenomena under investigation. The typical optical remote sensing sensors makes use of visible near infrared, short-wave infrared, mid-wave and thermal infrared (Table 1.1) for vegetation studies (Warner et al. 2009). Based on the number of spectral bands and band width, optical remote sensing systems are classified into the panchromatic (single band with broad wavelength), multispectral (few broad spectral bands) and hyperspectral (a large number of contiguous narrow spectral bands) remote sensing (Lillesand et al. 2004). While studying vegetation characteristics, a major problem associated with conventional broadband (panchromatic and multispectral) remote sensing techniques is that the spectral information is averaged over broadband widths, and as a result the valuable information available in narrow spectral absorption features is masked (Curran 1989a; Thenkabail et al. 2000). In this regard,

hyperspectral (or narrowband) sensors overcome the limitations associated with multispectral sensors for characterising vegetation parameters. In the past, significant progress has been made in the visible-near infrared and short-wave infrared (VNIR- SWIR; 0.4–2.5 µm) hyperspectral remote sensing to quantify vegetation biophysical (Todd et al. 1998a; Underwood et al. 2003; Mutanga and Skidmore 2004a; Cho et al. 2007) and biochemical (Kokaly and Clark 1999; Lamb et al. 2002; Huang et al. 2004a; Ferwerda et al. 2005; Mutanga et al. 2005; Mutanga and Skidmore 2007a) characteristics. The application of mid-wave and thermal infrared (2.5–14 µm) hyperspectral remote sensing for characterising vegetation is still rudimentary (Ribeiro da Luz and Crowley 2010; Fabre et al. 2011). Using mid infrared and thermal infrared hyperspectral remote sensing, this thesis addresses the identification of plant species and estimation of leaf water content, which are of prime significance among many other vegetation parameters.

Table 1.1: Classification of electromagnetic spectrum in to various spectral domains (Warner et al. 2009). Names of different spectral regions, their acronyms and spectral ranges are shown.

Name of the spectral regions	Acronyms	Range (µm)
Visible - Near Infrared	VNIR	0.4 – 1.1
Short Wave Infrared	SWIR	1.1 – 2.5
Mid Infrared	MIR	2.5 – 6.0
Thermal Infrared	TIR	7.5 – 14.0

1.2 Hyperspectral mid-wave to thermal infrared remote sensing and vegetation parameters

Using broadband (also called multispectral) remote sensing, vegetation parameters are mostly derived by establishing an empirical relationship between different spectral vegetation indices (for example, NDVI, RVI, SAVI or TSAVI) and ground-measured vegetation variables (Carlson and Ripley 1997; Duchemin 1999; Thenkabail et al. 2000; Moleele et al. 2001; Wylie et al. 2002; Zhao et al. 2007; Lokupitiya et al. 2010). Broadband vegetation indices, despite their wide use in ecological and agricultural studies, have certain limitations. For instance, broadband NDVI (the most popular vegetation index) saturates at high level of leaf area index (LAI; the total surface area of leaves per unit area of land surface) (Gao et al. 2000) and is inconsistent with different canopy structures and atmospheric conditions (Huete 1988; Todd et al. 1998a). These limitations make the estimation of vegetation parameters from multispectral broadband sensors challenging because the spectral reflectance at fixed broad bands saturates at high vegetation density and making the broad band indices less effective (Mutanga and Skidmore 2004c). Moreover, using broad bands sensors data, the information available in narrow spectral absorption features is masked

due to the averaging effect over a wide bandwidth (Curran 1989a; Thenkabail et al. 2000).

The advent of hyperspectral (or narrowband) sensors overcomes many of the limitations associated with multispectral sensors for characterising vegetation parameters. Comparisons have been made in various studies between broadband and narrowband vegetation indices for estimating biophysical parameters; in most cases, narrow band indices performed more accurately than broadband indices for different types of vegetation (Elvidge and Chen 1995a; Thenkabail et al. 2000; Hansen and Schjoerring 2003; Schlerf et al. 2005). Besides biophysical parameters, various foliar biochemicals have successfully been estimated using hyperspectral data (Curran et al. 2001; Clevers et al. 2002; Cho and Skidmore 2006; Mutanga and Skidmore 2007b; Asner and Martin 2008; Schlerf et al. 2010). Hyperspectral data were also found very useful in assessing vegetation stress caused by insufficient availability of foliar nutrients such as nitrogen, potassium, calcium (Jago et al. 1999; Mutanga et al. 2004) and water (Suárez et al. 2008).

So far, vegetation parameters has been successfully estimated from hyperspectral data in the visible, near-infrared and shortwave infrared (VNIR–SWIR) (Curran et al. 2001; Clevers et al. 2002; Cho and Skidmore 2006; Mutanga and Skidmore 2007b; Darvishzadeh et al. 2008a; Schlerf et al. 2010). However, hyperspectral data from the VNIR–SWIR alone is not sufficient to explain the structural and chemical characteristics of vegetation. For example in the VNIR-SWIR, the spectral features result from the combination of primary absorption features and their overtones, which make it very difficult to assign variation in spectral reflectance at certain wavebands to a unique chemical constituent (Curran 1989a). Moreover, the spectral profiles of plant species in the VNIR–SWIR (0.4–2.5 μm) are mostly similar in shape because vegetation reflectance in this domain is dominated by spectral absorption features of common chemical components weighted by their concentrations (Kokaly and Clark 1999).

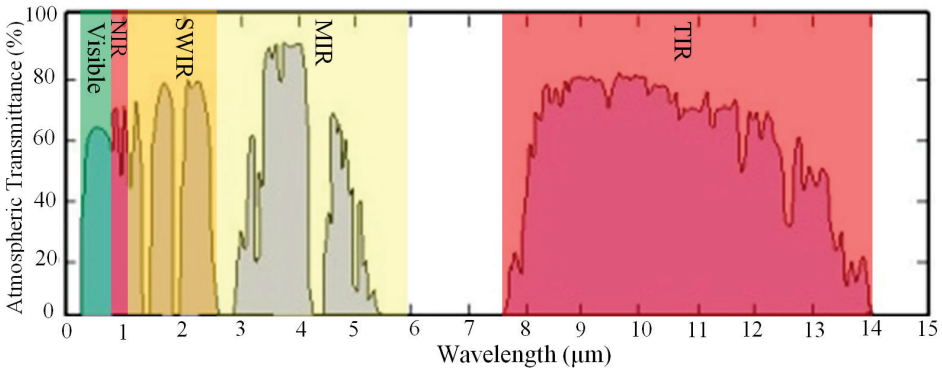

Figure 1.1: The atmospheric windows at various spectral domains, the grey areas highlight the spectral domains suitable for remote sensing applications.

Fundamental absorption features related to various compounds (i.e. cellulose, lignin, water) and leaf structure (i.e. thickness, wax, hairs) occur in the mid-wave (MIR) and thermal infrared (TIR) domains (Ribeiro da Luz 2006; Fabre et al. 2011; Gerber et al. 2011). The mid-wave (MIR) and thermal infrared (TIR) domain also offer numerous atmospheric windows (Fig. 1.1) for remote sensing. The atmospheric windows are the spectral regions where most of the reflected or emitted electromagnetic energy is transmitted through the layers of atmosphere. Despite primary absorption features and strong and wide atmospheric windows in the MIR and TIR, little is known about the optical properties of the vegetation in these spectral domains (Ribeiro da Luz 2006; Gerber et al. 2011). In the past, the spectral characteristics of plant leaves in the MIR and TIR were mostly overlooked due to a number of challenges (Ribeiro da Luz and Crowley 2007), such as lack of equipment (i.e. TIR spectroradiometers), low signal to noise ratios (SNR), and the subtle and complex nature of the spectral features of vegetation. However, some studies have nevertheless brought to light the potential of this spectral domain for characterizing vegetation parameters. Gates and Tantraporn (1952) were the first to measure leaf reflectance spectra in the TIR. They used seven spectral bands and noticed that older leaves reflect more light compared to the younger leaves (Gates and Tantraporn 1952). Almost three-and-half decades later, another study found a small change associated with leaf senescence in the TIR reflectance spectra (8–14 µm) (Salisbury 1986). Using Directrional Hemispherical Reflectance (DHR) in the MIR and TIR (2.5–13.5 µm), Salisbury and Milton (1988) found that different plant species have distinct TIR spectra. Investigating the spectral variability of drying leaves between 2.5 and 20 µm revealed that wavelengths less than 6 µm are strongly influenced by the variation in leaf water status (Elvidge 1988). In these early studies, remote sensing technology in the MIR and TIR was not well developed and leaf spectra were measured using spectrometers with a few spectral bands and low signal to noise ratios. However, the MIR

and TIR are now covered by the latest generation of hyperspectral sensors such as the laboratory based Bruker FTIR spectrometer, point based field level Midac FTIR spectrometer, Telops Hyper-Cam (field imager), Airborne Hyperspectral Imager (AHI), Mid-wave infrared Airborne Spectrographic Imager (MASI600), Thermal Airborne Spectrographic Imager (TASI600), Spatially Enhanced Broadband Array Spectrograph System (SEBASS; airborne) (Schlerf et al. 2012). These sensors have high signal to noise ratios (SNR) as well as high spatial and spectral resolution and make it possible to explore the potential use of MIR and TIR remote sensing in vegetation studies. The more recent studies in the MIR and TIR revealed that the spectral response of fresh plants is dominated by leaf epidermal materials (i.e. cell wall and cuticular membrane; Ribeiro da Luz 2006) and leaf water content (Fabre et al. 2011; Gerber et al. 2011). Leaves of different plant species differ in their chemical composition and external leaf tissue, and as a result have different spectral features in the MIR and TIR (Ribeiro da Luz and Crowley 2007). These absorption features in the TIR are related to the fundamental molecular vibrations of various compounds present in plant leaves (Ribeiro da Luz 2006). Besides spectral absorption features in the TIR, the fundamental water absorption features in the mid-wave infrared display very high specific absorption coefficients (Fig. 1.2) compared with the VNIR–SWIR and show strong absorption features at 2.90, 4.65, and 6.08 µm (Wieliczka et al. 1989; Fabre et al. 2011; Gerber et al. 2011). Thus variation in the MIR and TIR spectral signatures related to different plant species and leaf water content, can act as fingerprint for discriminating vegetation species (Ribeiro da Luz and Crowley 2007, 2010) and potentially be viable spectral regions for monitoring leaf water status.

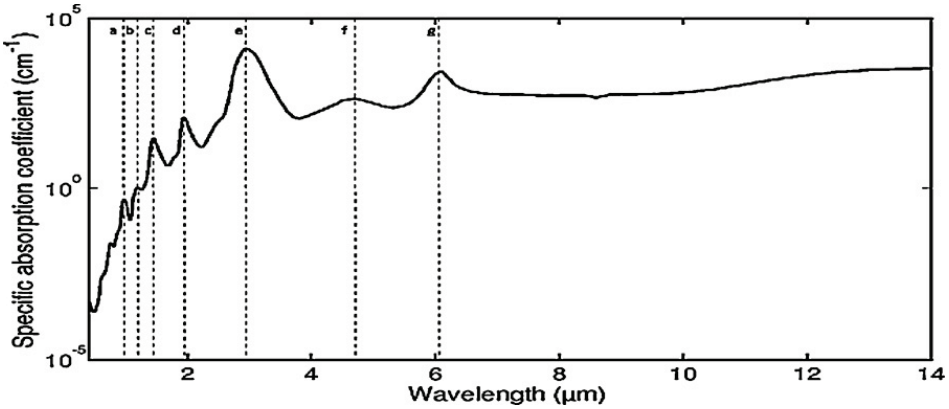

Figure 1.2: Specific absorption coefficients of water reported by Wieliczka et al. (1989) and Gerber et al. (2011). There are strong absorption features at 2.90 µm (line "e"), 4.65 µm (line "f") and 6.08 µm (line "g").

This thesis aims to identify vegetation species and to estimate leaf water content from laboratory measured mid to thermal infrared spectra. Among

others, the identification of plant species and the estimation of leaf water content are vegetation parameters of key importance. Knowledge of plant species and their spatial distribution is necessary for sustainable management of an ecosystem and conserving biological diversity (Schmidt et al. 2004). Spatial distribution maps of vegetation species helps in biodiversity assessment, resource inventories and holds great economic values (e.g. in forestry, agriculture, medicinal plants; Cho et al. 2010). The conventional floristic survey techniques for identification of plant species requires detailed study of plant morphology and extensive field work (Ribeiro da Luz 2006). The identification of plant species using remote sensing has therefore attracted scientists from many disciplines (Schmidt et al. 2004; Adam and Mutanga 2009).

Leaf water content (which is the second vegetation parameter covered in this thesis) is a fundamental constituent of plant leaves (accounts for about 50-90% of the total mass of fresh leaves), being a vital indicator of plant health, physiological condition as well as an important regulator in sustaining plant growth and development. Leaf water content is an important factor for maintaining leaf structure and shape, photosynthesis and thermal regulation. Assessing the variability of vegetation water is essential for monitoring of drought risk (Claudio et al. 2006a; Ghulam et al. 2007) and predicting wildfire (Ustin et al. 1998), estimating crop yield and irrigation scheduling (Bauer et al. 1986; Peñuelas et al. 1993; Peñuelas et al. 1997; Jones and Tardieu 1998). Remote sensing spectroscopy offers an effective way to estimate the variations in water content at leaf and canopy level (Cheng et al. 2011).

In this thesis the potential of a laboratory based mid to thermal infrared spectra is investigated. A laboratory spectrometer can measure the spectral signature of plant leaves in thousands of spectral bands under controlled laboratory environment compared to imaging spectrometers that remotely measure the reflectance of plant canopies in hundreds of narrow and contiguous spectral bands (Goetz et al. 1985). The spectral measurements acquired from imaging spectrometers are more complex than those from the laboratory spectrometers due to the impact of various factors such as atmospheric condition, canopy structure, viewing geometry, distance between the target and sensor, spatial and spectral resolution, and seasonal variation (Clark et al. 2005). Therefore, the possibility to characterize vegetation parameters from imaging spectroscopy could benefit from laboratory research in which vegetation parameters are accurately estimated using higher quality spectroscopic data measured in a controlled laboratory environment.

1.3 Research objectives and thesis structure

The two main objectives of this study were:

(a) To investigate the potential of leaf emissivity spectra in the mid to thermal infrared (2.5 – 14 µm) for the discrimination of plant species. It is assumed that the variability in the laboratory measured emissivity spectra of various species is statistically significant at different parts of the mid to thermal infrared spectrum.

(b) To examine whether retrieval of leaf water content can be quantified using laboratory measured mid to thermal infrared spectra. This research aimed to investigate the variation in the laboratory measured mid-wave and thermal infrared spectral response of dehydrating leaves and to locate the spectral region sensitive to the variation in leaf water content. Further, we aimed to model the leaf water content based on the optimal sensitive wavebands combination. The strength of optimal waveband combinations using laboratory measured spectra were tested at the airborne level by simulating data to the Mid-wave infrared Airborne Spectrographic Imager (MASI600). We also assessed the performance of different spectral regions for estimating leaf water content across the entire spectrum from visible to thermal infrared (0.40-14.0 µm).

Structurally this thesis comprised of seven chapters with five standalone papers submitted to the peer-reviewed international ISI journals. Four papers have been accepted and the remaining one is under review. The chapters are in the following order.

Chapter 2 is about identifying plant species using mid-wave infrared (2.5–6.0 µm) and thermal infrared (8–14.0 µm) emissivity spectra. In this chapter one-way ANOVA followed by post-hoc TukeyHSD test is used to identify the key spectral bands for the discrimination of thirteen vegetation species.

Chapter 3 is a continuation of the problem addressed in chapter 2. In this chapter, an optimization technique called genetic algorithms coupled with spectral angle mapper (as an objective function) has been used to identify optimal bands in mid and thermal infrared emissivity spectra (2.5–14.0 µm) for the identification of plant species.

Chapter 4 investigates whether leaf water content can be accurately retrieved from mid to thermal infrared spectra using continuous wavelet analysis. The spectral regions sensitive to the variation in leaf water content are identified and used to model leaf water content.

Chapter 5 is a continuation of chapter 4, and investigates the potential of three newly proposed indices for the retrieval of leaf water content from mid to thermal infrared spectra. The performance of the proposed indices is also assessed for simulated data of the Mid-wave infrared Airborne Spectrographic Imager (MASI600).

Chapter 6 investigates and assesses the strength of the entire spectra (from visible to thermal infrared) for the estimation of leaf water content. The reflectance and first derivative spectra in the visible to thermal infrared domain were assessed using various water stress indices and multivariate regression analysis using partial least square regression (PLSR).
Chapter 7 summarizes the findings of this study in the context of species identification and leaf water retrieval using mid-wave and thermal infrared data. This chapter also describes directions and recommendations for future research.

Chapter 2

Identifying plant species using mid-wave infrared (2.5 – 6 µm) and thermal infrared (8 – 14 µm) emissivity spectra[1]

[1] This chapter is based on:
Ullah, S., Schlerf, M., Skidmore, A.K., & Hecker, C. (2012). Identifying plant species using mid-wave infrared (2.5–6 µm) and thermal infrared (8–14µm) emissivity spectra. *Remote Sensing of Environment, 118*, 95-102.

Abstract

Plant species discrimination using remote sensing is generally limited by the similarity of their reflectance spectra in the visible, NIR and SWIR domains. Laboratory measured emissivity spectra in the mid infrared (MIR; 2.5 µm - 6 µm) and the thermal infrared (TIR; 8 µm - 14 µm) domain of different plant species, however, reveal significant differences. It is anticipated that with the advances in airborne and space borne hyperspectral thermal sensors, differentiation between plant species may improve. The laboratory emissivity spectra of thirteen common broad leaved species, comprising 3024 spectral bands in the MIR and TIR, were analyzed. For each wavelength the differences between the species were tested for significance using the one way analysis of variance (ANOVA) with the post-hoc Tukey HSD test. The emissivity spectra of the analysed species were found to be statistically different at various wavebands. Subsequently, six spectral bands were selected (based on the histogram of separable pairs of species for each waveband) to quantify the separability between each species pair based on the Jefferies Matusita (J-M) distance. Out of 78 combinations, 76 pairs had a significantly different J-M distance. This means that careful selection of hyperspectral bands in the MIR and TIR (2.5 µm - 14 µm) results in reliable species discrimination.

2.1 Introduction

Knowledge of plant species and their spatial distribution is essential for the sustainable management of an ecosystem (Schmidt et al. 2004). The conventional floristic survey techniques for identification of plant species require detailed study of plant morphology and extensive field work (Ribeiro da Luz 2006). Some plants can only be identified when flowering, and as a result many species remain unidentified in regions of high plant diversity with flowering occurring at different times of the year. Moreover, some regions are difficult to access using conventional floristic surveys, resulting in the identification and mapping of species being costly in terms of time, money and labour (Taylor et al. 1993).

Hyperspectral sensors, because of their high spectral detail in contiguous bands, form a valuable tool for identifying various plants species (Ustin and Xiao 2001; Kokaly et al. 2003; Schmidt and Skidmore 2003; Rosso et al. 2005; Vaiphasa et al. 2005; Belluco et al. 2006; Judd et al. 2007; Pengra et al. 2007; Adam and Mutanga 2009; Pu 2009; Cho et al. 2010), mapping their chemical composition (Curran 1989b; Asner 1998; Kokaly 2001; Clevers et al. 2002; Ferwerda et al. 2005; Mutanga et al. 2005; Blackburn and Ferwerda 2008; Schlerf et al. 2010) and quantifying yield and biomass (Todd et al. 1998b; Gao et al. 2000; Thenkabail et al. 2000; Mutanga and Skidmore 2004c). The absorption features in the short-wave infrared (VIS–SWIR; 0.4–2.5 μm) traditionally form the basis of vegetation characterization and are dominated by the water and pigment content of plant leaves. In comparison to VIS-SWIR spectra the MIR and TIR region has hardly been used in research.

To date, vegetation spectra have been perceived to be featureless in the TIR (2.5 –14 μm) region of the electromagnetic spectrum. In this spectral domain, the spectral characteristics of plant leaves are mostly overlooked due to a number of challenges (Ribeiro da Luz and Crowley 2007), such as lack of equipment (i.e. a spectroradiometer sensitive to the TIR), low signal to noise ratio, and the subtle and complex nature of the spectral features of vegetation. However, technical advances in the use of TIR helped discover that the spectral response of fresh plants is dominated by leaf epidermal materials (i.e. cell wall and cuticular membrane; Salisbury 1986). Leaves of different plant species differ in chemical composition of their external leaf tissue, resulting in different spectral features, which can act as fingerprint for discriminating vegetation species (Salisbury 1986; Salisbury and Milton 1988; Silverstein and Webster 1998; Kirkland et al. 2002; Ribeiro da Luz and Crowley 2007, 2010).

Very few scientists have attempted to investigate plant leaf spectra in the MIR and TIR. Salisbury (1986) was the first to recognize visual variation in

bi-conical reflectance of 13 vegetation types in the laboratory. Soon afterwards, the DHR reflectance of dry plant material was measured and the spectral features were attributed to cellulose and lignin (Elvidge 1988). Some scientists have attempted to identify vegetation in the field and airborne level (French et al. 2000; Ribeiro da Luz and Crowley 2007, 2010), differentiating vegetation species with varying degrees of success. Hyperspectral (narrow band) sensors in the MIR and TIR region may improve discrimination of vegetation species.

This paper investigates the potential of leaf emissivity spectra in discriminating plant species. On the basis of laboratory spectra it is hypothesized that the variability in the emissivity spectra of various species is significant. The emissivity spectra are then inverted to allow species identification.

2.2 Materials and Methods

2.2.1 Leaf sampling

This study was conducted in Enschede, the Netherlands, between July and September, 2010. Leaves were collected from a total thirteen plant species (Table 2.1), eleven of which were local and two were tropical (Asplenium nidus and Spathiphyllum; obtained from a local nursery) species. The species were identified by an experienced taxonomist.

In order to sample positional variation, leaves were collected from the upper, middle and lower part of the tree, both on the sun and the shaded side. The leaves, attached to small twigs, were brought to the laboratory within 5 minutes, and placed in moist cotton to avoid desiccation. Spectral measurements were recorded as soon as possible.

Table 2.1: Thirteen plant species, their common name, Latin name, code, and the number of leaves per species measured using a laboratory spectroradiometer (2.5 µm-14 µm).

Common name	Species	Species code	Sample size
Norway maple	*Acer platanoides*	AP	35
Hawai'I birdnest fern	*Asplenium nidus*	AN	35
Redosier dogwood	*Cornus sericea*	CS	35
Japanese knotweed	*Fallopia japonica*	FJ	35
Maidenhair tree	*Ginkgo biloba*	GB	35
English ivy	*Hedera helix*	HH	35
Ilex	*Ilex opaca*	IL	35
Sweetgum	*Liquidambar styraciflua*	LS	35
Oriental planetree	*Platanus orientalis*	PO	35
Cherry laurel	*Prunus laurocerasus*	PL	35
Rhododendron	*Rhododendron caucasicum*	RH	35
Peace Lily	*Spathiphyllum cochlearispathum*	SP	35
Largeleaf linden	*Tilia platyphyllos*	TP	35

2.2.2 Leaf spectral measurements

The Directional Hemispherical Reflectance (DHR) spectrum of each leaf was acquired using a Bruker VERTEX 70 FTIR (Fourier transform infrared; Bruker Optics GmbH, Ettlingen, Germany) spectrometer. The spectrometer was continuously purged of water vapour and carbon dioxide using nitrogen (N2) gas. An integrating sphere (with sample port of 30 mm and with the sample beam of 25 mm diameter) is attached to the external port of the spectrometer. The integrating sphere has a glass pearl blasted surface which is coated with gold (about 3 microns thick) to achieve a highly diffuse reflecting surface. The incoming energy enters the sphere is redirected by a folding mirror onto the sample at the bottom of the sphere. The incidence angle on the sample surface is 10 degrees off-normal which prevent the specularly reflected energy from escaping through the entrance hole. A mid-band mercury-cadmium-tellurium (MCT) detector (ranging from 10000 – 600 cm-1 or 1–16.70 µm) cooled with liquid nitrogen was used to measure the DHR spectra of the adaxial (upper) surface of the leaf sample. Thirty five (35) leaves were measured per species, thus in total 455 leaves were measured. The measured leaves were collected from at least ten different plants of the same species. Each leaf measurement was referenced against a calibration measurement of gold plate (infragold; Labsphere reflectance technology) with high reflectance (approximately 0.96). The DHR spectra of the plant leaves were measured between 2.5–14 µm, with a spectral resolution of 4 cm-1. Leaf sample were placed on a black surface to absorb transmitted radiance through the leaf and to minimize transparency features in the 3.5 and 5.7 µm range, as was proposed by Gerber et al. 2011. Each leaf spectrum resulted from the averaging of 1000 scans. The spectral region 6–

8 µm was excluded from the analysis because the spectra were noisy in this region. The DHR spectra were converted to emissivity using Kirchhoff's law (ε=1-R) (Nicodemus 1965; Salisbury et al. 1994). Kirchhoff's law holds for opaque objects and the spectroscopic study in the TIR domain recognized plant leaves as opaque objects (Coblentz 1913; Gates and Tantraporn 1952). The applicability of the Kirchhoff's law in this study is based on the assumption of a negligible influence on transmittance in the mid infrared domain, as a result of fresh leaves being measured on a black surface (Fabre et al. 2011; Gerber et al. 2011).

2.2.3 Data processing and analysis

Using narrowband sensor data with a large number of wavebands for classification purposes requires a large number of training samples, and is a labour intensive process (Schmidt and Skidmore 2003). To avoid these limitations and to identify bands between 2.5 and 14 µm (n = 3024) sensitive to species discrimination, the one way analysis of variance (ANOVA) and spectral separability (Jefferies Matusita Distance) tests were used. The usefulness of the selected wavebands for multiple class species classification was tested using quadratic discriminant analysis. The reason for selecting these methods was that for optimal feature selection no single technique has been proven to be universally superior (Yang et al. 2005; Adam and Mutanga 2009). Prior to conducting the tests, the distribution of the spectral emissivity values across each waveband was tested for normality and the homogeneity of variance (homoscedasticity) was verified for every spectral band.

2.2.3.1 Statistical tests (one way ANOVA)

The one way ANOVA followed by a post-hoc Tukey honestly significance difference (Tukey HSD) test were used to test for each waveband whether the variance of mean emissivity was greater between plant species than within a single plant species.

The null hypothesis for *n* vegetation species and *i* wavebands was formulated as:

H_0: $\mu_1 (i) = \mu_2 (i) = \ldots = \mu_n (i)$ (1)

and the alternative hypothesis as:

H_1: not all μ_n (i) are equal (2)

where μ_n represents the mean emissivity of the n^{th} species (n =1, 2, 3,…,13) and *i* denotes the spectral waveband.
A rejection of the null hypothesis was followed by multiple comparisons. For all the possible pair-wise combinations of species, a comparison was made at

each waveband using the post-hoc Tukey HSD test. Tukey HSD is a conservative post-hoc test and is preferred when the number of groups (vegetation species in this case) is large and threatens to inflate the Type 1 error (Yandell 1997). The total number of pair combinations was calculated as n*((n-1)/2)) and equalled 78. ANOVA was tested at a 99 percent (p < 0.01) confidence level.

Following the one way ANOVA with post-hoc Tukey HSD test, important wavebands for spectral discrimination between the 13 vegetation species (78 pairs) were identified by counting, for each waveband, the vegetation pairs where the mean emissivity difference was statistically significant.

2.2.3.2 Distance analysis between plant species

The one way ANOVA coupled with a post-hoc pair-wise comparison resulted in a frequency plot of statistically different means of emissivity per waveband. This frequency plot indicated the wavebands comparatively important for differentiating vegetation species. Twofold criteria were used for selecting the bands for separability analysis from the frequency plot. Firstly, to cover the whole spectrum between 2.5 and 14 µm, bands were selected equally from two different atmospheric windows (2.5– 6 µm and 8–14 µm) of the electromagnetic spectrum. Secondly, the band to be used should have at least 62 significantly different pairs out of a total 78 (80 percent). Six spectral bands fulfilling these criteria were used for analysing the separability of the 13 vegetation species based on the Jeffries Matusita (J-M) distance index (Schmidt and Skidmore 2003; Vaiphasa et al. 2005; Adam and Mutanga 2009). The Jeffries–Matusita (J-M) distance is the average distance between two class density functions (Richards 1993; Schmidt and Skidmore 2003).

Being a parametric test, the J-M distance calculation could not be executed over the whole spectrum of wavebands with large counts of vegetation pairs due to the singularity problem of matrix inversion (Vaiphasa et al. 2005; Adam and Mutanga 2009). The square of the J-M distance values ranges between 0 and 2, with a larger J-M distance value indicating higher separability between group pairs (Richards 1993). In this study we used a J-M distance of ≥1.94 (≥ 97 percent of 2) as a threshold of spectral separablilty between group pairs, which is even stricter than the value of 1.90 that is commonly used in remote sensing practice (Thomas et al., 2003; ENVI software's user guide RSI Inc). The J-M distance was calculated using equation (3).

$$J - M_{ij} = \sqrt{2(1 - e^{-\alpha})} \quad (3)$$

with

$$\alpha = \frac{1}{8}(\mu_i + \mu_j)^T \left(\frac{C_i + C_j}{2}\right)^{-1} (\mu_i + \mu_j) + 2\, ln\left(\frac{\left(\frac{1}{2}\right)|C_i + C_j|}{\sqrt{|C_i| x |C_j|}}\right) \quad (4)$$

where *i* and *j* are the two species being compared; C_i = the covariance matrix of the spectral response of *i* species; μ_i = the mean vector of signature of *i*; *T* = transposition function; *ln* = natural logarithm function; $|C_i|$ = the determinant of C_i.

2.2.3.3 Quadratic discriminant analysis (QDA)

The J-M distances only measures pair-wise class distances. To overcome the limitations of a pairwise analysis, discriminant analysis was performed. Linear discriminant analysis is a method used in statistics, pattern recognition and machine learning to find a linear combination of features which characterize or separate two or more classes of objects (Jackson and Landgrebe 2002; Shi et al. 2008; Sankaran and Ehsani 2011). In remote sensing, discriminant analysis using spectral data has been applied to distinguish aquatic plant species (Peñuelas et al. 1993), forest species (Foody and Cutler 2003), and other types of vegetation. To test the discriminative power of the six selected wavebands for many plant species (multi-class problem) a quadratic discriminant analysis (QDA) with stratified 10-fold cross-validation was run in Matlab Statistics Toolbox (www.mathworks.com). The training set was randomly divided into 10 disjoint subsets. Each subset was roughly of equal size and roughly the same class proportions. One subset was removed, the classification model was trained using the other nine subsets, and the trained model was used to classify the removed subset. For 10 runs we computed the average confusion matrix and the average overall accuracy as well as producer and user accuracies.

2.3 Results

2.3.1 Statistical analysis

Plant emissivity signatures for the 13 vegetation species (Figure 2.1) revealed different features and crossovers across wavelength regions in the MIR and TIR. Using one way ANOVA, the overall results were statistically significant (F=137.77, p=0.000), indicating that the mean emissivity of at least one pair was statistically different at each spectral band. The p-value plot (Figure 2.2) shows where, along the entire wavelength region, the mean emissivities of all plant species are not equal (i.e. statistically different at $p < 0.01$) and are likely to be spectrally separable. The Tukey HSD post-hoc test resulted in 78 possible pair combinations for the 13 vegetation species. For

illustrative purposes, four pairs of vegetation species were randomly selected for statistical comparison (Figure 2.3). The results indicate that the differences between the emissivity spectra were statistically significant for different vegetation species at different wavelength regions. The shaded area (Figure 2.3) represents the wavebands where the mean emissivity of one vegetation type differed statistically significantly from the other.

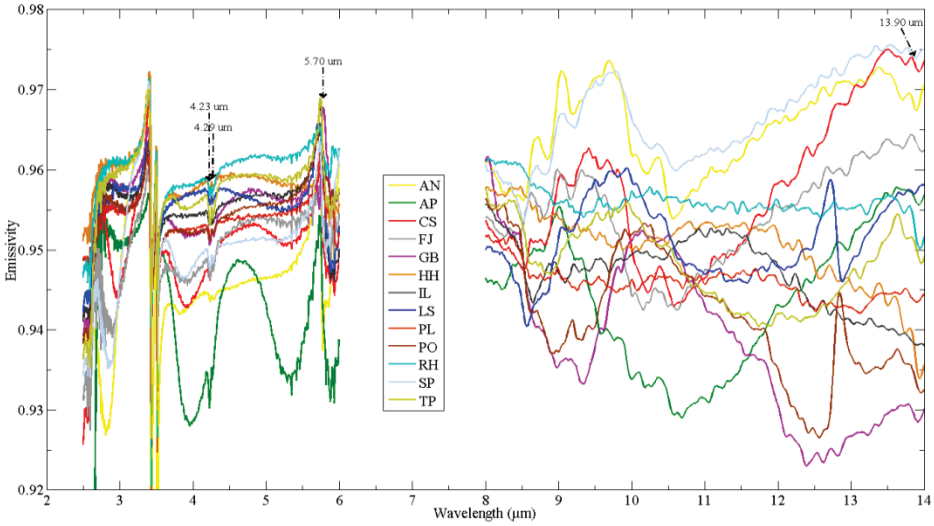

Figure 2.1: The emissivity spectra of 13 vegetation species, each spectra is the average of 35 leaves measured. The wavebands between 6 and 8 µm were removed. The arrows at 4.23, 4.29 13.70 µm represent CO2 features, and arrow at 5.70 µm indicate a spectral feature caused by water vapour.

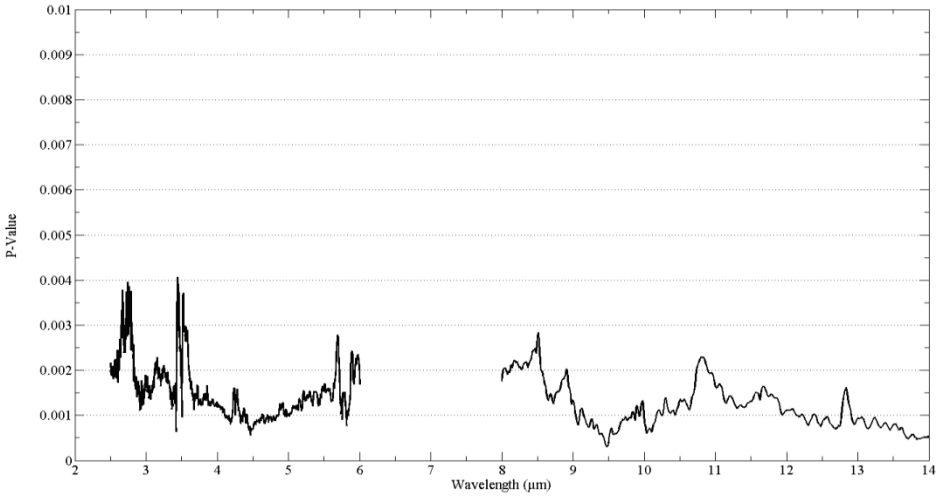

Figure 2.2: The significance (P) value plot of the ANOVA test. The P value shows that the mean emissivity of vegetation species at every spectral band is significantly different ($P < 0.01$).

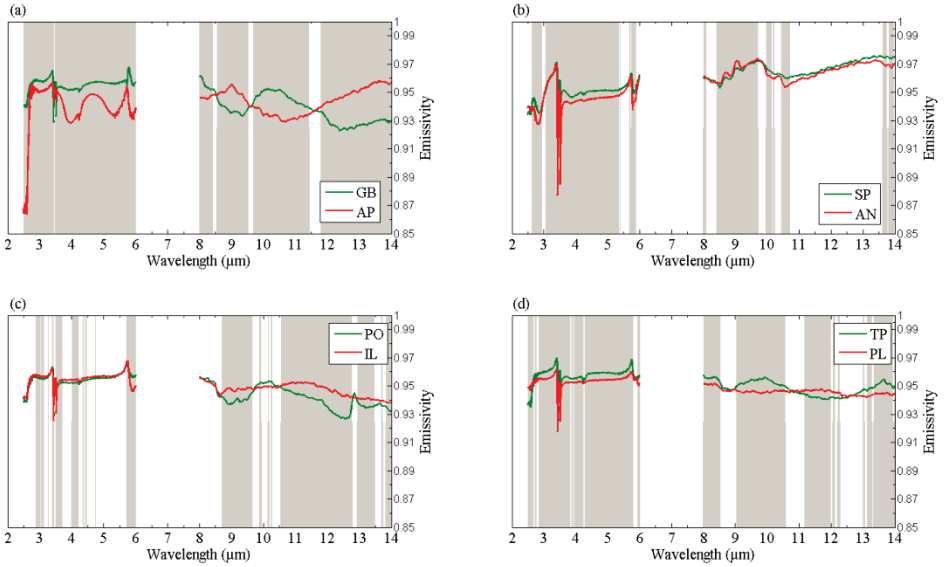

Figure 2.3: The results of a multiple comparison test for (a) GB versus AP, (b) SP versus AN, (c) PO versus IL and (d) TP versus PL. The gray areas represent the wavebands where the species were statistically significantly different from each other. The wavebands 6 – 8 μm were removed from the analysis.

The results of the frequency analysis (Figure 2.4) indicate the count of pairs having a mean emissivity that is statistically significantly different per wavelength. The maximum number of pairs at a particular waveband was 71 (or 91 percent) of the maximum possible number of pairs (78). The minimum count of statistically different pairs was 28. From the 3024 wavebands, 781 wavebands revealed more than 62 species pairs were separable, corresponding to 80 percent of the total number of pairs.

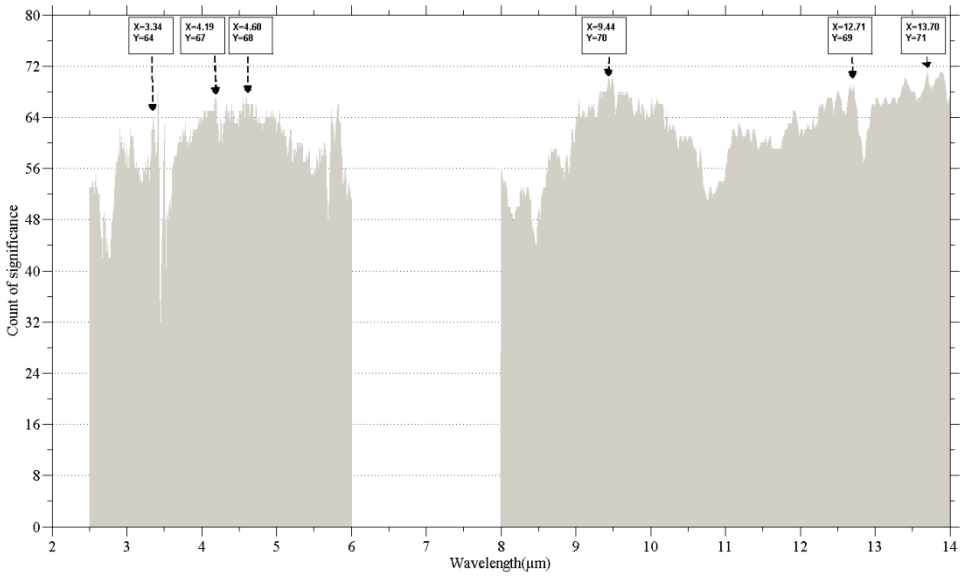

Figure 2.4: Frequency of statistical difference resulting from one way ANOVA with post-hoc Tukey HSD test (99% significance level, $p < 0.01$) of the mean emissivity of 13 different vegetation types. Prominent features in the frequency distribution are labelled. For instance, at 3.34 μm, 64 out of 78 species pairs have significantly different spectral emissivity.

The wavebands where single vegetation species differed significantly from the twelve other species are indicated in Figure 2.5. This graph shows where a single species can be differentiated from all other measured species based on emissivity spectra. All 13 species have at least one waveband where the mean emissivity is different from the means of the remaining twelve species. The maximum number of vegetation species that were statistically different at a particular single waveband occurred at four spectral positions (2.92 μm, 4.97 – 5.01 μm, 13.40–13.41 μm, 13.70 – 13.71 μm). Figure 2.5 quantifies what can be seen in Figure 2.1, namely that the mean emissivity spectra of Acer platanoides (AP) and Asplenium nidus (AN) show marked differences to other vegetation species in the 2.5– 6 μm region, whereas the mean emissivity spectra of Ginkgo biloba (GB) and Fallopia japonica (FJ) show the greatest difference around 12 – 14 μm.

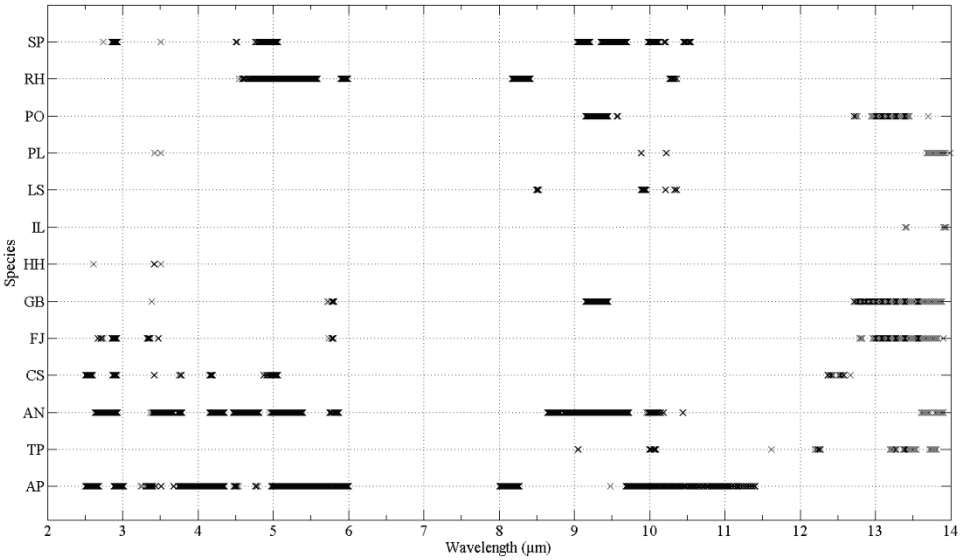

Figure 2.5: A cross (x) indicates a waveband where a certain plant species was significantly different ($p < 0.01$) to all other twelve species. The wavelength region 6 - 8 µm was excluded from the analysis.

2.3.2 Distance analysis (Jeffries-Matusita (J-M) distance)

The frequency plot (Figure 2.4) shows that some wavebands have higher counts of vegetation pairs with statistically significant differences in emissivity and that those bands can comparatively differentiate more species pairs. For calculating the J-M distance, six bands were selected based on the criteria mentioned in section (2.2.3). The bands should have at least 80 percent (62) of the vegetation pairs being statistically significantly different in their mean emissivity, and the selected bands should be spread across the whole spectrum more or less equally.

Three of the bands that were chosen for the separability analysis are located in first atmospheric window (2.5–6 µm), and the remaining three bands are located in the second atmospheric window (8–14 µm) (Figure 2.4). The selected bands were:

3.34 µm (with 64 statistically significantly different pairs)

4.19 µm (with 67 statistically significantly different pairs)

4.60 µm (with 68 statistically significantly different pairs)

9.44 µm (with 70 statistically significantly different pairs)

12.71 µm (with 69 statistically significantly different pairs)

13.70 µm (with 71 statistically significantly different pairs)

The separability index (J-M distance) was calculated between each vegetation pair using the six selected spectral bands. The results show (Table 2.2) that separability between most of the vegetation pairs was greater than the acceptable J-M distance threshold of 1.94. For 97.5 percent of the species pairs the two species were separable in feature space. The only two pairs had an unacceptable J-M distance (i.e. the two species were not separable in feature space) were Spathiphyllum vs Liquidambar styraciflua (with a J-M distance value of 0.92) and Prunus laurocerasus vs Ginkgo biloba (with a J-M distance value of 1.91).

2.3.3 Quadratic discriminant analysis

The average overall classification accuracy of 10 test runs and (i.e. the discriminative power of the six wavebands) was 92 percent (Table 2.3). Most of the plant species were accurately classified, plant species AP and AN with 100 percent producer accuracy and user accuracy. As the most prominent misclassification, samples of SP were incorrectly classified as CS, FJ were incorrectly labelled LS, and TP as RH.

Table 2.2: The J-M distance between all 13 species using six bands (3.34, 4.19, 4.60, 9.44, 12.71, and 13.70 µm). The species pairs having a separability level below the defined threshold (J-M index of 1.94) are highlighted in gray.

	AP	AN	CS	FJ	GB	HH	IL	LS	PL	PO	RH	SP	TP
AP	-	2	2	2	2	2	2	2	2	2	2	2	2
AN	-	-	2	2	2	2	2	2	2	2	2	2	2
CS	-	-	-	1.99	2	2	2	2	2	2	2	1.99	2
FJ	-	-	-	-	2	2	2	2	2	2	2	2	2
GB	-	-	-	-	-	2	2	2	1.91	2	2	2	2
HH	-	-	-	-	-	-	2	2	2	2	2	2	2
IL	-	-	-	-	-	-	-	2	2	2	2	2	2
LS	-	-	-	-	-	-	-	-	2	2	2	0.92	2
PL	-	-	-	-	-	-	-	-	-	2	2	2	2
PO	-	-	-	-	-	-	-	-	-	-	2	2	2
RH	-	-	-	-	-	-	-	-	-	-	-	2	1.99
SP	-	-	-	-	-	-	-	-	-	-	-	-	2
TP	-	-	-	-	-	-	-	-	-	-	-	-	-

Table 2.3: The error matrix resulted from QDA using six bands (3.34, 4.19, 4.60, 9.44, 12.71, and 13.70 μm). The values along diagonal represent the truly classified cases.

	AP	AN	CS	FJ	GB	HH	IL	LS	PL	PO	RH	SP	TP	Row total	User accuracy
AP	35	0	0	0	0	0	0	0	0	0	0	0	0	35	100
AN	0	35	0	0	0	0	0	0	0	0	0	0	0	35	100
CS	0	0	34	1	0	0	0	0	0	0	0	0	0	35	97
FJ	0	0	0	31	0	0	0	4	0	0	0	0	0	35	89
GB	0	0	0	0	33	0	0	0	0	2	0	0	0	35	94
HH	0	0	0	0	0	31	0	0	0	0	2	0	2	35	89
IL	0	0	0	0	0	1	30	0	4	0	0	0	0	35	86
LS	0	0	0	0	0	0	1	31	0	0	3	0	0	35	89
PL	0	0	0	0	0	0	2	0	33	0	0	0	0	35	94
PO	0	0	0	0	0	0	2	0	1	32	0	0	0	35	91
RH	0	0	0	0	0	0	0	0	0	0	34	0	1	35	97
SP	0	0	4	0	0	0	0	0	0	0	0	31	0	35	89
TP	0	0	0	0	0	2	0	1	0	0	4	0	28	35	80
Column Total	35	35	38	32	33	34	35	36	38	34	43	31	31	455	
Producer Accuracy	100	100	89	97	100	91	86	86	87	94	79	100	90	**Overall Accuracy = 92 %**	

2.4 Discussion

The visible and near-infrared reflectance spectra have been widely used for species discrimination, but MIR and TIR emissivity spectra has received little attention in discriminating vegetation species. The visual analysis of the mean emissivity spectra of various vegetation species showed crossing-over due to the differences in the absolute value of mean emissivity at different spectral bands (Figure 2.1). This study proved that these differences were statistically significant, allowing vegetation species to be discriminated. The results of a one way ANOVA with Tukey HSD (Figure 2.2) revealed the wavebands, where differences between vegetation species were statistically significant. Two atmospheric windows (3–6 μm and 8 –14 μm) in the MIR and TIR contained significantly different vegetation pairs making them important regions for discriminating between vegetation species (Figure 2.4). The J-M distance measured between each pair further assisted in discriminating vegetation types. Almost all pairs had a high J-M distance (2 or close to 2) and were above the threshold value (1.94) of separability. Results of QDA confirmed that the selected wavebands are suitable to perform a very accurate (i.e. above 90 percent accuracy) multiple species discrimination, although reported accuracies are more conservative compared to J-M distance analysis. However, QDA did not confirm the poor discrimination between LS and SP that was found in J-M distance analysis.

Spectral discrimination of vegetation types in the MIR and TIR might be possible due to variation in the composition of the superficial epidermal layer of plant leaves producing unique emissivity features. To date, which spectral feature is responsible for which chemical compound remains unclear. The emissivity signature of plant leaves is dominated by a feature associated with major classes of cellulous of the epidermis (Elvidge 1988; Ribeiro da Luz and Crowley 2007). The selection of features in the atmospheric window 3 to 6 μm may be attributed to water content in the plant leaves (Gerber et al. 2011). The higher number of differentiable vegetation pairs (Figure 2.4) at selected bands in the second atmospheric window of 8 to14 μm (9.44, 12.71, and 13.70 μm) may be attributed to the surface/volume scattering of cellulose and cuticle (Ribeiro da Luz and Crowley 2007). The cuticle structures of plant species are unique (Holloway 1982). Cuticle is composed of many organic compounds, including polymethylen, cutan, cutin and long chain lipids, and is covered by epicuticular waxes (Holloway 1982 ; Heredia 2003; Ribeiro da Luz 2006; Ribeiro da Luz and Crowley 2010).

The possibility of distinguishing vegetation species based on laboratory measured emissivity spectra is an important prerequisite for future airborne and space borne floristic mapping. However, field conditions impose several challenges; it is difficult to calibrate remotely sensed signals in the MIR

(around 3 µm) due to the overlap of the reflected and emitted energy from the surface. Another potential remote sensing problem is the effect of canopy cavities (cavity effect) causing blackbody emittance in the TIR and reducing the spectral contrast in the signal. This phenomena is more pronounced with small and needle leaved species as well as species that form funnel-like leaf arrangements (Ribeiro da Luz and Crowley 2010). Given field conditions, such as atmospheric condition, canopy structure, distance between the target and sensor, spatial and spectral resolution, and seasonal variation, this study can only be extended to field, airborne and space borne level if the sensing system has a high signal to noise ratio (SNR) to allow small spectral differences in plant canopies to be distinguished.

Although most of the vegetation type pairs were separable, there were two species pairs with separability indices (J-M distance value) below the defined threshold of 1.94. These barely separable species were *Spathiphyllum cochlearispathum* vs *Liquidambar styraciflua* (0.92) and *Prunus laurocerasus* vs *Ginkgo biloba* (1.91), though in remote sensing, the separability threshold is often set at ≥1.90 (Thomas et al. 2003), meaning the second pair would not be excluded. The similarity in the emissivity spectra of the unseparable pairs may be attributed to the closeness of the physiochemical properties of the leaves (Ribeiro da Luz and Crowley 2010).

2.5 Conclusion

This study investigated the potential of high resolution MIR and TIR emissivity spectra for differentiating between vegetation species at laboratory level. It is concluded that laboratory emissivity spectra of different vegetation species contain sufficient information to discriminate vegetation types and have potential for floristic mapping. The results of the study showed that vegetation types have characteristic emissivity signatures which are statistically significantly different from other species. The frequency plot helped to understand which part of the electromagnetic spectrum has high potential for discriminating vegetation types. The outcome of this study is that the possibility exists to extend this kind of work and, with the advancement of hyperspectral MIR and TIR sensors, implement it in the field and at airborne level.

Chapter 3

Using a genetic algorithm as an optimal band selector in the mid-wave and thermal Infrared (2.5–14 μm) to discriminate vegetation species[2]

[2] This chapter is based on:
Ullah, S., Groen, T.A., Schlerf, M., Skidmore, A.K., Nieuwenhuis, W., & Vaiphasa, C. (2012). Using a Genetic Algorithm as an Optimal Band Selector in the Mid and Thermal Infrared (2.5–14 μm) to Discriminate Vegetation Species. *Sensors, 12*, 8755-8769.

Abstract

Genetic variation between various plant species determines differences in their physio-chemical makeup and ultimately in their hyperspectral emissivity signatures. The hyperspectral emissivity signatures, on the one hand, account for the subtle physio-chemical changes in the vegetation, but on the other hand, highlight the problem of high dimensionality. The aim of this paper is to investigate the performance of genetic algorithms coupled with the spectral angle mapper (SAM) to identify a meaningful subset of wavebands sensitive enough to discriminate thirteen broadleaved vegetation species from the laboratory measured hyperspectral emissivities. The performance was evaluated using an overall classification accuracy and Jeffries Matusita distance. For the multiple plant species, the targeted bands based on genetic algorithms resulted in a high overall classification accuracy (90%). Concentrating on the pairwise comparison results, the selected wavebands based on genetic algorithms resulted in higher Jeffries Matusita (J-M) distances than randomly selected wavebands did. This study concludes that targeted wavebands from leaf emissivity spectra are able to discriminate vegetation species.

3.1 Introduction

Hyperspectral sensors, because of their high spectral detail over contiguous narrow bands, have proven to be a valuable tool for discriminating plants species (Ustin and Xiao 2001; Schmidt and Skidmore 2003; Adam and Mutanga 2009; Cho et al. 2010) compared to multispectral resolution sensors (Landgrebe 2003). However, due to high dimensionality, working with hyperspectral data poses challenging problems such as redundancy, intensive computation, and singularity of covariance matrix inversion (Hughes 1968; Shahshahani and Landgrebe 1994; Vaiphasa et al. 2007; Hao and Qu 2009; Zhou et al. 2010). To overcome these problems, the dimensionality of hyperspectral data needs to be reduced without compromising the information content. The dimensionality of the data is reduced through either band extraction or band selection (Hao and Qu 2009). In band selection a subset of the original bands is selected without affecting the physical meaning of the selected bands. In band extraction a certain number of bands are selected after transforming the original dataset (Rui and Mingyi 2005). Band selection is often preferred to band extraction as the physical meaning of the data remains unchanged (Lee and Landgrebe 1993; Ifarraguerri and Chang 2000; Kaewpijit et al. 2003; Du 2004; Hao and Qu 2009).

Genetic algorithms constitute problem solving optimization methods based on the philosophy of genetics and natural selection through "survival of the fittest" (Holland 1975; Goldberg 1989). A genetic algorithm is a popular band selector and dimensionality reduction procedure for spectral analysis (Leardi 1994; Leardi and Lupiáñez González 1998; Fang et al. 2003; Vaiphasa et al. 2007; Kawamura et al. 2010). The genetic algorithm as a band selector has performed with higher accuracy than other band selection algorithms for both synthetic (Siedlecki and Sklansky 1989) and real remote sensing data (Yu et al. 2002; Fang et al. 2003; Vaiphasa et al. 2007; Kawamura et al. 2010). In remote sensing, genetic algorithms selected spectral bands for classification with hyperspectral data, as well as bands sensitive to the chemical content of plants and soils (Fang et al. 2003; Kawamura et al. 2010). The majority of the studies used genetic algorithms as a band selector where the class information was broad (i.e. the spectral signatures of the different classes were distinct from each other) (Anderson et al. 1976) and the genetic algorithms easily selected bands that differentiated between various classes. Using visible to short-wave infrared (VIS–SWIR; 0.4–2.5 μm) spectra, Vaiphasa et al. (2007) discriminated between sixteen mangrove plant species with similar spectral characteristics. The present study extends the genetic algorithms to the mid and thermal infrared for optimal band selection for discriminating plant species.

Till recently, vegetation spectrum in the mid to thermal infrared (2.5–14 μm) was perceived as a line without any spectral features (Ribeiro da Luz and Crowley 2007). However, the introduction of spectroradiometers sensitive to mid and thermal infrared revealed that certain spectral features are associated with the composition of leaf epidermal materials (i.e. cell walls and cuticular membranes), which can act as a fingerprint for discriminating vegetation (Ribeiro da Luz 2006; Ribeiro da Luz and Crowley 2007, 2010; Ullah et al. 2012b). The present study attempts to discriminate between 13 broadleaf vegetation species using genetic algorithms from high resolution mid to thermal infrared data (2.5–14.0 μm, comprising 3,024 spectral bands). The possibility of using genetic algorithm-based selected features for distinguishing vegetation species (from laboratory measured emissivity spectra) will be an important prerequisite for adjusting band positions of air-borne and space-borne floristic mapping campaigns.

3.2 Materials and Methods

3.2.1 Leaf sampling

The dataset of leaf samples used in this study was the same as used in the (Ullah et al. 2012b). The leaves were collected (between July and September 2010) from thirteen plant species (Table 3.1) species. To avoid pseudo-replication, leaves were collected from at least ten different plants of the same species. Leaves were acquired from different part of the plant (both on the sun and the shaded side). The leaves, attached to small twigs, were brought to the laboratory within 5 minutes, and placed in moist cotton to avoid desiccation. Spectral measurements were recorded as soon as possible.

3.2.2 Spectral measurements

A Bruker VERTEX 70 FTIR spectrometer (Bruker Optics GmbH, Ettlingen, Germany) was used to acquire the Directional Hemispherical Reflectance (DHR) spectrum of each leaf. Nitrogen (N2) gas was used to continuously purge the spectrometer from water vapor and carbon dioxide. A mid-band mercury-cadmium-tellurium (MCT) detector cooled with liquid nitrogen was used to measure the DHR spectrum of the adaxial (upper) surface of the leaf samples between 2.5 and 14 μm (Figure 3.1), with a spectral resolution of 4 cm−1. Thirty five (35) leaves were measured per species, thus 455 leaves were measured in total. Each leaf measurement was referenced against a calibration measurement of gold plate (infragold; Labsphere reflectance technology) with a high reflectance (approximately 96%). One thousand (1,000) scans were averaged to produce each leaf spectrum. The spectra between 6 to 8 μm were noisy (due to water absorption) and were excluded from the analysis. The DHR spectra were converted to emissivity using

Kirchhoff's law (Emissivity = 1 − R) (Nicodemus 1965; Salisbury and Milton 1988; Salisbury et al. 1994). For further detail about the spectrometer and data acquisition see Hecker et al. 2011 and Ullah et al. 2012b.

Table 3.1: The plant species used for spectral measurements. Thirty five (35) leaves were measured per species.

Species	Species code
Acer platanoides	AP
Asplenium nidus	AN
Cornus sericea	CS
Fallopia japonica	FJ
Ginkgo biloba	GB
Hedera helix	HH
Ilex opaca	IL
Liquidambar styraciflua	LS
Platanus orientalis	PO
Prunus laurocerasus	PL
Rhododendron caucasicum	RH
Spathiphyllum cochlearispathum	SP
Tilia platyphyllos	TP

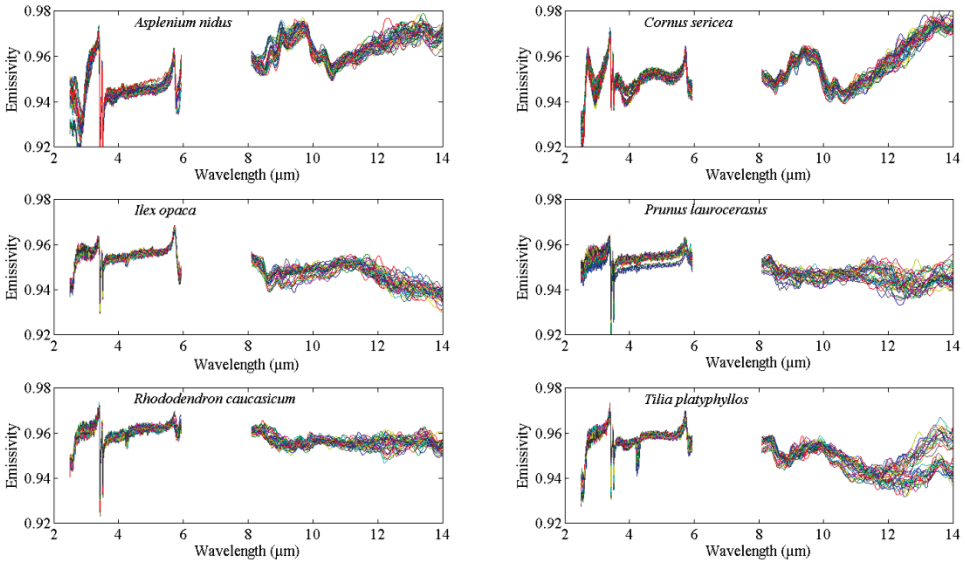

Figure 3.1: The spectral emissivity profiles of the six plant species in the mid-wave and thermal infrared domain.

3.2.3 Concept of genetic algorithm

Genetic algorithms, introduced for the first time by Holland (1975), are a popular type of evolutionary optimization computation based on the concept of natural selection. The innovation behind genetic algorithms is the random

(stochastic) model that uses a population of solutions rather than a single solution. During each iteration, solutions are represented in the form of a "chromosome", with selected wavelength bands positioned as "genes". The algorithm commences with a population of random solutions, termed the first generation. A fraction of these solutions, with the best "fitness" according to a pre-defined objective function are then selected to produce (i.e. undergo the mechanism of crossover and mutation) a second generation that consists of hybridized offspring of the first generation. Of this second generation, again the solutions with the highest fitness are selected to reproduce a third generation, and so on, until the improvement in fitness between subsequent generations levels off to a pre-set threshold. Parameters that have to be selected before starting the algorithm are the chromosome size (i.e. how many bands can be selected per solution), the population size (i.e. the number of solutions per generation), the fraction of a generation that is selected to be the "parents" for the new generation, and when to stop the algorithm. The reproduction operators, objective function, and selection mechanism are summarized in the next subsection, while the detailed practical implementation (step by step procedure) can be found in Goldberg (1989). The genetic algorithms script was written at the Faculty of Geo-Information Science and Earth Observation (ITC), the Netherlands.

3.2.3.1 Reproduction operators

For problem solving, the selected chromosomes directly undergo crossover and mutation. In the crossover operation the two selected parent chromosomes merge and produce offspring (new chromosomes) that share the properties of both parents. A single point crossover was used in this study, where two parent chromosomes split into four segments (two segments per parent). Then the exchange of gene segments produces two offspring from every two parents. In mutation, a single gene (band, in this case) in the offspring chromosome is randomly altered and as a result the characteristics of the offspring differ from the parental chromosome combination.

3.2.3.2 Objective function

An objective function is required to assign a value to each chromosome. The associated value of each chromosome is an indication how well it fits the solution it represents. The spectral angle mapper (SAM) nearest neighbour classifier was used to evaluate the fitness values (in this case the overall classification accuracy) of the chromosome population during the process of evolution. The SAM determines the spectral similarity between two spectra (i.e. target and reference) by calculating the angle between them in an n-dimensional space. To calculate the fitness function, half of the spectra of each species (17 spectra per species) were used for training purposes, and

the remaining half for validation purposes. For each species, the average spectrum of training dataset was used as a reference spectrum.

3.2.3.3 Selection

On the basis of fitness value (i.e. the classification accuracy resulted from the SAM), the parent chromosomes were selected to reproduce offspring using random (roulette wheel) selection. The chromosomes with higher fitness values have a higher chance of being selected for reproduction and to generate a new chromosome.

3.2.3.4 Preliminary parameters and chromosome size

The initial parameters were configured as follows: Population size = 1,000, maximum number of generations = 500, crossover probability = 1, probability of mutation = 0.01, elite count (i.e. the number of chromosomes with best fitness values in the current generation that are guaranteed to survive into the next generation; these chromosomes are called elite children) = 2.

In order to define the number of genes in a chromosome for maintaining high classification accuracy, the genetic algorithms were run with different gene numbers per chromosome. The minimum threshold for class separability (i.e. classification accuracy) was set to 85% (Anderson et al. 1976). The minimum number of genes in a chromosome that exceeded the defined threshold was five. There was little increase in the classification accuracy when the genetic algorithm was executed with chromosomes with six bands (Figure 3.2). Therefore, a chromosome with five bands was chosen for further analysis.

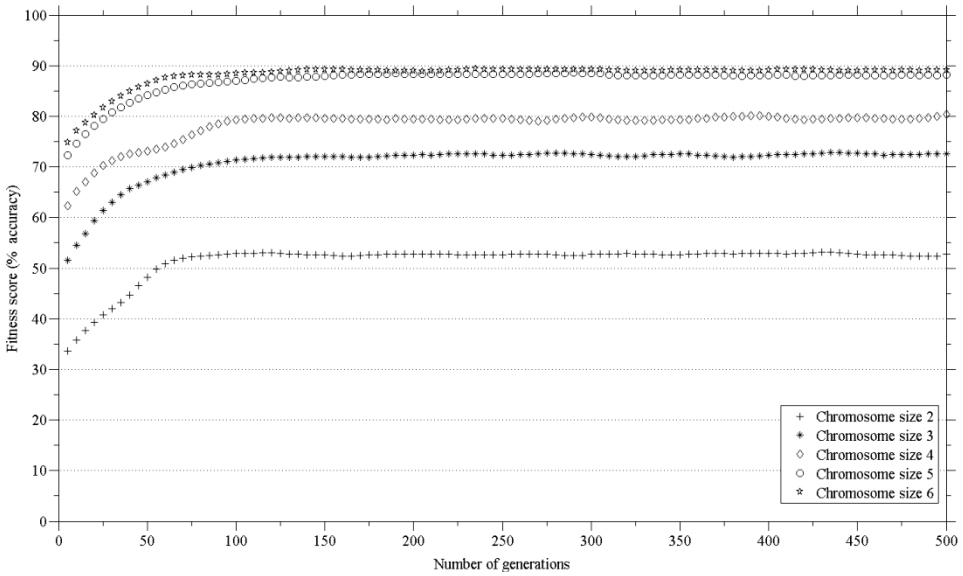

Figure 3.2: Performance of different sized chromosomes (number of bands in the chromosome) for the classification of 13 vegetation species.

The consistency of the genetic algorithms for discriminating vegetation species was checked by repeating the analysis 40 times. The data was reshuffled at the beginning of each run. The algorithms start with a random initial population and undergo selection (based on fitness score), crossover, mutation and elite count processes.

3.2.4 Evaluating the performance of the genetic algorithm

The performance of the genetic algorithms in separating the species was assessed by using the Jeffries Matusita (J-M) distance (Richards and Jia 2006). The J-M distance is the average distance between two class density functions. The J-M distance takes into account the distance between class mean and the distribution of values from the means. Another advantage is that it can be executed over a number of bands (unlike M-statistics). The J-M distance is a parametric test, of which values range between 0 and 2, providing an easy comparison of class separability (Schmidt and Skidmore 2003; Adam and Mutanga 2009; Cho et al. 2010). The J-M distance was calculated between each pair of species using the genetic algorithm based winner chromosome (using the bands selected on the basis of the genetic algorithm) as well as a randomly selected chromosome. Prior to conducting the tests, the distribution of the spectral emissivity values across selected waveband was tested for normality and the homogeneity of variance (homoscedasticity) was verified for every spectral band.

The average J-M distance between each species pair selected using the genetic algorithm's selected bands were compared with the average J-M distance derived from the randomly selected bands. The significance of difference in the J-M distances between the genetic algorithm based bands and randomly selected bands was tested using a t-test.

3.3 Results

3.3.1 Length of the chromosome

The results (Figure 3.2) compare the fitness score against chromosome size for the thirteen species. The minimum number of genes in a chromosome that exceeded the defined threshold (classification accuracy of 85%) was five. There was no substantial increase in the classification accuracy using a six, compared to a five, band chromosome (Figure 3.2).

3.3.2 Band pruning based on genetic search algorithms

Illustrating the process of evolution, Figure 3.3 shows the result of a single run. The vertical (y) axis represents the count of the genes selected, while the horizontal axis (x) represents the wavelength. At the beginning (1st generation) the population consisted of randomly selected genes from all wavebands, and as the evolution proceeded the bands started to converge.

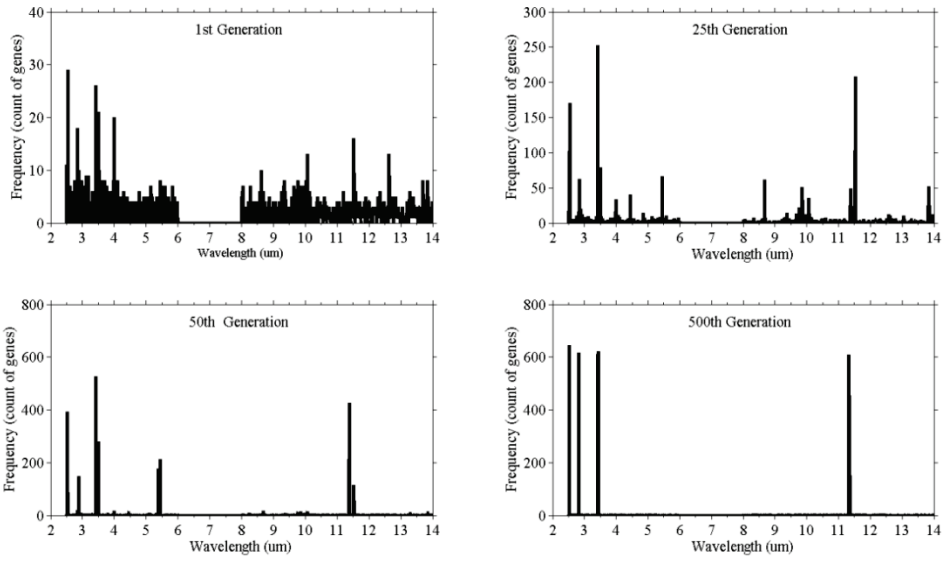

Figure 3.3: The graphical representation of gene convergence, the frequency (count of genes selected in the population) clustered around certain wavebands as the number of generations increases.

The overall classification accuracy using the winning chromosome genes are illustrated in Table 3.2. The results (Table 3.2) show that the classification accuracies of the winning chromosome were above the set threshold (85%) for both training and testing datasets.

Table 3.2: The average confusion matrix (of 40 runs) for the training and testing dataset, the bands selected by genetic algorithms during training are used for evaluation by the testing dataset.

	PL	RH	SP	TP	AP	AN	CS	FJ	GB	HH	IL	LS	PO
PL	17	0	0	0	0	0	0	0	0	0	0	0	0
RH	0	15	0	0	0	0	0	1	0	0	0	1	0
SP	0	0	15	0	0	0	0	0	0	0	2	0	0
TP	0	0	0	17	0	0	0	0	0	0	0	0	0
AP	0	0	0	0	17	0	0	0	0	0	0	0	0
AN	0	0	0	0	0	17	0	0	0	0	0	0	0
CS	0	0	0	0	0	2	15	0	0	0	0	0	0
FJ	0	0	0	0	0	0	0	17	0	0	0	0	0
GB	0	0	0	0	0	0	0	0	17	0	0	0	0
HH	0	0	0	0	0	0	0	0	0	17	0	0	0
IL	0	0	0	0	0	0	0	0	0	0	17	0	0
LS	0	0	0	0	0	0	0	0	0	1	0	16	0
PO	0	0	0	0	0	0	0	0	0	0	0	0	17
Overall classification accuracy of training dataset = 96.83 %													
	PL	RH	SP	TP	AP	AN	CS	FJ	GB	HH	IL	LS	PO
PL	12	0	0	0	0	0	0	0	0	0	2	3	0
RH	0	13	0	4	0	0	0	0	0	0	0	0	0
SP	0	0	12	0	0	0	5	0	0	0	0	0	0
TP	0	2	0	12	0	0	0	0	0	0	0	3	0
AP	0	0	0	0	17	0	0	0	0	0	0	0	0
AN	0	0	0	0	0	17	0	0	0	0	0	0	0
CS	0	0	0	0	0	0	17	0	0	0	0	0	0
FJ	0	0	0	0	0	0	0	17	0	0	0	0	0
GB	0	0	0	1	0	0	0	0	16	0	0	0	0
HH	0	0	0	0	0	0	0	0	0	17	0	0	0
IL	0	0	0	0	0	0	0	0	0	0	17	0	0
LS	0	0	0	0	0	0	0	0	0	0	0	17	0
PO	0	0	0	0	0	0	0	0	0	0	0	0	17
Overall classification accuracy of testing data = 90.50 %													

The genetic algorithm was run 40 times to check consistency. The wining chromosomes along with classification accuracies (based on the SAM) are reported in Appendix 1. The fitness scores of all winning chromosomes were above the defined threshold (classification accuracy over 85%). The frequency of the selected genes showed genes clustering around certain wavebands (Figure 3.4). The high frequency occurring at certain wavebands represents that waveband's importance for the separating of species. The selected genes were grouped into eight waveband regions based on the mean and standard deviation (Table 3.3). Five of those lie in the mid infrared (2.5–6 μm) and the remaining three regions belong to the thermal infrared (8–12 μm).

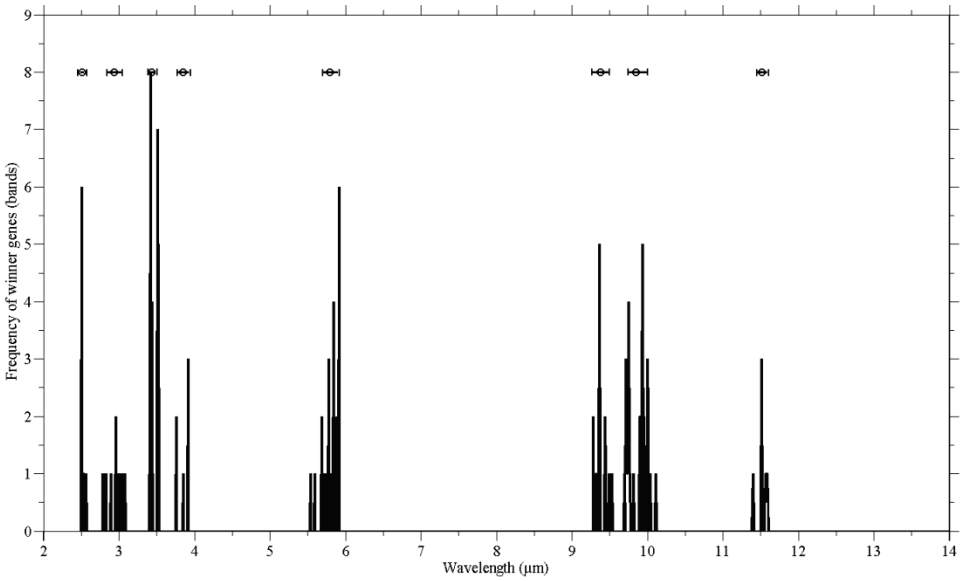

Figure 3.4: The vertical bars represent the number of winning genes at a certain wavelength region for all 40 runs. The horizontal bar at the top shows the spread (mean and standard deviation) of the spectral regions from which the winning bands are selected.

3.3.3 Evaluation of the performance of genetic algorithm

The Jeffries Matusita (J-M) distances between different species pairs calculated using the bands selected by the genetic algorithm, were compared with the randomly selected bands. The five selected bands (resulting from the genetic algorithms and the random selection) were used to calculate the J-M distance between each species. The average J-M distance values of genetic algorithm based selected bands were higher than the value of randomly selected bands. The result of the t-test (Table 3.4) confirms that the differences between most J-M distances (74 out of 78 ≈95%), based on genetic algorithms and random selection, are statistically significant at a 95% confidence level ($p \leq 0.05$).

Table 3.3: Summary of the clustering of selected genes (wavebands), the number of genes, spectral range, means wavelength location and standard deviation.

Group	Spectral region	No. of genes	Wavelength range (μm)	Mean wavelength (μm)	Standard deviation (μm)
A	Mid infrared	26	2.50–2.54	2.52	±0.020
B	Mid infrared	12	2.84–3.03	2.94	±0.097
C	Mid infrared	69	3. 40–3.48	3.44	±0.041
D	Mid infrared	6	3.77–3.93	3.85	±0.078
E	Mid infrared	30	5.70–5.90	5.80	±0.099
F	Thermal infrared	16	9.27–9.48	9.36	±0.107
G	Thermal infrared	35	9.74–10.00	9.87	±0.121
H	Thermal infrared	7	11.46–11.58	11.52	±0.064

Table 3.4: The results of t-test (p-values) between Jeffries Matusita (J-M) distances calculated from genetic algorithms and randomly selected wavebands.

	AP	TP	AN	CS	FJ	GB	HH	IL	LS	PL	PO	RH	Sp
AP	-	0.00	0.02	0.11	0.01	0.00	0.00	0.00	0.01	0.13	0.02	0.01	0.01
TP	-	-	0.00	0.00	0.00	0.00	0.00	0.00	0.16	0.00	0.00	0.00	0.00
AN	-	-	-	0.01	0.00	0.00	0.00	0.00	0.00	0.00	0.00	0.00	0.00
CS	-	-	-	-	0.00	0.00	0.00	0.00	0.14	0.00	0.00	0.00	0.02
FJ	-	-	-	-	-	0.01	0.00	0.00	0.01	0.00	0.01	0.00	0.00
GB	-	-	-	-	-	-	0.03	0.00	0.00	0.01	0.00	0.00	0.03
HH	-	-	-	-	-	-	-	0.01	0.00	0.00	0.00	0.00	0.01
IL	-	-	-	-	-	-	-	-	0.00	0.00	0.00	0.00	0.00
LS	-	-	-	-	-	-	-	-	-	0.01	0.00	0.00	0.02
PL	-	-	-	-	-	-	-	-	-	-	0.00	0.00	0.00
PO	-	-	-	-	-	-	-	-	-	-	-	0.01	0.00
RH	-	-	-	-	-	-	-	-	-	-	-	-	0.00
Sp	-	-	-	-	-	-	-	-	-	-	-	-	-

3.4 Discussion

This study tested the applicability of genetic algorithms for the selection of bands from the mid and thermal infrared emissivity spectra to discern thirteen vegetation species. The visible to shortwave infrared domain have been widely used for discriminating vegetation species, but mid to thermal infrared emissivity spectra have received little attention. The outcome of the study (Table 3.2 and Appendix 1) demonstrated that the genetic algorithm

based selected bands (subset of five bands) achieved an overall accuracy of more than 85%.

The improved classification accuracy of the bands selected by genetic algorithms compared to the randomly selected bands could be attributed to the fact that genetic algorithms provide several possible solutions, evaluate them on the basis of an objective function and pick the best one for the next generation.

The validity of the combination of genetic algorithm based selected bands used for the spectral discrimination of vegetation species in the mid to thermal infrared emissivity spectra may be attributed to the spectral positioning of the selected bands. The emissivity spectra of the different plant species contain unique features due to the variation in physio-chemical composition of the superficial epidermal layer of the plant leaves. The emissivity signature of plant leaves is dominated by a feature associated with major classes of cellulous of the epidermis (Holloway 1982 ; Elvidge 1988; Siedlecki and Sklansky 1989; Leardi 1994; Achenbach et al. 1995; Leardi and Lupiáñez González 1998; Heredia 2003). The selected waveband positions, between 2.5 to 6 μm, may be attributed to the physical makeup of the surface, as well as the water and chemical content of different plant leaves (Ribeiro da Luz 2006; Fabre et al. 2011; Gerber et al. 2011). The clustering of the winning genes at around 3.00 μm may be due to OH band stretching and bending in the water molecule (Richards and Jia 2006; Ribeiro da Luz and Crowley 2007; Zhou et al. 2010). The selection of bands at the wavelength position of 3.44 μm may be due to the presence of different amounts of nonacosane (a compound in wax occurring on the leaf surface), as a result of the stretching of the CH2 bond of methylene in leaf surface waxes (Silverstein and Webster 1998; Maréchal and Chanzy 2000; Kacuráková and Wilson 2001). The stretching of carbonyl group (C=O) in ester has been linked to a spectral features at 5.80 μm (Ramirez et al. 1992; Silverstein and Webster 1998). Different amounts of leaf cutin and cutan (which are composed of esterified monomers) may be linked to the selection by the genetic algorithm of features at 5.80–5.92 μm (Figure 3.4). The bands selected between 9.40–9.70 μm (Figure 3.3) could be attributed to cellulose thickness, creating two prominent features at 9.47 μm and 9.68 μm, associated with the C-O band stretching (Maréchal and Chanzy 2000; Ribeiro da Luz and Crowley 2007). The next spectral region winner bands were selected from (mean at 9.87 μm and standard deviation ±0.121 μm) may have resulted from differences in hemicellulose and other pectins (Wilson et al. 2000; Fry 2004). The winning gene clustering at 11.50 μm (mean 11.50 and standard deviation ±0.121 μm, Figure 3.4) may have resulted from the presence of different aromatic compounds in the plant species (Ribeiro da Luz 2006).

Discriminating vegetation species using laboratory measured emissivity spectra is prerequisite for the future vegetation mapping campaigns from air-borne and space-borne data. However, there are a number of problems associated with extending this work to field level. The calibration of remotely sensed signals in the MIR (around 3 μm) is complicated by the difficulty associated with the overlap of reflected and emitted energy in the MIR. Other problems associated with field condition are the distance between target and sensor, spectral and spatial resolution, atmospheric condition, and seasonal changes. The cavity effect of plant leaves causes blackbody emittance in the TIR and reduces spectral contrast in the signal. The cavity effect problem is noticeable in small and needle leaved species and also in species with funnel-like leaf arrangements (Ribeiro da Luz and Crowley 2010). One could extend this study to a field, air-borne, and space-borne by using a sensing system with high signal to noise ratio (SNR) that allows small spectral differences in plant to be characterized.

3.5 Conclusions

This study has demonstrated the potential of genetic algorithms as band selectors using high resolution mid to thermal infrared emissivity spectra to differentiate between vegetation species at laboratory level. It is concluded that the bands selected by genetic algorithms are more useful for discriminating vegetation species than randomly selected bands are, when using laboratory emissivity spectra. The genetic algorithm based selected bands were actually found to have potential for floristic mapping. Bands selected with genetic algorithms may correspond to physiochemical characteristics of vegetation leaves (as seen in the previous studies) as leaves of different species possess unique surface materials. The genetic algorithm based selected bands help to understand the section of the electromagnetic spectrum that has a high potential for discriminating vegetation types, which may be useful when designing new sensors for vegetation studies. The outcome of this study is that the genetic algorithm band selection procedure can differentiate between plant species using laboratory measured thermal emission spectra. It would be very interesting to extend this work to the field and at airborne level with the advancement of hyperspectral thermal infrared sensors.

Chapter 4

An accurate retrieval of leaf water content from mid to thermal infrared spectra using continuous wavelet analysis[3]

[3] This chapter is based on:
Ullah, S., Skidmore, A.K., Naeem, M., & Schlerf, M. (2012). An accurate retrieval of leaf water content from mid to thermal infrared spectra using continuous wavelet analysis. *Science of The Total Environment, 437*, 145-152

Ullah, S., Skidmore, A.K., Naeem, M., & Schlerf, M. (2012). Estimation of leaf water content from far infrared (2.5 -14 μm) spectra using continuous wavelet analysis. In, *Geoscience and Remote Sensing Symposium (IGARSS), 2012 IEEE International* (pp. 4817-4820)

Abstract

Leaf water content determines plant health, vitality, photosynthetic efficiency and is an important indicator of drought assessment. The retrieval of leaf water content from the visible to shortwave infrared spectra is well known. Here for the first time, we estimated leaf water content from the mid to thermal infrared (2.5 – 14.0 μm) spectra, based on continuous wavelet analysis. The dataset comprised 394 spectra from nine plant species, with different water content achieved through progressive drying. To identify the spectral feature most sensitive to the variations in leaf water content, first the Directional Hemispherical Reflectance (DHR) spectra were transformed into a wavelet power scalogram, and then linear relations were established between the wavelet power scalogram and leaf water content. The six individual wavelet features identified in the mid infrared yielded high correlations with leaf water content (R^2 = 0.86 maximum, 0.83 minimum), as well as low RMSE (minimum 8.56%, maximum 9.27%). The combination of four wavelet features produced the most accurate model (R^2 = 0.88, RMSE = 8.00%). The models were consistent in terms of accuracy estimation for both calibration and validation datasets, indicating that leaf water content can be accurately retrieved from the mid to thermal infrared domain of the electromagnetic radiation.

4.1 Introduction

Leaf water content is a key indicator of plant health, vigour and photosynthetic efficiency (Harry 2006). Accurate retrieval of plant water content plays a crucial role in assessing drought risk (Bauer et al. 1986), predicting wildfire and monitoring the physiological condition of vegetation (Peñuelas and Filella 1998) and biomass (Mutanga et al. 2005; Cho et al. 2007; Ullah et al. 2012c), while in the agriculture domain it helps in scheduling irrigation and estimating crop yields (Peñuelas et al. 1993; Peñuelas et al. 1997). Conventional methods of estimating leaf water content in the field are time consuming and location specific. Remote sensing is an effective alternative to field sampling for the retrieval of leaf water content, being non-destructive and providing continuous spatial coverage of a large area (Hunt et al. 1987; Peñuelas et al. 1993; Zhang et al. 1997; Sepulcre-Cantó et al. 2006).

Leaf water content is the quantity of water in a leaf and is conventionally represented as gravimetric water content (GWC: water mass in leaf relative to either the fresh (GWCf; Garnier and Laurent 1994) or dry leaf weight (GWCd; Chuvieco et al. 2002) or equivalent water thickness (EWT: mass of leaf water per unit leaf area; Datt 1999). As leaf area is not always easy to measure (conifer needles in particular), gravimetric water content is preferred to equivalent water thickness (Cheng et al. 2011).

Leaf water status has been successfully estimated using the near infrared and shortwave infrared (Aldakheel and Danson 1997; Datt 1999; Ceccato et al. 2001; Zygielbaum et al. 2009). Leaf water molecules absorb electromagnetic energy throughout the shortwave infrared (1.30 – 2.50 μm), where there is strong absorption at 1.45 μm, 1.90 μm and 2.10 μm, and weak overtones are located at 0.75 μm and 1.20 μm (Datt 1999). In contrast, the mid and thermal infrared (2.5 – 14 μm) domain is mostly ignored because of a number of challenges, including unavailability of spectroradiometers (i.e. sensitive to the mid to thermal infrared), and the subtle variations in vegetation spectra (Salisbury and Milton 1988; Kirkland et al. 2002; Ribeiro da Luz and Crowley 2007). Research in the mid to thermal infrared suggests that the plants spectra is dominated by leaf water content and leaf epidermal materials (Boyd and Petitcolin 2004; Ribeiro da Luz and Crowley 2010; Ullah et al. 2012a; Ullah et al. 2012b). However, there is no literature relevant to the successful retrieval of leaf water content and water stress indices from multiple species. Gerber et al. (2011), who measured the mid to thermal infrared response of fresh and completely dried leaves but not intermediate moisture levels, noticed considerable variation in the mid infrared spectral response, highlighting that the mid infrared may be used for quantifying leaf water content.

The leaf water content needs to be matched to the spectral response. In this study, continuous wavelet transformation (which is an emerging tool for analysing spectral signals) was used to recognize subtle changes in the hyperspectral data by decomposing it into different scale (or frequency) components (Mallat 1991; Cheng et al. 2010b). The continuous wavelet analysis has been successfully used to estimate vegetation biophysical/biochemical parameters from hyperspectral signals in the visible to shortwave infrared (Pu and Gong 2004; Cheng et al. 2010b; Cheng et al. 2011).

This paper investigates the potential of laboratory measured mid to thermal infrared Directional Hemispherical Reflectance (DHR) spectra for the retrieval of leaf water content based on a continuous wavelet analysis. More specifically, the aim was to assess the accuracy (R2 and RMSE) of a continuous wavelet decomposed spectral features for the retrieval of leaf water content, and to identify the spectral region sensitive to the variation in leaf water content of nine different plant species.

4.2 Materials and Methods

4.2.1 Leaf collection and measurement of leaf water content

The study took place at the Geo-Science Laboratory, Faculty of Geo-Information Science and Earth Observation (ITC), between 15th July and 30th August, 2011. Leaves (6 or 10 leaves per species) were collected from nine plant species (Table 4.1). To investigate the variation in the spectral response associated with different leaf water content, we acquired leaves from three different plants of the same species. The preliminary visual analysis showed that each single leaf was healthy. Within 30 minutes, spectral measurements were made of the fresh leaves in the laboratory (Kumar et al. 2010). Different levels of leaf water content were obtained by successively air drying the leaves and taking measurements after every four hours. The leaf water content was precisely measured before and after recording the spectra by using a digital weight balance with 100 µg accuracy. Prior to measuring the final (completely dry leaf) water content level, leaves were oven dried at 60°C for 90 minutes.

The gravimetric leaf water content was estimated using the following equation:

$$LWC_f = 100(M_w - M_d)/ M_w \quad (1)$$

where Mw represent the wet leaf mass and Md is the mass of completely dried leaf (dried in oven for 90 minutes at last succession). LWCf is the leaf water content relative to wet leaf mass.

Table 4.1: The plant species studied, leaf sample size per species, successive drying phases, and the total number of spectra per species measured using a laboratory spectroradiometer (2.5 – 14 µm). The species were identified by an experienced taxonomist.

Species name	Common name	Sample size	Drying phases	spectra per species
Acer platanoides L.	Norway Maple	6	5	30
Cornus sericea L.	Redosier Dogwood	6	6	36
Fallopia japonica (Houtt.)	Japanese Knotweed	6	5	30
Platanus orientalis L.	Oriental Planetree	10	6	60
Rhododendron caucasicum Pall.	Rhododendron	6	8	48
Tilia platyphyllos Scop.	Largeleaf Linden	10	6	60
Liquidambar styraciflua L.	Sweetgum	10	7	70
Fagus sylvatica L.	European Beech	6	4	24
Aesculus hippocastanum L.	Horse-Chestnut	6	6	36
				Total measured spectra = 394

4.2.2 Spectral measurements

The Bruker VERTEX 70 FTIR spectroradiometer was used to acquire the DHR spectrum of each leaf between 2.5 and 14 µm, with a spectral resolution 4 cm-1. The H2O vapour and CO2 gas were continuously expelled from the spectroradiometer using N2 gas. The DHR spectra of the leaf samples (upper surface) were measured using mercury-cadmium-tellurium (MCT) detector cooled with liquid nitrogen. A gold plate (also called infragold) was used to calibrate the spectral measurements of each leaf sample. The DHR spectra of leaves with different water contents were measured progressively at various drying levels, as described above. The spectral measurement per species varied from 24 to 70, depending on the dehydration speed and the number of leaves (per species) selected at the initial stage (Table 4.1). A total of 394 spectra were measured (Table 4.1). Two thirds (n = 262 samples) of the total data were (randomly) used for calibration and one third (n = 132 samples) for validation purposes.

4.2.3 Wavelet analysis and feature selection procedure

The DHR spectra were processed by adapting a continuous wavelet transformation routine as described in Cheng et al. (2011). Wavelet transformation is an emerging tool for analysing hyperspectral data and facilitating the recognition of subtle changes by decomposing hyperspectral data into different scale (or frequency) components (Mallat 1991). Since 1991, wavelet transformation has been widely used in the biological and medical sciences (Crowe et al. 1992; Chen et al. 1993; Chmelka and Kozumplik 2005), geophysics (Corso et al. 2003; Zarrouk and Bennaceur 2009), as well as chemistry (Chen et al. 2004; Ma and Shao 2004). In remote sensing, wavelet analysis has been used in classification based on texture (Zhu and Yang 1998; Kiema 2000; Li 2004; Soulard and Carré 2011; Myint and Mesev 2012), landscape heterogeneity (Murwira and Skidmore 2005, 2006, 2010), image fusion (Pajares and de la Cruz 2004; Amolins et al. 2007; Li 2008; Wan et al. 2010), reduction of hyperspectral data dimensionality (Kaewpijit et al. 2003; Chen and Qian 2011), discrimination of plant species (Koger et al. 2003; Banskota et al. 2011) and estimation of vegetation biophysical/biochemical parameters from hyperspectral signals (Pu and Gong 2004; Blackburn 2007). More recently, wavelet analysis has been used to estimate moisture content in plant leaves from visible near infrared and shortwave infrared hyperspectral data (Cheng et al. 2010b; Cheng et al. 2011).

The wavelet transforms are further bifurcated into a discrete and a continuous wavelet transform (Chen et al. 2004; Cheng et al. 2010b; Cheng et al. 2011). Compared with the discrete wavelet transform, the continuous wavelet is quite simple to perform, the coefficients are easily interpretable and (unlike DWT) it does not require inverse transformation to construct the original signal (Bruce et al. 2001; Chen et al. 2004; Kalacska et al. 2007; Cheng et al. 2011). The coefficients of continuous wavelet transformation (CWT) can be directly compared with the original spectra wavebands and possess information about the position and shape of the vegetation's spectral features (Blackburn and Ferwerda 2008).

Continuous wavelet routine is the linear transformation of a hyperspectral signal into a set of coefficients using the mother wavelet function f (λ) (where λ=1, 2, 3, …k, k represent the number of wavebands). The continuous wavelet ψa,b(λ) can be created from the scaling and shifting of the mother wavelet ψ(λ) (Bruce et al. 2001; Cheng et al. 2010b; Cheng et al. 2011);

$$\psi a,b(\lambda)=\frac{1}{\sqrt{a}}\psi\left(\frac{\lambda-b}{a}\right) \quad (2)$$

where a and b are positive real numbers and represent the scaling and shifting factor, respectively. The scale factor a represents the width of the wavelet and the shifting factor b denotes the position.

$$Wf(a,b)=\langle f, \psi_{a,b}\rangle = \int_{-\infty}^{+\infty} f(\lambda)\ , \psi_{a,b}(\lambda)d\lambda \quad (3)$$

The continuous wavelet coefficients (Wf (a,b) consist of a two dimensional matrix (j×k matrix) called a scalogram. One dimension (1,2,…j) is the scale and the other dimension is the wavelength (1,2,3…k). The length of all scale components is equal to the spectrum under investigation.

The low and high scale constituents capture, respectively, the characteristics of the narrow features and overall shape of the spectra (Ferwerda and Jones 2006; Cheng et al. 2011). The scalogram (wavelet coefficients) shows the magnitude of correlation between the scale and shifted mother wavelet, and represents the similarity of the localized spectral signature to the mother wavelet (Rivard et al. 2008; Cheng et al. 2010a; Cheng et al. 2011). The variation in the shape and depth of leaf spectra due to different amounts of leaf water content can be quantified by using the wavelet coefficient (scalogram).

A Gaussian second derivative (or Mexican hat) was used as the mother wavelet foundation (Torrence and Compo 1998) because of the resemblance of the spectral feature to Gaussian (Miller et al. 1990). The Mexican hat effectively supports a range of [-5, 5] for scale a = 1 (Du et al. 2006). Instead of using all possible scale decompositions, the dyadic scales (21, 22, 23,……, and 211) were used to decompose the spectra in order to avoid intensive computation as well as to reduce the dimension of the scalogram and the volume of data. For simplicity, the dyadic scale (21, 22, 23,……, and 211) of the scalogram is represented as scale 1,2,3….,11 in the upcoming sections. The continuous wavelet analysis was executed using the Matlab software package (The MathWorksTM,Natick, Massachusetts, USA).

To select the wavelet features (i.e. single units in the wavelet scalogram) most sensitive to leaf water content, a four-step procedure was followed (Figure 4.1). In step 1, the wavelet power (wavelet scalogram) was computed for all spectra using the continuous wavelet transform function. The wavelet scalogram is a function of scale and wavelength (μm). In step 2, a Pearson correlation (R2) was computed between leaf water content and the wavelet scalogram in order to detect the spectral features sensitive to the variation in leaf water content. Then, all significant ($p < 0.05$) features were arranged in descending order based on R2, and a threshold (of the top 1%) was applied to select spectral features highly sensitive to variations in leaf water content. The features demarcated by this threshold were adjacent

(consecutive) in scale and wavelength dimension and clustered in a wavelet region sensitive to leaf water content. To avoid multicollinearity of consecutive wavelet features, at step 4 an individual feature with the highest R2 was selected from each spectral region. The sparsely dispersed individual features (selected at step 4) represent the most sensitive features and were expressed in scale as well as wavelength dimension.

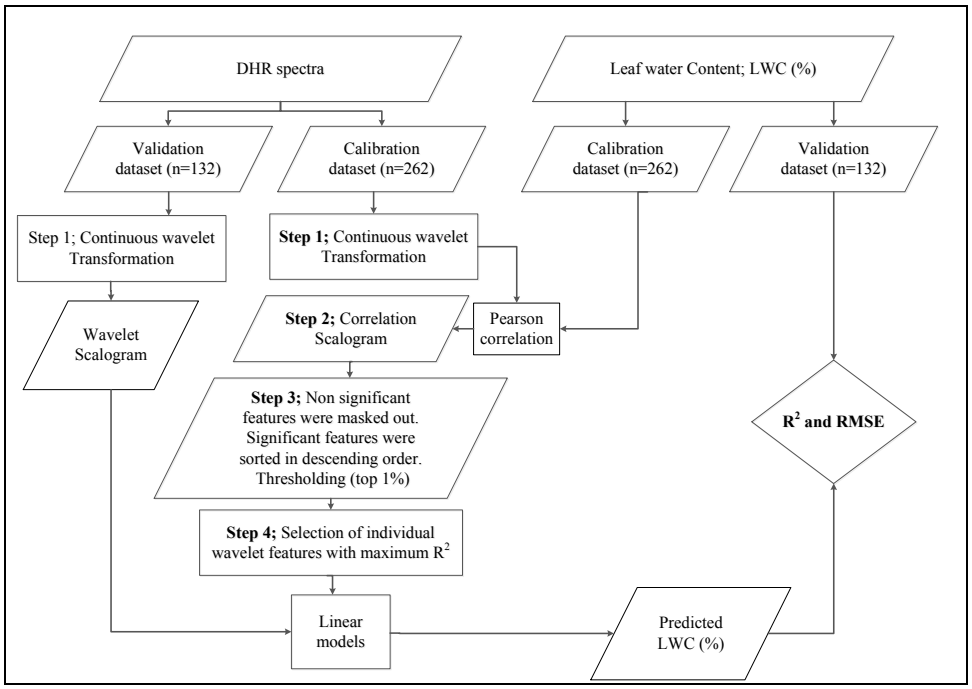

Figure 4.1: Schematic representation of the method followed for the retrieval of leaf water content from Directional Hemispherical Reflectance (DHR) spectra between 2.5 and 14 µm.

4.2.4 Statistical analysis

The entire dataset consisted of DHR spectra (394 in total) for nine plant species, and the associated leaf water content (one measurement per spectrum). The dataset was randomly divided into calibration (66%; 262 samples) and validation (34 %; 132 samples) subsets. The calibration dataset consisted of four (or six depending on the number of leaves measured per species) samples per species, while the validation dataset acquired two (or four) samples per species per drying phase. The calibration dataset was used to identify the sensitive wavelet features by following the procedure discussed in section 4.2.3. Simple linear regression was used to model the relationship of individual wavelet features (independent variable) with leaf water content (dependent variable), while stepwise multiple linear regression was used to model the relationship between multiple wavelet

features and the leaf water content. The models resulting from the calibration dataset were applied to the validation dataset, and the predictive performance assessed using R^2 and RMSE (Figure 4.1).

4.3 Results

4.3.1 Variation in the spectral response (mid to thermal infrared) and leaf water content

Different plant species exhibited considerable variation in the leaf water content. The means and spreads of the leaf water content for nine plant species are shown in (Figure 4.2). In general, a similar spectral response was observed with varying leaf water content in all species. Fresh leaves exhibited the lowest mid and thermal infrared reflectance (Figure 4.3), and reflectance increased as leaf water content decreased. In the mid infrared, the variation in reflectance was more pronounced between 2.5 – 3.0 µm (reflectance reached a maximum of 30%) and 3.5– 5.8 µm (reflectance reached a maximum of 16%). The absorption feature at 3.05 µm and 4.65 µm is linked to water in the leaf (Ribeiro da Luz 2006; Fabre et al. 2011). The water absorption band at 4.65 µm (Fabre et al. 2011) became weaker, as the leaf water content decreased, while the cellulose and lignin maxima at 4.00 µm and 5.52 µm became prominent.

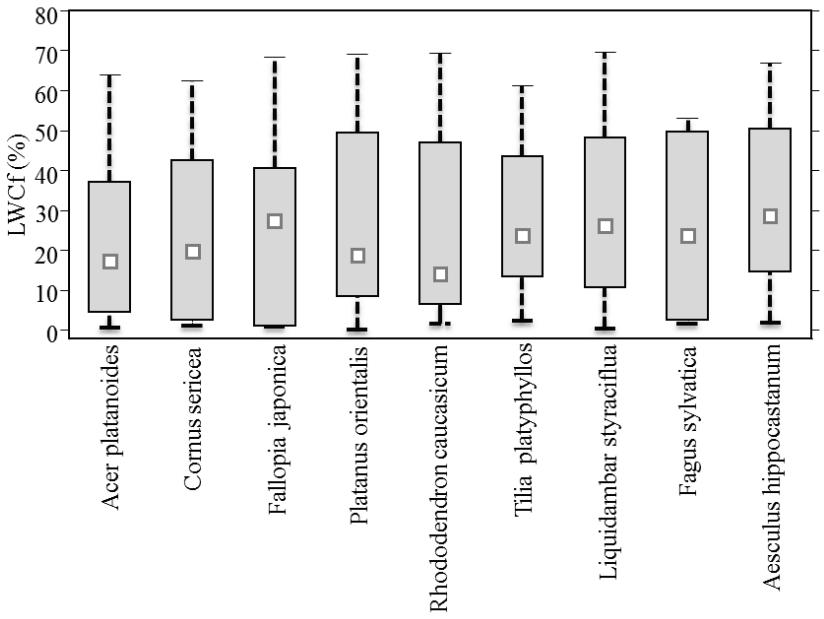

Figure 4.2: Boxplots showing the means and spreads of leaf water content in different plant species.

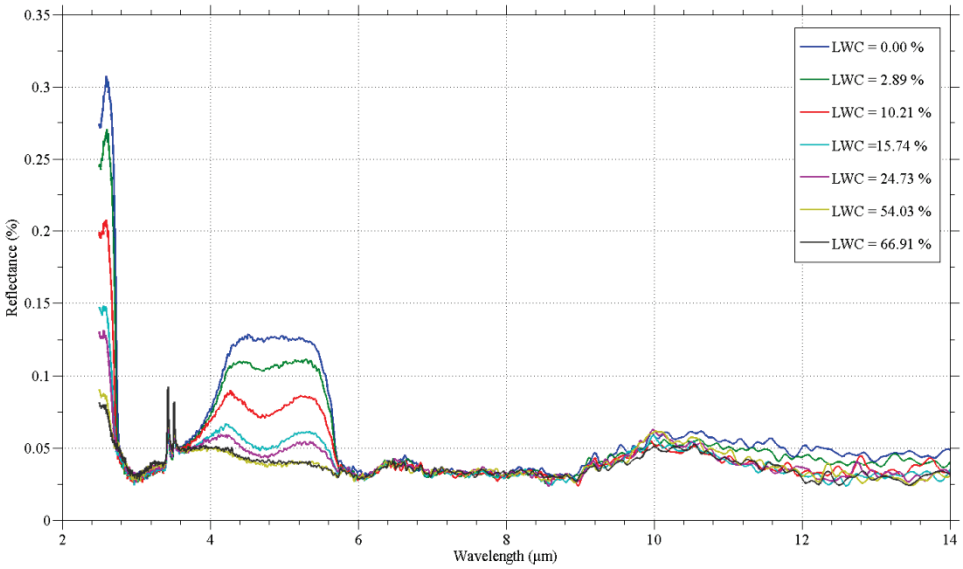

Figure 4.3: The DHR spectra in the mid and thermal infrared of *Liquidambar styraciflua* leaves with different water content. The reflectance markedly increases between 2.5 – 3.0 µm and 3.5 – 5.8 µm as the leaf water content decreases.

The summary statistics indicated that leaf water content relative to the wet leaf weight in the calibration subset varied between 0.0% (completely dried) and 69.2%, with an average of 27.7% and standard deviation of 23.3%. The validation subset ranges between 0.0% and 69.7%, with an average of 28.7% and standard deviation of 23.1% (Table 4.2).

Table 4.2: Summary statistics of the leaf water content (LWCf) of calibration and validation datasets.

Data type	Sample size	Min LWC_f (%)	Max LWC_f (%)	Mean LWC_f (%)	StDev LWC_f (%)
Calibration	262	0.0	69.2	27.7	23.3
Validation	132	0.0	69.7	28.7	23.1

4.3.2 Wavelet features sensitive to leaf water content

The transformation of DHR spectra using continuous wavelet analysis highlighted six spectral features (single feature per spectral region). The correlation scalogram (Figure 4.4(a)) showed regions with high R2 located in the mid infrared (2.5 – 6 µm), and the positions (wavelength and scale) are illustrated in Figure 4.4(b). The R2 varied from 0. 87 (feature A, Figure 4.4(b), Table 4.3) located at wavelength 3.302 µm, to R2 = 0.84 at wavelength 2.508 µm (feature E, Figure 4.4(b), Table 4.3). The combination of the spectral features using stepwise multiple linear regression resulted in a

high coefficient of determination (adjusted R2 = 0.89). Stepwise regression produced the highest accuracy model (Table 4.3) by the inclusion of four wavelet features (A, B, E, D).

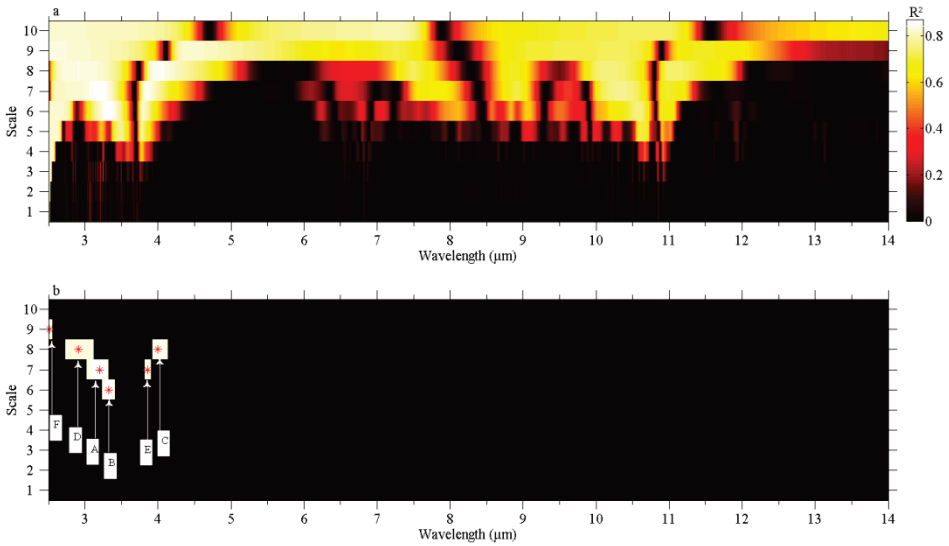

Figure 4.4: The correlation scalogram (a) and the selected wavelet features sensitive to leaf water content (b). The bright portion (a) represents the wavelet regions with high correlation (R^2) with leaf water content and the dark region represents those that are less sensitive to variation in the leaf water content. The vertical axis represents the wavelet scale, while the horizontal axis displays the wavelength.

Table 4.3: Summary of the selected wavelet features, the wavelet features, their spectral location, scale, correlation with leaf water content for calibration and validation data, RMSE of predicted versus measured leaf water content, and relation of the selected features to the existing literature.

Feature	Wavelet feature location		Calibration data		Validation data		Features related to
	Wavelength	Scale	R^2 (%)	Stat. Sig	R^2 (%)	RMSE (%)	
A	3.203 μm	7	0.876	$P < 0.01$	0.863	8.56	Water at 3.05 μm
B	3.329 μm	6	0.875	$P < 0.01$	0.862	8.60	
C	3.999 μm	8	0.856	$P < 0.01$	0.849	8.98	Lignin at 4.00 μm
D	2.910 μm	8	0.855	$P < 0.01$	0.841	9.22	Water at 2.91 um
E	3.857 μm	7	0.855	$P < 0.01$	0.841	9.24	Lignin at 4.00 μm
F	2.508 μm	9	0.839	$P < 0.01$	0.831	9.49	Water at 2.50 um
A,B,E,D	Stepwise regression		0.890	$P < 0.01$	0.883	8.00	

4.3.3 Validating the modeled leaf water content from the selected features

The models resulting from the calibration dataset were applied to a validation dataset. Among individual wavelet features, the most accurate model (R2 = 0.86, RMSE = 8.56%) was produced at wavelength 3.203 µm and scale 7 (feature A; Table 4.3). The stepwise regression model based on a calibration dataset estimated the leaf water content with the highest accuracy (R2 = 0.88, RMSE = 8.0%) (Table 4.3, Figure 4.6). The validation results (Figure 4.5 and Figure 4.6) show that data points are dispersed close to the 1:1 line, except for higher leaf water content (above 40 %). The DHR reflectance and wavelet power saturate at higher (above 40%) leaf water content (Figure 4.7).

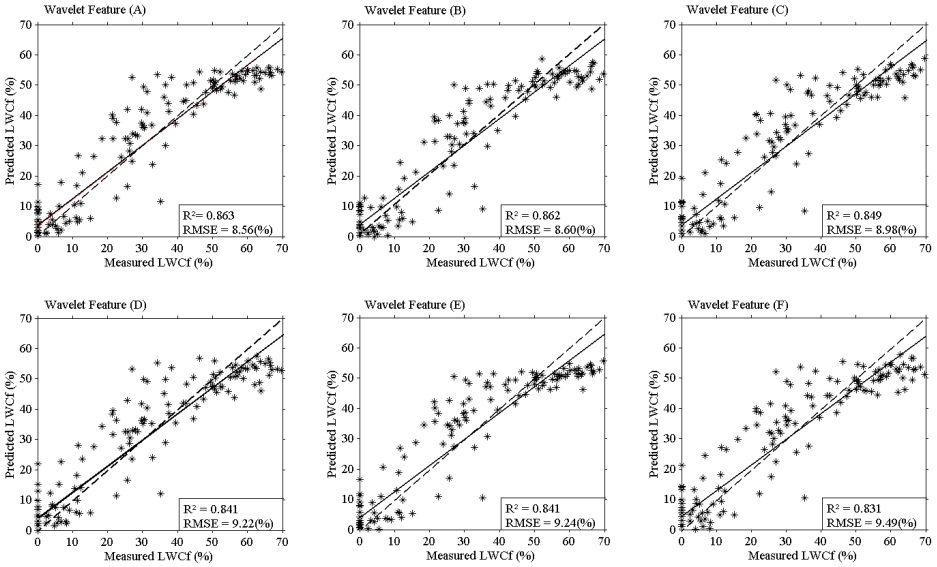

Figure 4.5: Comparison of measured LWC_f (%) with predicted LWC_f (%) based on the model developed from individual wavelet features.

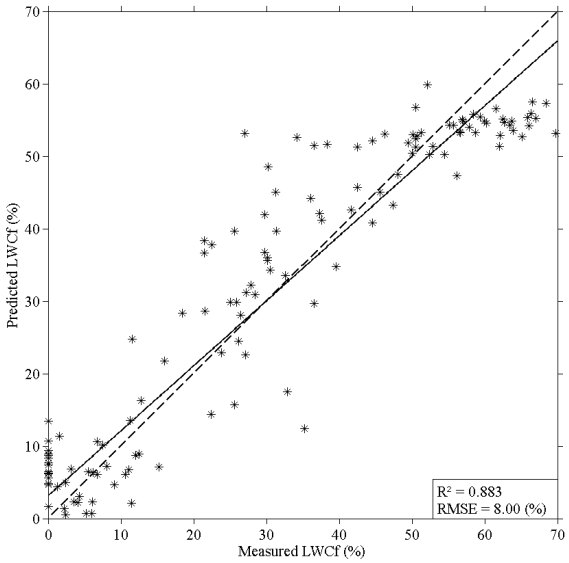

Figure 4.6: Measured versus predicted LWC_f (%) based on combined wavelet features using stepwise regression model.

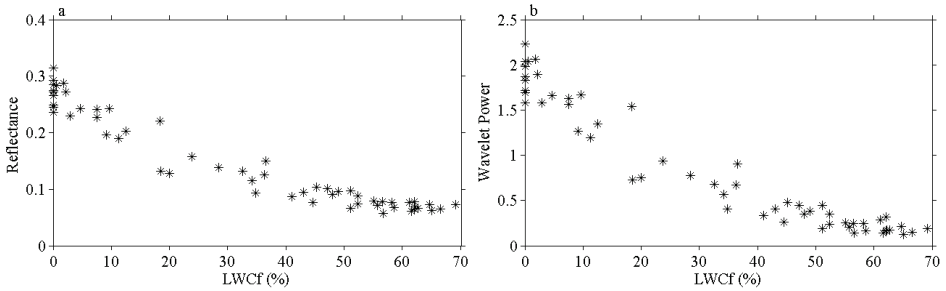

Figure 4.7: The variation in leaf reflectance (a) and wavelet power (b) at 2.508 µm as a function of leaf water content LWC_f(%). The sensitivity of leaf reflectance and wavelet power was low with high water content.

4.4 Discussion

This study quantified for the first time the relationship between DHR spectra (mid to thermal infrared; 2.5 – 14 µm) and leaf water content using continuous wavelet analysis. Retrieving leaf water content using the mid to thermal infrared resulted in a more accurate estimate of leaf water content (R2 = 0.88) than when using visible to shortwave infrared (Cheng et al. 2011) (R2 =0.77). In other words, our results complement knowledge from the visible to short wave infrared (0.4 – 2.5 µm) domain that leaf water content relates to remotely sensed spectra (Aldakheel and Danson 1997; Datt 1999; Ceccato et al. 2001; Zygielbaum et al. 2009) and especially that

higher explained model variance is obtained using the mid infrared and thermal infrared.

The variation in the mid infrared and thermal infrared spectral response with changing water content (i.e. high reflectance with low leaf water content and vice versa) agrees with results from Fabre et al. (2011) and Gerber et al. (2011). The spectral reflectance increased as leaf water content decreased and this impact was more noticeable when the leaf water content fell below 40% (Figure 4.7). The asymptotic behaviour at high leaf water content (above 50 %) was attributed to the poor sensitivity of the wavelet feature to leaf water content due to saturation of DHR spectra. A similar result was observed when leaf water content was estimated from the visible near infrared and shortwave infrared domain (Datt 1999; Ceccato et al. 2001; Cheng et al. 2011).

The selected wavelet features that significantly explain foliar water content were located only in the mid infrared, with no features from thermal infrared being selected, thus confirming recent findings by other researchers (Fabre et al. 2011; Gerber et al. 2011). The selected wavelet features were spectrally positioned at the edge of the water, cellulose and lignin absorption features. The wavelet features at 2.508 μm (feature F), 2.910 μm (D), 3.203 μm (A), and 3.329μm (B) could be attributed to the absorption bands related to leaf water content (Ribeiro da Luz 2006; Fabre et al. 2011; Gerber et al. 2011). The wavelet features at 3.857 μm and 3.999 μm were at the leading edge of spectral features (i.e. the cellulose and lignin spectral peak at 4.00 μm). These features became prominent with the reduction in leaf water content (Figure 4.3).

An accurate retrieval of leaf water content was achieved despite the influence of variation in leaf structure from different plant species. The continuous wavelet analysis has proved an effective tool for analyzing DHR spectra (comprising thousands of bands) and selecting spectral features related to leaf water content. The continuous wavelet analysis segregated the water absorption features into various scales. The different scaled features contain information on both narrow and broad absorption features related to leaf water and dry matter contents. The correlation scalogram (which resulted from the correlation between wavelet power and leaf water content of numerous samples) facilitated the selection of features that were most sensitive to the variations in leaf water content.

This study successfully estimated leaf water content, as well as demonstrated the practicality of the continuous wavelet analysis method in the mid and thermal infrared (Blackburn 2007; Rivard et al. 2008; Cheng et al. 2010b; Cheng et al. 2011). However, upscaling our results to field conditions may

pose several challenges. In this study, all the selected wavelet features belong to the mid infrared domain. In the mid infrared, the reflected and emitted radiation overlap that make the remotely sensed signals difficult to calibrate. Because of field conditions, including canopy structure, spectral resolution, spatial resolution, atmospheric condition, and seasonal variation, we anticipate that successful results will be predicated on sensing systems with strong signal to noise ratios (SNR), allowing subtle differences in the spectral signature of plant canopies to be sensed. An interesting extension to the work will be to develop and compare radiative transfer models in the middle and thermal infrared (Darvishzadeh et al. 2008a).

4.5 Conclusion

This study aimed to investigate the potential of mid to thermal infrared spectra for the retrieval of leaf water content at laboratory level using continuous wavelet analysis. It is concluded that mid-wave infrared spectra contain sufficient information to retrieve leaf water content with high accuracy (R2 = 0.88, RMSE = 8.00%). The selected wavelet features are characterized by water and dry matter (cellulose and lignin) absorption wavebands. This study suggests that the retrieval of leaf water content may be explored from airborne mid-wave infrared sensors at canopy level.

Chapter 5

Evaluation of three proposed indices for the retrieval of leaf water content from the mid-wave infrared (2 – 6 µm) spectra[4]

[4] This chapter is based on:
Ullah, S., Skidmore, A.K., Groen, T.A., & Schlerf, M. (2013). Evaluation of three proposed indices for the retrieval of leaf water content from the mid-wave infrared (2–6 µm) spectra. *Agricultural and Forest Meteorology, 171–172*, 65-71

Abstract

The retrieval of leaf water content based on various indices derived from the visible to shortwave infrared (0.4–2.5 μm) have been frequently reported. The mid-wave infrared (2.5–6.0 μm) domain has surprisingly received little attention, though the main water absorption bands are located in the mid-wave infrared. This research aimed to investigate the potential of three newly proposed narrowband indices for retrieving leaf water content from the mid-wave infrared. The proposed indices were named as Mid-wave infrared Normalized Difference Water Index (MNDWI), Mid-wave infrared Simple Ratio Water Index (MSRWI) and Mid-wave infrared Simple Difference Water Index (MSDWI). Linear relations were established between the indices (calculated from all possible two-band combinations) and leaf water content. The performance of each index was evaluated based on R^2 and RMSE. The proposed indices yielded high correlation with leaf water content, and among them MNDWI produced the most accurate model (R^2 = 0.89 and RMSE = 7.65%) followed by MSDWI (R^2 = 0.86 and RMSE = 8.66%) and MSRWI (R^2 = 0.85 and RMSE = 8.86%). In conclusion, the findings of this study suggest that mid-wave infrared has the potential to retrieve leaf water content.

5.1 Introduction

Leaf water content is a fundamental constituent of plant leaves, being a vital indicator of plant health, physiological condition as well as an important regulator in sustaining plant growth and development. Leaf water content is an important factor for maintaining leaf structure and shape, photosynthesis and thermal regulation. The spatial and temporal variability of vegetation water is essential for monitoring of drought risk, predicting wildfire and estimating crop yield (Bauer et al. 1986; Peñuelas et al. 1993; Peñuelas et al. 1997; Jones and Tardieu 1998; Datt 1999; Harry 2006).

Although the traditional method of measuring leaf water content in the field is reliable, it is time consuming, expensive and lacks continuous spatial coverage. Remote sensing is an effective alternative to field sampling being non-destructive and providing continuous spatial coverage over a large area (Bauer et al. 1986; Hunt et al. 1987; Hunt and Rock 1989; Peñuelas et al. 1993; Peñuelas et al. 1997; Sepulcre-Cantó et al. 2006).

Leaf water content has been widely retrieved using spectral data collected in the visible, near infrared and shortwave infrared (VNIR and SWIR) (Hunt et al. 1987; Hunt and Rock 1989; Danson et al. 1992; Peñuelas et al. 1993; Aldakheel and Danson 1997; Peñuelas et al. 1997; Ceccato et al. 2001; Ceccato et al. 2002a; Ceccato et al. 2002b; Zygielbaum et al. 2009; Cheng et al. 2011). In the VNIR and SWIR, the strong water absorption wavebands are located at 1.45 μm, 1.90 μm, 2.10 μm and overtones are positioned at 0.75 μm and 1.20 μm (Datt 1999). Based on the water absorption wavebands, different band ratio indices such as the water index (WI; Peñuelas et al. 1997) and normalized difference water index (NDWI; Gao 1996) have been developed and used for the retrieval of leaf water content in VNIR-SWIR (Hunt et al. 1987; Gao 1996; Peñuelas et al. 1997; Ceccato et al. 2001; Ceccato et al. 2002a; Ceccato et al. 2002b). The existing research in the visible to short wave infrared reported that as the leaf water content increases the water retrieval indices tend to saturate, thereby reducing the accuracy of estimating leaf water content (Datt 1999; Ceccato et al. 2001; Cheng et al. 2011).

In contrast, little attention has been paid to the mid-wave infrared (2.5 – 6 μm) domain due to a number of challenges such as a lack of equipment (i.e. a spectroradiometer sensitive to the mid-wave infrared), a low signal to noise ratio, and the overlap between reflected and emitted radiation from the surface (Ribeiro da Luz 2006; Ribeiro da Luz and Crowley 2007; Gerber et al. 2011). However, recent technical advances in the mid-wave infrared hyperspectral sensors have demonstrated its potential for environmental modeling and characterizing the vegetation which covers 65 % of the

terrestrial surface (Boyd and Petitcolin 2004; Ribeiro da Luz 2006; Ribeiro da Luz and Crowley 2007, 2010; Fabre et al. 2011; Gerber et al. 2011; Ullah et al. 2012b). More recently, Gerber et al. (2011) and Fabre et al. (2011) noticed considerable variation in the spectral response within the mid-wave infrared (2.5 – 6 µm) as leaves dry, suggesting that this region may be used for accurately quantifying leaf water content. The fundamental water absorption features in the mid-wave infrared exhibited very high specific absorption coefficients compared with the VNIR–SWIR and showed strong absorption features at 2.90, 4.65, and 6.08 µm (Wieliczka et al. 1989; Fabre et al. 2011; Gerber et al. 2011) suggesting the mid-wave infrared domain may potentially be viable for monitoring leaf water status. Here we propose three narrow band mid-wave infrared indices; Mid-wave infrared Normalized Difference Water Index (MNDWI), Mid-wave infrared Simple Ratio Water Index (MSRWI) and Mid-wave infrared Simple Difference Water Index (MSDWI) to accurately retrieve leaf water content.

The current study aimed to (1) investigate the variation in the laboratory-measured mid-wave infrared spectral response of dehydrating leaves from nine plant species; (2) locate the sensitive waveband combination for monitoring leaf water content; (3) model the leaf water content based on the optimal sensitive wavebands combination of the spectral indices; (4) validate the performance of the developed indices by establishing an empirical relationship between measured leaf water content (progressively drying leaf) and predicted leaf water content and (5) to evaluate the performance of the proposed indices using simulated data of the Mid-wave infrared Airborne Spectrographic Imager (MASI600).

5.2 Materials and method

5.2.1 Leaf sampling and leaf water content measurement

We collected leaves (6 or 10 leaves per species) from nine different (Table 5.1) plant species. To examine the difference in the spectral response related with different leaf water content, leaves were collected from at least three different plants of the same species. A preliminary visual inspection showed that each leaf was in good physical shape.

The leaves, attached to small twigs, were placed in moist cotton in the laboratory to avoid desiccation. Within 30 minutes, spectral measurements were made on the fresh leaves (Kumar et al. 2010). Different levels of leaf water content were achieved by successively air drying the leaves and taking measurements after every four hours. To avoid leaf rolling with dehydration, leaves were placed in cardboard plates. The leaf water content was precisely

measured before and after recording the spectra by using a digital weight balance with 100 µg accuracy. Prior to measuring the final (fully dry leaf) water content level, leaves were oven dried at 60 °C for one and a half hours.

The following equation was used to estimate the gravimetric leaf water content:

$$LWCf = 100(Mw - Md)/ Mw \quad (1)$$

where Mw represents the wet leaf weight (leaf mass at a given water content) and Md is the weight of fully dried leaf (dried in an oven for one and a half hours at last succession). LWCf represents the leaf water content relative to wet leaf weight.

Table 5.1: Nine plant species, their common name, Latin name, leaf sample size per species, number of leaf drying phases, and the sum of spectra per species measured.

Species name	Common name	Sample size	Drying phases	Spectra per species
Acer platanoides	Norway Maple	6	5	30
Cornus sericea	Redosier Dogwood	6	6	36
Fallopia japonica	Japanese Knotweed	6	5	30
Platanus orientalis	Oriental Planetree	10	6	60
Rhododendron caucasicum	Rhododendron	6	8	48
Tilia platyphyllos	Largeleaf Linden	10	6	60
Liquidambar styraciflua	Sweetgum	10	7	70
Fagus sylvatica	European Beech	6	4	24
Aesculus hippocastanum	Horse-Chestnut	6	6	36
	Calibration Dataset = 262		Validation dataset =132	Total = 394

5.2.2 Spectral reflectance measurements

The Directional Hemispherical Reflectance (DHR) spectrum of the adaxial (upper) surface of each leaf was acquired using a Bruker VERTEX 70 FTIR (Fourier transform infrared; Bruker Optics GmbH, Ettlingen, Germany) spectrometer (Ullah et al. 2012b). The spectrometer was continuously purged of water vapour and carbon dioxide using nitrogen (N2) gas (Hecker et al. 2011). Each leaf measurement was referenced against a calibration measurement of gold plate (infragold; Labsphere reflectance technology) with high reflectance (approximately 0.96). The Directional Hemispherical Reflectance (DHR) spectra of the plant leaves were measured between 2.5 and 14 µm, with a spectral resolution of 4 cm-1. To absorb transmitted

radiance and to minimize transparency features in the 3.5 to 5.7 µm range, leaf samples were placed on a black surface (Gerber et al. 2011). Leaves with different water contents (resulted from progressive drying) were subjected to DHR spectral measurements. The spectral measurement per species varied from 24 to 70 (Table 5.1), depending on the speed of desiccation and the number of leaves (per species) chosen at the preliminary stage. A total of 394 spectra were measured (Table 5.1). For calibration purpose, two thirds (n = 262 spectra) of the total data were used while the remaining one thirds (n = 132 spectra) were used for validation purposes.

5.2.3 Simulation at Mid-wave infrared Airborne Spectrographic Imager (MASI600)

To test the potential of the proposed indices at airborne level, the laboratory spectra were simulated as Mid-wave infrared Airborne Spectrographic Imager (MASI600). The MASI600 is a pushbroom hyperspectral sensor operating in the mid-wave infrared (3 – 5 µm), having 64 continuous spectral bands with a spectral resolution (FWHM) of 32 nm. The MASI600 can acquire data at a maximum altitude of 3048m (above sea level). The spatial resolution varies between 1m and 3.5m (depend on the altitude of the platform) with a spatial coverage of 600 pixels.

5.2.4 The proposed mid-wave infrared indices

In contrast to the VNIR- SWIR (0. 40– 2.50 µm), the fundamental vibration molecules of water exhibited a strong specific absorption coefficients (Figure 5.1) in the mid-wave infrared at 2.90, 4.65, and 6.08 µm (Wieliczka et al. 1989; Fabre et al. 2011; Gerber et al. 2011). Recent investigation of leaf hyperspectral spectra in the mid-wave infrared has revealed that spectral features related to water markedly fluctuate with varying leaf water content (Fabre et al. 2011; Gerber et al. 2011). In the mid-wave infrared, weak spectral features are related to other leaf biochemicals such as lignin and cellulose (Ribeiro da Luz 2006; Ribeiro da Luz and Crowley 2007, 2010; Ullah et al. 2012b). These variations in the mid-wave infrared spectra with different leaf water contents, suggest a potentially suitable domain for developing spectral indices and monitoring leaf water status.

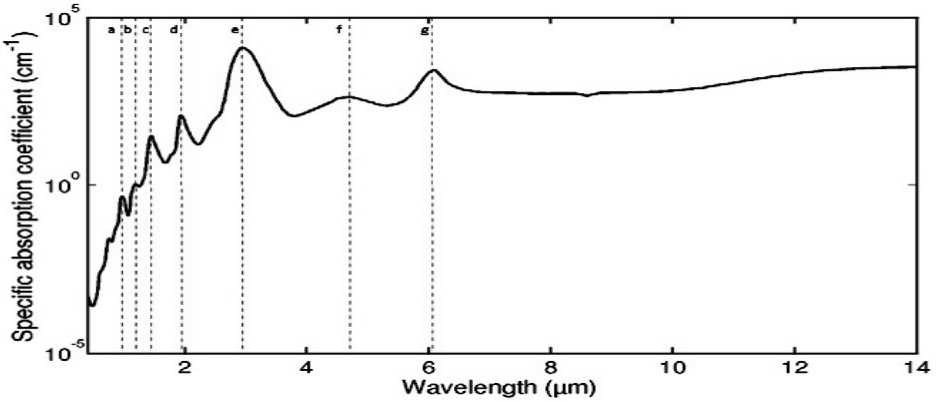

Figure 5.1: Specific absorption coefficients of water reported by Wieliczka et al. (1989). There are strong absorption features at 2.90 μm (line "e"), 4.65 μm (line "f") and 6.08 μm (line "g").

To quantify the variations in the mid-wave infrared spectral responses of dehydrating leaves, three newly proposed narrow band indices were used. These indices were named the Mid-wave infrared Normalized Difference Water Index (MNDWI), the Mid-wave infrared Simple Ratio Water Index (MSRWI) and the Mid-wave infrared Simple Difference Water Index (MSDWI). The detailed name, abbreviation and formula for these indices are summarized in Table 5.2. For each spectral index, all possible two-waveband combinations were calculated. The mid-wave infrared spectra were composed of 2420 wavebands; thus a total of 5856400 (2420 x 2420) combinations were evaluated for the retrieval of leaf water content.

Table 5.2: The summary of the proposed spectral indices (name, abbreviation and formulas) investigated in this study.

Name	Abbreviation	Equation
Mid-wave infrared Normalized Difference Water Index	MNDWI	$(R_{\lambda1}-R_{\lambda2})/(R_{\lambda1}+R_{\lambda2})$
Mid-wave infrared Simple Ratio Water Index	MSRWI	$R_{\lambda1}/ R_{\lambda2}$
Mid-wave infrared Simple Difference Water Index	MSDWI	$R_{\lambda1}-R_{\lambda2}$
where $R_{\lambda1}$ and $R_{\lambda2}$ are the reflectance values at two different wavebands		

5.2.5 Statistical analysis

To determine the best band combination for estimating leaf water content from the proposed indices, a simple linear regression was used to establish a relationship between an index values (calculated for all possible band combinations) and leaf water content using calibration dataset. The coefficient of determination R2 was used to evaluate the strength of the relation between proposed indices and leaf water content. To visualize the highest accuracy band combinations, R2 values were plotted in coloured

contour maps. For each index, the most sensitive waveband regions containing the 100 highest R2 were identified, and marked with small rectangle on the contour map. The regression models of the most sensitive waveband combinations were then used to predict the leaf water content of an independent testing dataset. The accuracy of predicting leaf water content was assessed using R2 and RMSE.

5.3 Results

5.3.1 Variation in the DHR spectra with leaf water content

The descriptive statistics of calibration subset shown that leaf water content ranges between 0.0% (completely dried) and 69.2% with an average of 27.7% and standard deviation of 23.3%. The coefficient of variation (0.84) indicated a high variability in the calibration data (Table 5.3). The validation subset varied between 0.0% and 69.7% and the coefficient of variation (0.80) shows a high variability in the testing data (Table 5.3).

Table 5.3: Descriptive statistics of measured leaf water content (LWC_f).The sample size, minimum, maximum, mean, standard deviation and coefficient of variation (CV) of the calibration and validation datasets are listed.

Data type	Sample size	Min LWC_f (%)	Max LWC_f (%)	Mean LWC_f (%)	StDev LWC_f (%)	Coefficient of Variation (CV)
Calibration	262	0.0	69.2	27.7	23.3	0.84
Validation	132	0.0	69.7	28.7	23.1	0.80

In the mid-wave infrared, fresh leaves exhibited the lowest reflectance (Figure 5.2), with the reflectance increasing as leaf water content decreased. In the mid-wave infrared, the variation in reflectance was more noticeable between 2.50 – 3.00 μm (reflectance reached a maximum of 30%) and 3.50 – 5.80 μm (reflectance reached a maximum of 16%). The spectral absorption bands at 3.05 μm and 4.65 μm are associated with water in the leaf (Ribeiro da Luz 2006; Fabre et al. 2011). The water absorption features at 4.65 μm became weaker, as the leaf water content declined, while the lignin and cellulose maxima at 4.00 μm and 5.52 μm became conspicuous (Fabre et al. 2011).

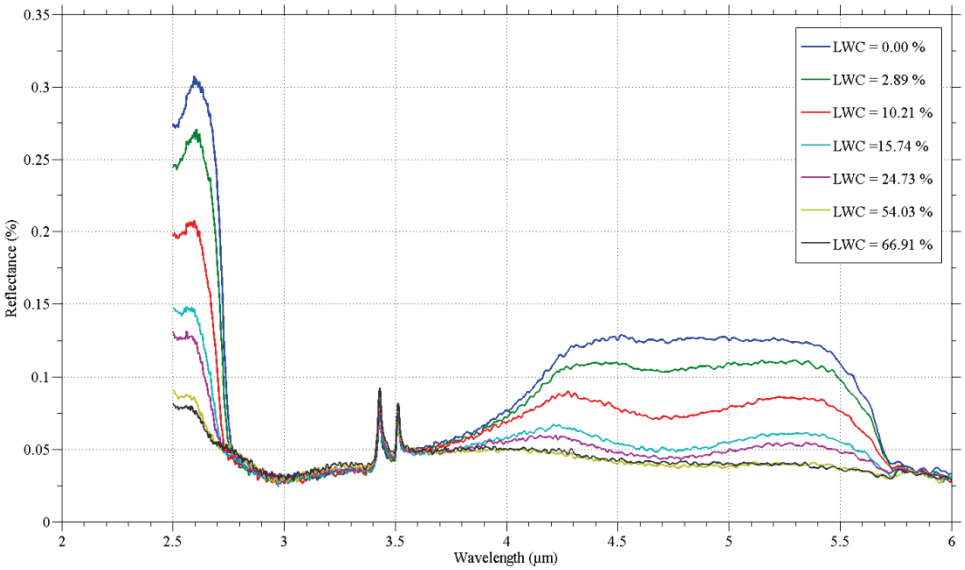

Figure 5.2: The mid-wave infrared DHR spectra of the *Liquidambar styraciflua* leaves with varying water contents. The reflectance markedly increases between 2.5 – 3.00 µm and 3.50 – 5.80 µm as the leaf water content decreases.

The leaf water content was negatively correlated to the spectral response across the entire mid-wave infrared (Figure 5.3). The correlation coefficients increased sharply between 2.6 and 2.8 µm and became flatter (plateau-like) at 2.9 µm. As the wavelength then increased, the coefficient decreased slowly up to around 3.4 µm. The two peaks at 3.43 and 3.51 µm are the Christiansen features related to the Reststrahlen bands of the very strong and consistent CH2 features mostly present in all plants (Ribeiro da Luz, 2006). The coefficients steeply decreased between 3.52 µm and 4.20 µm, with increasing wavelength. Between 4.30 µm and 5.50 µm, the coefficients varied only slightly; after 5.60 µm the correlation coefficients began to increase rapidly up to 5.80 µm.

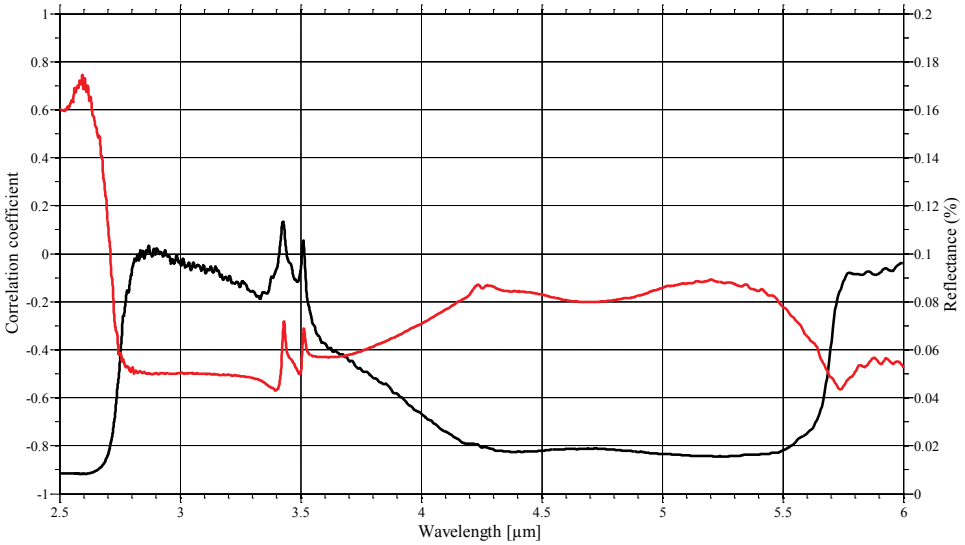

Figure 5.3: The correlation coefficients (black line) of leaf water content to the spectral response in the mid-wave infrared. The average DHR spectrum (red line) indicates typical vegetation reflectance features in the mid-wave infrared.

5.3.2 Relationship between leaf water content and spectral indices (MNDWI, MSRWI and MSDWI)

The coefficient of determination (R2) between leaf water content and the indices (MNDWI, MSRWI and MSDWI) showed wide variation with different two bands combination (Figure 5.4). For all designated indices, certain waveband combinations (λ1, λ2) appeared highly sensitive to leaf water content. The most sensitive wavebands combination for the MNDWI resulted in the highest R2 (0.91) compared to MSRWI (0.88) and MSDWI (0.88). The range of highest 100 R2 values (Table 5.4 and Figure 5.5) showed MNDWI was the most sensitive index in a linear relationship with leaf water content compared to MSRWI and MSDWI.

The most sensitive waveband regions (i.e. wavebands combination based on the highest 100 R2 values) were different for different indices (the blue rectangle in Figure 5.4). The range of the highest 100 waveband combinations of MNDWI, MSRWI and MSDWI are detailed in Table 5.4.

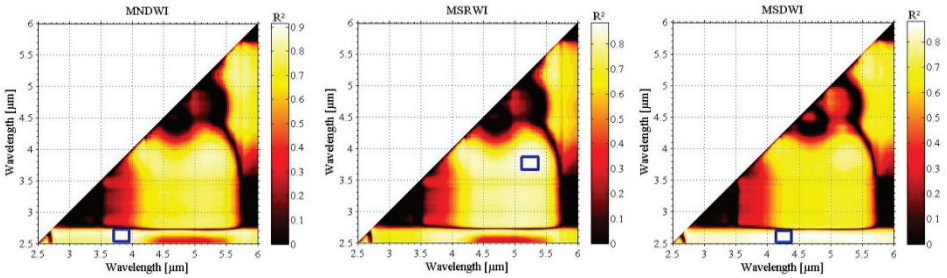

Figure 5.4: The contour map highlighting the relationship (R^2) between leaf water content and different indices calculated from all possible waveband combinations from 2.50– 6.00 μm. The sensitivity of different waveband combination is different. The blue rectangles represent the 100 waveband regions with the highest R^2.

Table 5.4: The sensitive wavebands ranges for different indices, the highest R^2 value, and regression equations as calculated using the calibration datasets. The validation RMSE and R^2 are displayed in the last two columns.

Index	Bands pair ranges		Calibration	Validation	
	λ1(μm)	λ2(μm)	R^2*	R^2	RMSE (%)
MNDWI	2.638–2.650	3.886– 3.948	0.91	0.89	7.65
SRDWI	3.814–3.900	5.150– 5.268	0.88	0.85	8.85
MSDWI	2.588– 2.593	4.220– 4.272	0.88	0.86	8.66
R^2* is the coefficient of determination resulting from the waveband combination with highest R^2 value.					

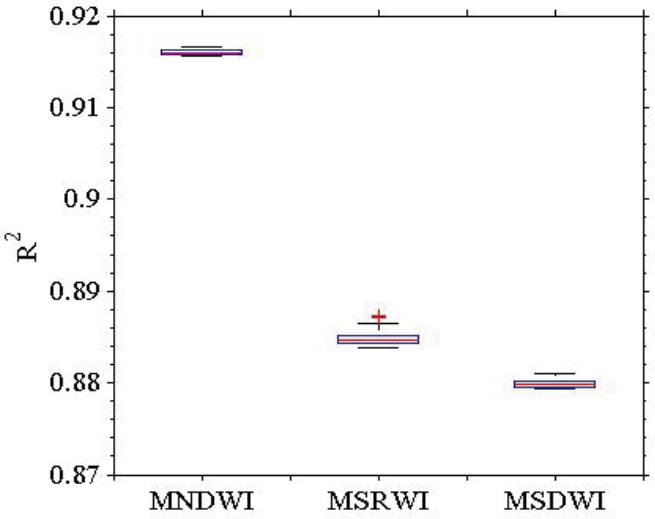

Figure 5.5: Boxplots represent the spread of R^2 of the 100 most sensitive waveband combinations for the three indices using calibration dataset. The MNDWI ranked with the highest average R^2 values followed by MSRWI and MSDWI.

5.3.3 Validation

The models resulting from the most sensitive wavebands pair (each of the three indices) using the calibration dataset were subsequently applied to a validation dataset. Among spectral indices, the leaf water content was estimated with the highest accuracy using MNDWI (R2 = 0.89, RMSE = 7.65%) compared to MSDWI (R2 = 0.86, RMSE = 8.66%) and MSRWI (R2 = 0.85, RMSE = 8.85%) (Table 5.4, Figure 5.6). The validation results (Figure 5.6) show that data points of the measured and predicted leaf water content (LWCf) are dispersed close to the 1:1 line, highlighting the reliable performance of these narrow spectral band indices.

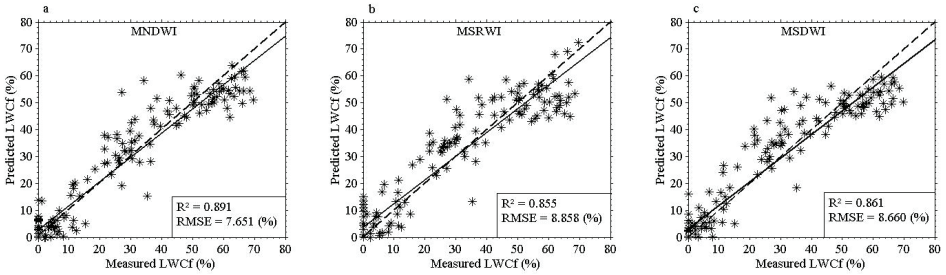

Figure 5.6: The relationship between measured and predicted leaf water content (LWC_f (%) based on the model developed from MNDWI, MSRWI and MSDWI; the highest correlation shown produced using MNDWI.

5.3.4 The simulation (MASI600) outcome

The leaf water content as predicted from simulated MASI600 spectra using MNDWI, MSRWI and MSDWI is shown in Figure 5.7. There is a wide variation in the coefficient of determination (R2) among the indices, with MSRWI predicting leaf water content with the highest accuracy (R2 = 0.83, RMSE = 9.31 %), compared with MNDWI (R2 = 0.80, RMSE = 10.15 %) and MSDWI (R2 = 0.74, RMSE = 11.74%). The most sensitive waveband combinations (i.e. waveband combinations resulting in the highest R2) were similar for MSRWI and MNDWI indices (Table 5.5).

Table 5.5: The sensitive waveband combinations of MASI600 for different indices, the R^2 value, and regression equations as calculated using the calibration datasets. The validation R^2 and RMSE are displayed in the last two columns.

Indices	Calibration				Validation	
	λ1(μm)	λ2(μm)	R^2	Regression Eq	R^2	RMSE (%)
MNDWI	3.771	5.000	0.83	y = 138.12x + 45.935	0.80	10.15
MSRWI	3.771	5.000	0.86	y = 91.403x - 45.329	0.83	9.31
MSDWI	3.992	4.180	0.76	y = 1582.8x + 45.228	0.74	11.74

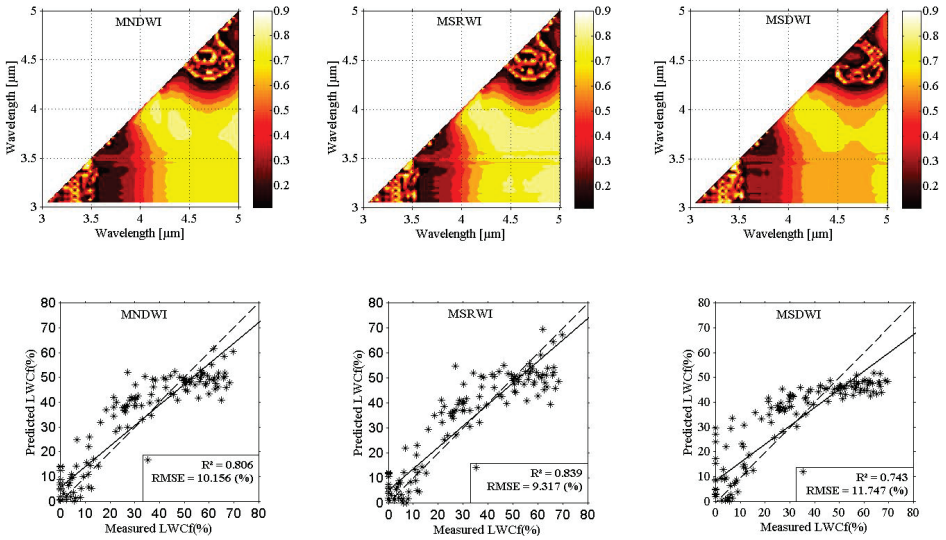

Figure 5.7: The relationship between leaf water content and the three proposed indices calculated from the spectra simulated at MASI600. The top row plots represent the results of the calibration dataset and the bottom row plots show the accuracy based on validation dataset.

5.4 Discussion

Leaf water content has been widely estimated using the visible and shortwave infrared with varying degree of success, while the mid-wave infrared has been ignored. This study quantifies and accurately estimates leaf water content for the first time from mid-wave infrared spectra (2.5 – 6 µm) using narrow band indices. Our results complement knowledge from the visible to short wave infrared (0.4 – 2.5 µm) domain that leaf water content relates to remotely sensed spectra (Hunt et al. 1987; Hunt and Rock 1989; Danson et al. 1992; Aldakheel and Danson 1997; Datt 1999; Ceccato et al. 2001; Ceccato et al. 2002a; Danson and Bowyer 2004; Claudio et al. 2006b; Colombo et al. 2008; Zygielbaum et al. 2009; Cheng et al. 2011). In this study using mid-wave infrared spectra, a strong relationship was found between leaf water content and the proposed indices. Existing research in the visible to short wave infrared reported that as the leaf water content increases, the water retrieval indices saturate and show an asymptomatic trend above approximately 40% leaf water content (Datt 1999; Ceccato et al. 2001; Cheng et al. 2011). This asymptotic behaviour reduced the accuracy of estimating leaf water content in the visible to short wave infrared. In the current study using narrow band indices developed from the mid-wave infrared, a subtle saturation effect was observed at higher leaf water content and the asymptomatic trend begins above 60% leaf water content. At this stage, it is very difficult to infer the superiority of any spectral region (visible to shortwave infrared or mid-wave infrared) for the retrieval of leaf water content and will require future work. The simultaneous spectral

measurements in the visible to shortwave infrared (0.4 -2.5 µm) and mid-wave infrared (2.5-6.0 µm) of leaves with varying leaf water content, will help to assess the strength of spectral domain for the retrieval of leaf water content.

The spectral reflectance in the mid-wave infrared increased as leaf water content decreased (Figure 5.2). The results of this study agrees with the finding of Fabre et al. (2011) and Gerber et al. (2011), where spectral variation is dominant in the mid-wave infrared with changing leaf water content. The correlation coefficient plot (Figure 5.3) indicates that there is considerable variation in the correlation coefficient across the entire mid-wave infrared and certain wavebands were more sensitive to the fluctuation in leaf water content. This was further confirmed by the colour contour map (Figure 5.4) of different narrow band combination showing wide range variation in R2 value. This strong correlation could be attributed to the presence of intense water absorption wavebands (Fabre et al. 2011; Gerber et al. 2011).

The indices used in this study showed an excellent capacity to retrieve leaf water content from the mid-wave infrared. The high R2 and low RMSE (Figure 5.6) highlights the importance of selected wavebands for the estimation of leaf water content. The selected optimal wavebands of the indices belong to the strong water absorption features, and exhibit high variation in reflectance with varying leaf water content (Ribeiro da Luz 2006; Fabre et al. 2011; Gerber et al. 2011).

The MNDWI performed more accurately (R2 = 0.89, RMSE=7.65%) compared to MSRWI and MSDWI. The average of the highest 100 R2 value (Figure 5.5) indicates that MNDWI showed high correlation with leaf water content from mid-wave infrared. Leaf water content was accurately retrieved regardless the influence of differences in leaf structure from various plant species. The correlation plot (which resulted from the relationship between water indices and leaf water content of several samples) assisted the selection of wavebands most sensitive to the variation in leaf water content.

The simulation result of the current study suggests that the selected wavebands could predict leaf water content from airborne sensor operating in the mid-wave infrared. However, several challenges associated with field conditions such as distance between target and sensor, spatial and spectral resolution, canopy structure, atmospheric condition, and seasonal variation may affect the up-scaling to canopy level.

5.5 Conclusion

This study tested three narrow band indices for the retrieval of leaf water content from mid-wave infrared domain. Based on the results, it is concluded that mid-wave infrared spectra contain sufficient information to accurately estimate leaf water content, and certain wavebands (2.588– 2.650 μm, 3.814– 3.900 μm, 4.220– 4.272 μm and 5.150– 5.268 μm) are highly correlated with leaf water content. The MNDWI yielded the highest accuracy when estimating leaf water content compared to MSRWI and MSDWI, suggesting that MNDWI is suitable for estimating leaf water content. It is recommended to explore the utility of this work at airborne and space-borne levels.

Chapter 6

Retrieval of leaf water content spanning the Visible to Thermal infrared spectra[5]

[5] This chapter is based on:
Ullah, S., Skidmore, A.K., Ramoelo, A., & Groen, T.A. (In review). Retrieval of leaf water content spanning the Visible to Thermal infrared spectra. *Remote Sensing of Environment*

Abstract

The objective of this study was to investigate the entire spectra (from visible to the thermal infrared; 0.390 µm -14.0 µm) to retrieve leaf water content in a consistent manner. Narrow-band spectral indices (calculated from all possible two band combinations) and a partial least square regression (PLSR) were used to assess the strength of each spectral region. The coefficient of determination (R^2) and root mean square error (RMSE) were used to report the prediction accuracy of spectral indices and PLSR models. In the visible-near infrared and shortwave infrared (VNIR-SWIR), the most accurate spectral index yielded R^2 of 0.89 and RMSE of 7.60%, whereas in the mid infrared (MIR) the highest R^2 was 0.93 and RMSE of 5.97%. Leaf water content was poorly predicted using two-band indices developed from the thermal infrared (R^2=0.33). The most accurate PLSR model resulted from MIR reflectance spectra (R^2=0.96, RMSE=4.74% and RMSECV=6.17%) followed by VNIR-SWIR reflectance spectra (R^2=0.91, RMSE=6.90% and $RMSE_{CV}$=7.32%). Using thermal infrared (TIR) spectra, the PLSR model yielded a moderate retrieval accuracy (R^2=0.67, RMSE=13.27% and $RMSE_{CV}$=16.39%). This study demonstrated that the MIR and SWIR domains were the most sensitive spectral region for the retrieval of leaf water content.

6.1 Introduction

An accurate estimation of leaf water content permits for example monitoring plant physiological status (Datt 1999), predicting drought risk (Bauer et al. 1986), precision agriculture (Peñuelas et al. 1993; Peñuelas et al. 1997) and assessing the risk of forest fire (Chuvieco et al. 2002). Remote sensing is a promising tool for assessing vegetation water status due to its capability of providing continuous spatial observations over large areas compared to point based measurements in the field (Hunt et al. 1987; Hunt and Rock 1989; Sepulcre-Cantó et al. 2006).

Retrieving leaf water content using remote sensing data, has been widely investigated in the visible near infrared (VNIR) and shortwave infrared (SWIR) spectra (Thomas et al. 1971; Danson et al. 1992; Aldakheel and Danson 1997; Ceccato et al. 2001; Cheng et al. 2011). Water molecules in leaves strongly absorb electromagnetic energy in the NIR (0.70 – 1.00 µm) and SWIR (1.40 – 1.90 µm) (Thomas et al. 1971; Datt 1999). The estimation of leaf water content using NIR is less effective, and the spectral response is less sensitive with changing leaf water content, compared to the SWIR (Datt 1999). Other studies found that leaf water content is strongly correlated with reflectance and derivative spectra at wavebands between 1.40 – 1.90 µm while wavebands between 1.90 – 25 µm are relatively less sensitive to the variation in leaf water content (Danson et al. 1992; Ceccato et al. 2001; Ceccato et al. 2002b; Champagne et al. 2003). The wavebands between 1.40 – 1.90 µm contain water absorption features and are strongly related to leaf water content (Hunt et al. 1987; Bowman 1989).

Very few studies attempted to estimate leaf water content using the MIR and TIR spectra. However, there are strong specific water absorption features located in the MIR (at 2.90, 4.65, and 6.08 µm) which may potentially be a suitable region for quantifying leaf water status (Wieliczka et al. 1989). Using visible to MIR (0.4 – 5.7 µm), Gerber et al. (2011) recently modelled the Directional Hemispherical Reflectance (DHR) and transmittance spectra of fresh and completely dried leaves. Using two different (independent) datasets, they noticed considerable variation with changing leaf water content in the MIR domain (Gerber et al. 2011). More recently, Fabre et al. (2011) studied the effect of leaf water content on spectral reflectance in the MIR to TIR (3.0–15.0 µm). The variation in spectral response of the three plant species used was more pronounced in the MIR compared to the TIR (Fabre et al. 2011). The variation in MIR spectra with varying leaf water content was quantified and resulted in a high correlation with leaf water content. This strong correlation led to the successful estimation of leaf water content from MIR spectra using various spectral transformation techniques (Ullah et al. 2012c; Ullah et al. 2013).

The above studies either used VNIR– SWIR or MIR and TIR but they did not sample the same target for the entire range from visible to thermal infrared to guarantee consistency in measurement. In the current study, we report on research where the same leaf samples were measured simultaneously across the visible to thermal infrared. Moreover, the intermediate water levels were acquired by successively dehydrating leaves. The main objective of this study was to assess the strength of the entire spectra (from visible to thermal infrared) for the estimation of leaf water content. The reflectance and first derivative spectra in the visible to thermal infrared domain were assessed using various water stress indices (e.g. by establishing univariate regression) and partial least square regression (PLSR; a type of multivariate regression analysis).

6.2 Material and Methods

6.2.1 Leaf sampling and measurements of leaf water content

Leaves (six samples per species) were collected from various plant species (Table 6.1) in the vicinity of the ITC building (in Enschede, the Netherlands) during July and August 2012. Before the first spectral measurements, leaves attached to small twigs, were keep moist in cotton to avoid desiccation (Kumar et al. 2010). The leaves were then progressively dehydrated at room temperature and measurements were taken after every four hours. Before the final reading, leaves were oven dried at 60 °C for one and a half hour. The leaves mass were precisely measured using a digital weight balance with 100 µg accuracy.

The leaf water content (LWCf) was calculated using the following formula (Ullah et al. 2013);

$$LWCf = 100(Mw - Md)/ Mw \quad (1)$$

where Mw represents the mass of the wet leaf and Md is the mass of completely dried leaf (dried in oven for 90 minutes at last succession). LWCf is the leaf water content relative to wet leaf weight.

We sampled 402 measurements from eleven different plant species. The number of leaves sampled per species and the dehydration phases are detailed in Table 6.1.

Table 6.1: Eleven plant species, their common name, Latin name, leaf sample size per species, successive drying phases, and the total number of spectra measured.

Common name	Species name	Sample size	Progressive drying phases	Total spectra
Maidenhair tree	*Ginkgo biloba*	6	6	36
English ivy	*Hedera helix*	6	8	48
Norway Maple	*Acer platanoides*	6	5	30
Redosier Dogwood	*Cornus sericea*	6	6	36
Japanese Knotweed	*Fallopia japonica*	6	5	30
Oriental Planetree	*Platanus orientalis*	6	6	36
Rhododendron	*Rhododendron caucasicum*	6	8	48
Largeleaf Linden	*Tilia platyphyllos*	6	6	36
Sweetgum	*Liquidambar styraciflua*	6	7	42
European Beech	*Fagus sylvatica*	6	4	24
Horse-Chestnut	*Aesculus hippocastanum*	6	6	36
	Calibration Dataset = 268		Validation dataset =134	Total= 402

6.2.2 Spectral measurements

The spectral measurements were recorded between 0.390 and 14.0 μm. To cover the entire spectral range (visible, NIR, SWIR, MIR and TIR); two different spectrometers were used for the measurements. The ASD FieldSpec® spectro-radiometer (Analytical Spectral Devices: Boulder, CO, USA) covered the VNIR-SWIR range (0.390–2.50 μm), whereas a Bruker VERTEX 70 FTIR (Fourier transform infrared; Bruker Optics GmbH, Ettlingen, Germany) spectrometer was used to acquire Directional Hemispherical Reflectance (DHR) between 2.50 –14.0 um. During spectral measurements of the leaf samples, the ASD and Bruker spectro-radiometers were used in random order to minimize the influence of different spectral instruments.

An ASD spectrometer, coupled with an integrating sphere, was used to measure reflectance spectra between VNIR and SWIR (0.390–2.50 μm; comprising 2110 spectral bands). The ASD is a portable spectrometer and can acquired spectra with a sampling interval of 1 nm. Two hundred (200) scans were averaged to a single spectrum in order to minimize the effect of noise (signal variance) on the final correlation analysis (see section 6.2.5). A calibrated reference standard (with approximately 99% reflectance) was used to convert raw radiance to reflectance.

A Bruker VERTEX 70 FTIR acquired DHR spectra between 2.5 and 14.0 μm of the adaxial surface of the leaf. The spectrometer was purged of water vapour and carbon dioxide using nitrogen gas. A Mercury Cadmium Telluride (MCT) detector (cooled with liquid N2) was used to measure leaf spectra with a spectral resolution of 4-cm (Hecker et al. 2011; Ullah et al. 2012a; Zaini et al. 2012). Each spectrum was calibrated using a high reflectance (approximately 0.96) gold plate (infragold; Labsphere reflectance technology). Each spectrum was calculated from the average of 1000 scans.

6.2.3 Pre-processing of spectra and spectral transformation

The spectra were smoothed using a Savitsky–Golay filter (Savitzky and Golay 1964), with 15 sample points and second order polynomials. The smoothed spectra were then used for calculating different indices and first derivatives reflectance (FDR).

6.2.4 Narrow bands moisture stressed indices

A narrow band simple ratio, simple difference and normalized difference indices (Hunt and Rock 1989; Gao 1996; Peñuelas et al. 1997) were calculated for all band combinations using the reflectance spectra. These indices have been reported in the literature for the VNIR–SWIR (Datt 1999; Ceccato et al. 2001; Zygielbaum et al. 2009), but are hardly used in the MIR and TIR (Ullah et al. 2013). Different naming conventions are used for the indices in the VNIR-SWIR and MIR and TIR for their interpretation (see details in Table 6.2).

Narrow band vegetation indices have been successfully used to estimate vegetation parameters (Mutanga and Skidmore 2004c; Darvishzadeh et al. 2008b). The notion of calculating vegetation indices (i.e. simple ratio, normalized difference indices) are based upon the contrast in the reflectance between two spectral bands (Rouse et al. 1974). In vegetation indices, a limited number of wavebands (which contain most of the information) are used from massive hyperspectral wavebands. The purpose of using vegetation indices is to minimize the variability in reflectance caused by various factors such as illumination condition, instrument noise, atmospheric condition and soil background (van Leeuwen and Huete 1996). To determine the best narrow band index, all possible combination of two bands were calculated and a combination that has the highest R^2 with leaf water content was located (Thenkabail et al. 2000; Mutanga and Skidmore 2004c).

Table 6.2: List of spectral indices used in this study.

Name	Acronym			Equation
	VNIR-SWIR	MIR	TIR	
Normalized Difference Water Index	NDWI	MNDWI	TNDWI	$(R_{\lambda1}-R_{\lambda2})/(R_{\lambda1}+R_{\lambda2})$
Simple Ratio Water Index	SRWI	MSRWI	TSRWI	$R_{\lambda1}/ R_{\lambda2}$
Difference Water Index	DWI	MDWI	TDWI	$R_{\lambda1}-R_{\lambda2}$
where $R_{\lambda1}$ and $R_{\lambda2}$ is the reflectance at two different wavebands				

6.2.5 Statistical analysis

6.2.5.1 Simple Linear regression

Simple linear regression was used to quantify the retrieval accuracy of leaf water content using the calculated indices. The data were randomly divided in to calibration and validation subsets. The model was trained with a calibration subset (n= 268; two third of the entire dataset) and was then used to predict the leaf water content in validation subsets (n= 134; one third of the entire dataset). The predicted leaf water content was plotted against the measured leaf water content, and the accuracy of each index reported using R^2 and RMSE.

6.2.5.2 Partial least square regression (PLSR)

A challenge associated with hyperspectral data is a high spectral dimensionality and a high degree of collinearity of the adjacent bands (Vaiphasa et al. 2005). Multivariate regression models based on hyperspectral data suffers from multi-collinearity especially when the numbers of predictors are equal or higher in number than sample observations and the input data lead to a high R2 (Curran 1989b). PLSR is a robust technique which can handle high dimensional hyperspectral datasets for predicting leaf bio-chemicals, while minimizing multi-collinearity and model over-fitting (Thomas and Haaland 1990). This technique has been successfully used to estimate several leaf bio-chemicals (Huang et al. 2004b; Asner and Martin 2008; Ramoelo et al. 2011). The Partial least square regressions (PLSR) were used to estimate leaf water content from both the reflectance and FDR spectra in the VNIR-SWIR, MIR and TIR. The increased use of PLSR in remote sensing (Lin et al. 2007; Asner and Martin 2008; Darvishzadeh et al. 2008b; Ramoelo et al. 2011) is due to the fact that PLSR can process multi-collinear predictors (hyperspectral data) by inputting all spectral bands simultaneously and select uncorrelated variables from a matrix of explanatory variables (Geladi and Kowalski 1986). The PLSR analysis was implemented using the TOMCAT toolbox in MATLAB. The independent variables were first mean centered prior to input to the PLSR. The lowest RMSECV (RMSE-leave-one-out cross validation) was adopted as

criterion to select the optimal number of components for model development (Darvishzadeh et al. 2008b). The accuracy of the models using different spectral domains was assessed using R2, RMSE and RMSECV.

6.3 Results

6.3.1 Effect of leaf water content on spectral responses

The leaf water content was variably correlated with reflectance across spectral bands (Figure 6.1). The correlation was low between leaf water and the blue part of the spectrum (0.390–0.430 µm) and increased in the green and red part of the visible spectrum (0.50-0.65 µm; Figure 6.1 a). The correlation attained a maximum between 1.4 and 2.2 µm (in the SWIR). In the MIR domain, leaf water content was strongly correlated with the Directional Hemispherical Reflectance (DHR) between 2.50 and 2.70 µm, and the correlation became weaker at 2.7 to 3.6 µm. After 3.6 µm the correlation increased to a maximum between 4.0–5.6 µm (Figure 6.1 b). In the thermal infrared the correlation plot (Figure 6.1 c) exhibited a flat line.

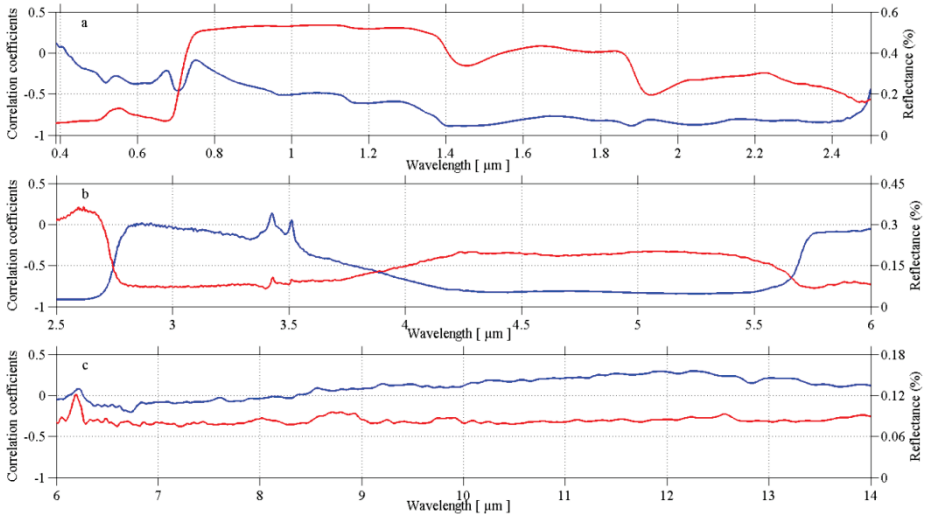

Figure 6.1: The relationship between spectral reflectance and the leaf water contents in the VNIR-SWIR (a), MIR (b) and TIR (c). The red line represents the average reflectance spectrum while the blue line is the correlation coefficient between leaf water content and spectral response.

6.3.2 Leaf water content and spectral indices

Using visible near infrared and shortwave infrared (VNIR-SWIR) spectra, the narrow-band indices (NDWI, SRWI and DWI) were calculated and leaf water content was estimated based on these indices. The indices with the most

sensitive waveband combinations yielded a high R2 (Figure 6.2) using the calibration dataset. The models derived from the calibration data were applied to the validation datasets in order to predict leaf water content. For the VNIR-SWIR domain, the prediction of leaf water content was high (R2=0.86 (minimum), RMSE=8.86% (maximum)) using the validation datasets. For all possible waveband combinations of the three indices, the most sensitive waveband combinations (with highest R2) were located in the SWIR region (i.e. the blue rectangle in Figure 6.2). For the VNIR and SWIR , the NDWI provided more accurate predictions of leaf water content compared to SRWI and DWI (Figure 6.3), though it is noted that in all three models (NDWI, SRWI and DWI) the predicted values underestimate the measured leaf water content above approximately 50% leaf water content.

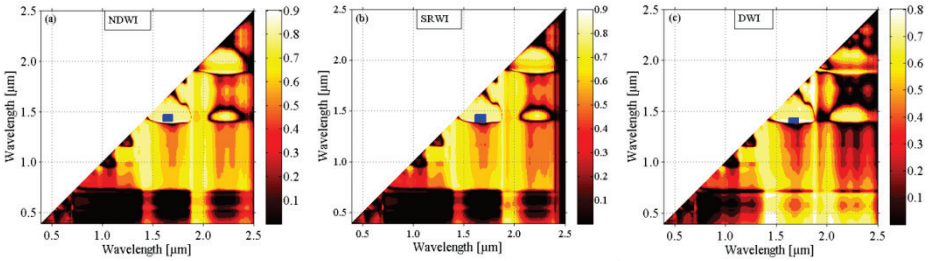

Figure 6.2: Contour map displaying the relationship (R^2) between leaf water content and different indices calculated from all possible waveband combinations from 0.390 – 2.50 μm. The blue rectangles represent the most sensitive waveband regions with the highest R^2.

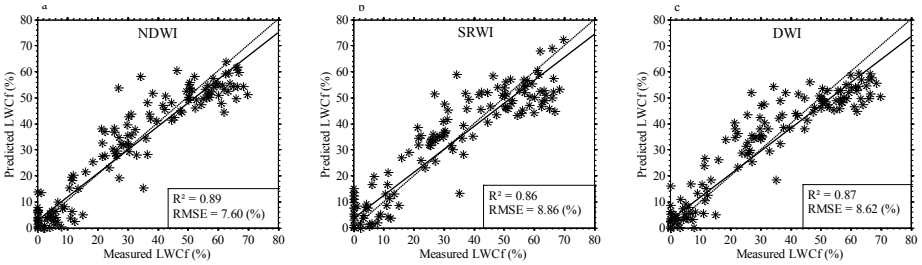

Figure 6.3: Scatterplots detailing the relationship between measured and predicted leaf water content using VNIR- SWIR. The solid line shows the regression line, while the dotted line is the 1:1 line. The NDWI performed more accurately compared to SRWI and DWI.

For the MIR, leaf water content was accurately estimated using narrow-band indices (MNDWI, MSRWI and MDWI). Using the calibration datasets, these indices yielded a high R2 (Figure 6.4). When the calibration model was applied to the independent validation datasets, leaf water content was accurately predicted (i.e. high R2 and low RMSE) (Figure 6.5 and Table 6.3). The indices developed from TIR spectra were less effective in estimating leaf water content. Using TIR, the maximum R2 achieved was 0.33 (from TNDWI)

and lead to a poor estimation (i.e. high RMSE) of leaf water content (Figure 6.6, Table 6.3).

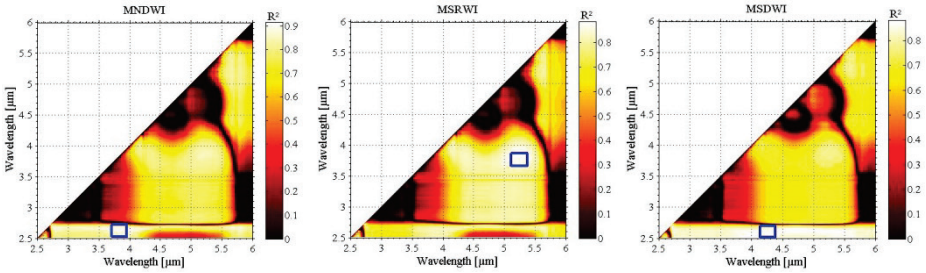

Figure 6.4: Contour map highlighting the relationship (R^2) between leaf water content and different indices calculated from all possible waveband combinations from 2.50–6.00 µm. The sensitivity of different waveband combination is different. The blue rectangles represent the most sensitive waveband regions with the highest R^2.

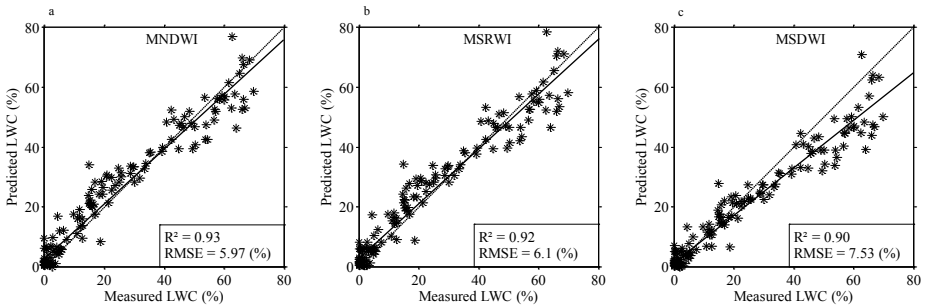

Figure 6.5: Scatterplot detailing the relation between measured and predicted leaf water content (LWC_f (%)). The predicted leaf water content is based on the calibration models developed from MNDWI, MSRWI and MSDWI; the highest correlation shown produced using MNDWI.

Table 6.3: The most sensitive wavebands for the different indices, selected on the basis of the highest R^2 values, and regression equations as calculated using the calibration datasets. The validation RMSE and R^2 are displayed in the last two columns.

Index	Most sensitive bands		Calibration		Validation	
	λ1(µm)	λ2(µm)	R^2	Regression Eq	R^2	RMSE (%)
NDWI	1.400	1.578	0.91	y=-0.002x+0.0368	0.89	7.60
SRWI	1.397	1.614	0.88	y=-0.0038x+1.0694	0.86	8.86
DWI	1.396	1.615	0.87	y=-0.0014x+0.0339	0.87	8.62
MNDWI	2.651	3.891	0.92	y = -0.0088x + 0.5562	0.93	5.97
MSRWI	3.814	5.219	0.92	y = 0.0092x + 0.5396	0.92	6.10
MDWI	2.591	4.220	0.91	y=-0.0024x+ 0.1519	0.90	7.53
TNDWI	6.730	11.310	0.34	y=-0.0032x+0.9632	0.33	31.22
TSRWI	6.730	11.310	0.33	y = -0.0019x - 0.0196	0.32	31.83
TDWI	6.730	11.460	0.34	y = -0.0002x - 0.0016	0.32	31.69

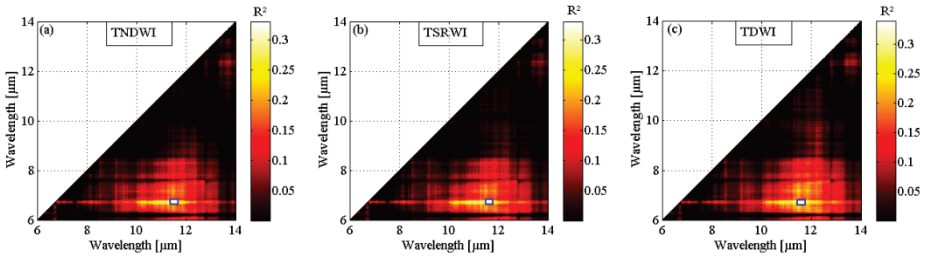

Figure 6.6: The relationships between leaf water content and narrow-band spectral indices in the TIR spectra. The rectangular region indicates the sensitive wavebands combination selected on the basis of the highest R^2 values.

6.3.3 Partial least square regression and leaf water content

Using the VNIR-SWIR reflectance spectra, the PLSR models (Figure 6.7) were slightly more accurate (R2=0.91, RMSE =6.90 % and RMSECV =7.32 %) than the PLSR models developed using the first derivative spectra (R2=0.90, RMSE =7.14% and RMSECV = 8.50%). The number of wavelength latent factors were equal (8 factors) for both the reflectance and first derivative spectra (Table 6.4).

Using reflectance and first derivative spectra in the MIR, both PLSR models yielded an accurate estimate of leaf water content (Figure 6.8). The models based on MIR reflectance spectra were more accurate (R2 =0.96, RMSE= 4.74 and RMSECV= 6.14) compared to the model developed from first derivative spectra using MIR (R2 =0.93, RMSE= 5.98 and RMSECV= 8.40). The number of factors involved in the models is detailed in Table 6.4. The PLSR models based on MIR was more accurate (i.e. high R2 and low RMSE) than the models developed using VNIR –SWIR spectra. The PLSR regression using TIR spectra, yielded the lowest R2 (0.67) and highest RMSE (13.27 %) and RMSECV (16.39) (Figure 6.9).

The PLSR models in all spectral domains (i.e. VNIR-SWIR, MIR and TIR) improved the prediction of leaf water content (i.e. results in a higher R2 and low RMSE) compared to the narrow band indices. The most significant improvement was noticed for retrieving leaf water content using the TIR reflectance, where R2 increased from 0.32 to 0.67 and RMSE decreased from 31.83% to 16.39 % (Table 6.3 and Table 6.4).

Table 6.4: The results of PLSR analysis for estimating leaf water content using the reflectance and first derivative spectra in the VNIR-SWIR, MIR and TIR.

	Spectral region	No. of factors	R^2	RMSE (%)	$RMSE_{CV}$ (%)
Reflectance spectra	VNIR-SWIR	8	0.91	6.90	7.32
	MIR	10	0.96	4.74	6.14
	TIR	9	0.67	13.27	16.39
First Derivative Spectra	VNIR-SWIR	8	0.90	7.14	8.50
	MIR	4	0.93	5.98	8.40
	TIR	4	0.63	14.21	23.95

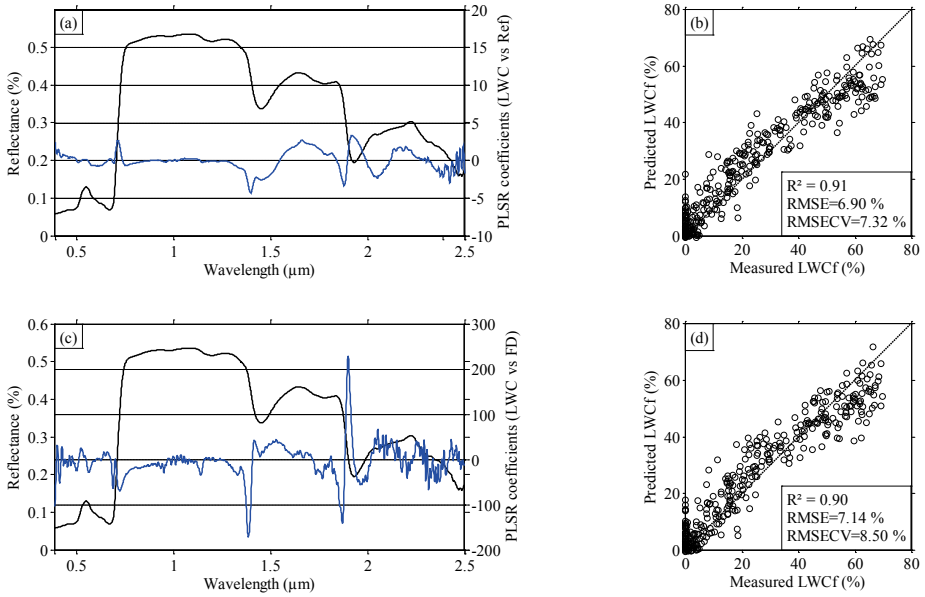

Figure 6.7: The PLSR coefficients (blue line) showing the importance of each waveband in developing the PLSR model for retrieving leaf water content from reflectance (a) and first derivative spectra (c) in the VNIR-SWIR. The average reflectance spectra (black line) are shown for reference purpose. The PLSR analysis using reflectance (b) predicted leaf water content more accurately (high R^2 and low RMSE and $RMSE_{CV}$) compared to the PLSR model developed from first derivative spectra (d).

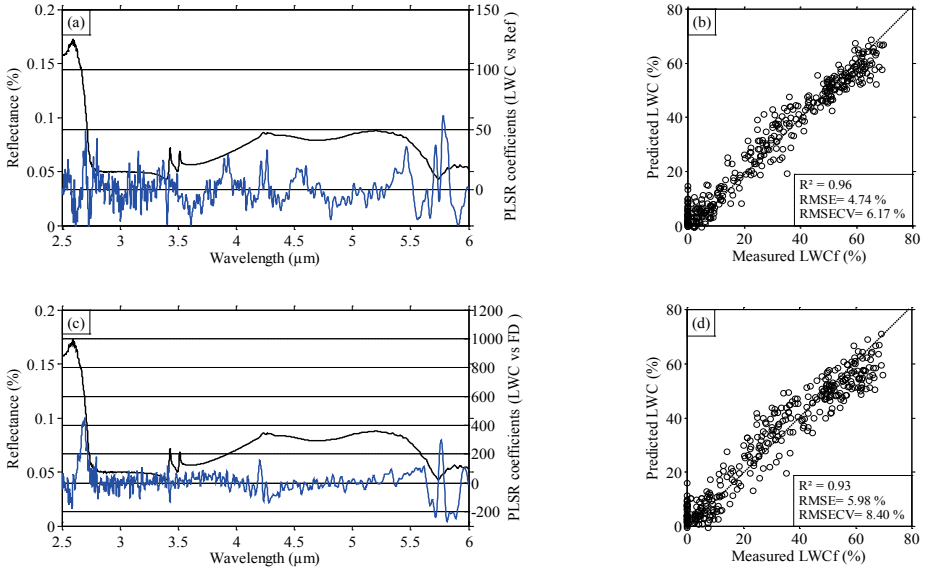

Figure 6.8: The PLSR coefficients (blue line) showing the importance of each waveband in developing the PLSR model for retrieving leaf water content from reflectance (a) and first derivative spectra (c) in the MIR. The average reflectance spectra (black line) are shown for reference purpose. The PLSR analysis using reflectance (b) predicted leaf water content more accurately (high R^2 and low RMSE and $RMSE_{CV}$) compared to the PLSR model developed from first derivative spectra (d).

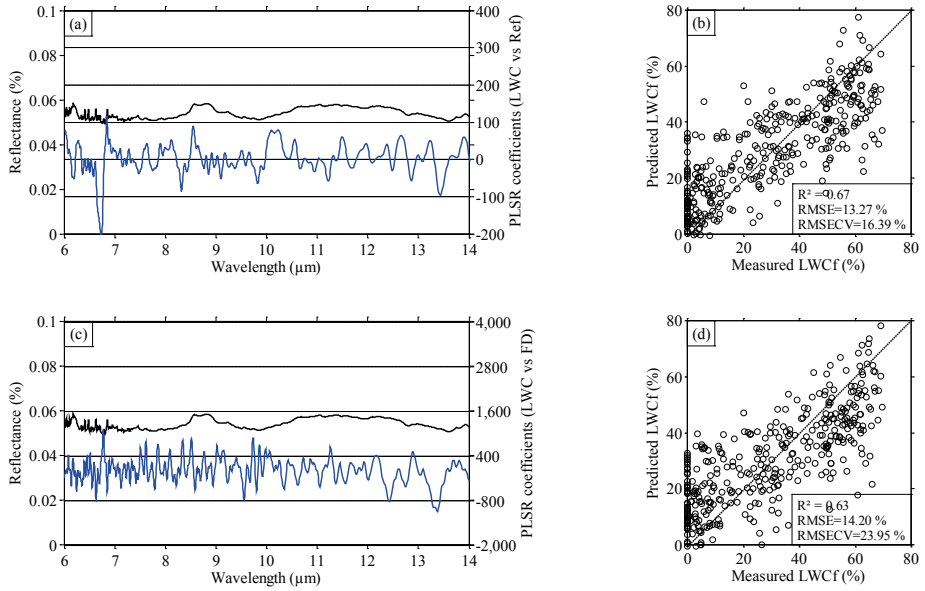

Figure 6.9: The PLSR coefficients (blue line) showing the importance of each waveband in developing the PLSR model for retrieving leaf water content from TIR reflectance spectra (a). The average TIR reflectance spectra (black line) are shown for reference purpose. The PLSR models using TIR reflectance spectra (b) and TIR first derivative spectra (d) yielded moderately accurate estimate of leaf water content.

6.4 Discussion

Remote sensing is potentially a viable tool to assess and monitor vegetation parameters from local (point sample) to global scales (Skidmore 2002). In the past, estimation of vegetation water content focused on the VNIR-SWIR (0.3-2.5 µm). The advent of sensor technology in the MIR (2.5-6.0 µm) and TIR (8.0-14.0 µm) enables the assessment and monitoring of vegetation functions or physiological status (Ribeiro da Luz 2006; Ribeiro da Luz and Crowley 2007, 2010; Ullah et al. 2012b). In this study, an empirical relationship between leaf spectra and leaf water content demonstrated that MIR and SWIR were the most sensitive spectral regions ($R^2 \geq 0.86$) for the estimation leaf water content. The TIR showed moderate affinity with leaf water content (maximum R^2 =0. 67), however the performance of TIR were less accurate compared to MIR and SWIR.

The correlation between reflectance spectra (across visible to thermal infrared) and the leaf water content (Figure 6.1) underlined that leaf water content is related to the spectral response, but the strength of the relationship varies across VNIR-SWIR/ MIR and TIR. The spectral response was strongly correlated with leaf water content (Figure 6.1) in the SWIR (1.4-2.5 µm) and MIR (2.5-2.7 µm and 3.7-5.6 µm). The findings of this study are in line with that of the previous studies where two band indices were used for the retrieval of leaf water or biochemical parameters (Hunt and Rock 1989; Gao 1996; Datt 1999; Ceccato et al. 2001; Ceccato et al. 2002a; Ceccato et al. 2002b; Zhang et al. 2012). Using narrow-band indices, the most sensitive waveband combinations were located at 1.60 µm, 1.397 µm (i.e. SWIR) and at 2.65 µm, 3.89 µm and 5.20 µm (i.e. MIR). These selected sensitive wavebands (from narrow-band indices) correspond to the slope and depth of water absorption features in the reflectance spectra (Datt 1999; Ceccato et al. 2001; Cheng et al. 2010b; Gerber et al. 2011; Ullah et al. 2012c). The selected wavebands in the SWIR (1.397 µm and 1.60 µm) are related to the absorption features associated with moisture, cellulose and starch in plant leaves (Curran 1989b; Thenkabail et al. 2004). The selected wavebands at 3.89 µm and 5.20 µm (MIR) are associated with cellulose maxima at 4.0 and 5.2 µm (Fabre et al. 2011).

The PLSR model of the MIR reflectance spectra yielded the highest accuracy (R^2= 0.96, RMSE= 4.74% and $RMSE_{CV}$= 6.14%) (Figure 6.8) compared to the VNIR-SWIR (Figure 6.7) and TIR (Figure 6.9). The PLSR models derived using first derivative spectra were less accurate than the model developed from reflectance spectra. The lower performance of the first derivative PLSR model may be due to consistent illumination conditions used in the experiment, as well as no influence of background soil/litter reflectance (Elvidge and Chen 1995b).

The PLSR model is emerging as an alternative to univariate statistical analysis for estimating leaf water content as it selects the most important variables for a parsimonious model (Lin et al. 2007; Asner and Martin 2008; Darvishzadeh et al. 2008b; Ramoelo et al. 2011) and can therefore be considered in general to be more practical for such analyses. Compared to narrow band indices, all the PLSR models in their respective spectral domains achieved relatively higher accuracy (Table 6.3 and Table 6.4). In this study, using the reflectance and first derivative spectra, the number of PLSR latent factors varied from 4 to 10 (Table 6.4).

The novelty of this study is the simultaneous and consistent sampling of the same target leaf while measuring the whole spectrum (from the visible to thermal infrared) for the retrieval of leaf water content. Integrating various imaging spectrometers data to cover the entire spectral range (i.e. visible to thermal) helps to identify the spectral bands for accurate retrieval of leaf water content at the field level and may provide a foundation for up-scaling to canopy level.

6.5 Conclusion

This study has used univariate and multivariate statistical techniques to examine the strength the VNIR-SWIR, MIR and TIR for the retrieval of leaf water content. Narrow band indices and PLSR were used in to analyze the spectral data. The strength of each model was assessed by comparing the differences in the R2 and RMSE and RMSECV. It is concluded that the PLSR models were more accurate (yielded high R2 and low RMSE) compared to narrow band indices in all spectral domains and is a practical and robust technique compared to univariate statistical analysis for estimating leaf water content. The strength of predicting leaf water content using SWIR and MIR (yielded high R2 and low RMSE) are higher than TIR. The SWIR and MIR proved highly sensitive spectral regions and hold promise for the estimation of leaf water content.

Chapter 7

Synthesis: Characterizing Vegetation Parameters Using Mid to Thermal Infrared Hyperspectral Remote Sensing

7.1 Introduction

Precise and up-to-date information on vegetation parameters is critical in various disciplines such as agriculture (e.g. modelling crop yield , productivity, irrigation scheduling; Broge and Mortensen 2002; Mkhabela et al. 2011), forestry (e.g. timber biomass, forest growth; Dong et al. 2003; Lim et al. 2003) and in ecology and range management (e.g. quality and availability of forage, species diversity; Schmidt and Skidmore 2003; Mutanga and Skidmore 2004b). Direct measurement of vegetation parameters in the field is reliable but expensive, time-consuming, labour-intensive and lacks spatial coverage. Remote sensing is an effective alternative to field sampling and is considered a practical means for quantifying vegetation parameters as it is cheap, non-destructive and can provide repetitive observation with continuous spatial coverage. However, using traditional multispectral remote sensing, the information contained in narrow spectral features is lost by averaging reflectance over wide wavebands. To overcome this limitation, the advent of hyperspectral remote sensing (in which spectra are composed of over 100 contiguous narrow-spectral-bands) has offered the possibility to accurately quantify vegetation parameters.

In the past, the use of visible near infrared and shortwave infrared (VNIR–SWIR; 0.4–2.5 μm) hyperspectral remote sensing for characterising vegetation has been wide-ranging (Curran 1989a; Asner 1998; Curran et al. 2001; Clevers et al. 2002; Banskota 2006; Cho and Skidmore 2006; Mutanga and Skidmore 2007b; Asner and Martin 2008; Blackburn and Ferwerda 2008; Schlerf et al. 2010) but the application of hyperspectral mid-wave and thermal infrared (MIR and TIR) are rare and inconclusive (Ribeiro da Luz 2006). The limited number of studies on spectral characteristics of plant leaves in the MIR and TIR may be due to the lack of equipment (i.e. a spectroradiometers sensitive to the MIR and TIR), low signal to noise ratios (SNR) and subtle and complex nature of the spectral features of vegetation (Ribeiro da Luz and Crowley 2007). However, due to significant technical advances in the MIR and TIR, this spectral domain is now covered by the latest generation of hyperspectral sensors such as Bruker FTIR spectrometer, MIDAC FTIR spectrometer, Telops Hyper-Cam, AHS, MASI600, TASI600, SEBASS (Schlerf et al. 2012). A few recent studies have used hyperspectral MIR and TIR to characterize vegetation parameters, and found that the spectral response of fresh plants is dominated by leaf epidermal materials (i.e. cell wall and cuticular membrane; Ribeiro da Luz 2006) and leaf water content (Fabre et al. 2011; Gerber et al. 2011). These studies suggest that the variation in the MIR and TIR spectral signatures related to the leaf epidermal materials of different plant species and leaf water content, can act as fingerprints for discriminating vegetation species (Ribeiro da Luz and

Crowley 2007, 2010) and potentially represent viable spectral regions for monitoring leaf water status.

This thesis investigates the potential of MIR and TIR spectra for identifying different plant species and to quantify leaf water content (which are important vegetation parameters among many others). A number of methodologies were developed to extract useful information regarding species identification and retrieving leaf water content. Exploring MIR and TIR for identifying plant species and retrieving leaf water content in itself is an innovative aspect of this thesis. Second the methodologies followed in this thesis to extract the valuable information from the MIR and TIR spectra are also rarely explored techniques. As this thesis addressed two distinct (species identification and estimation of leaf water content) problems, the reason for choosing these two parameters are discussed in subsection 7.2. We then synthesize the contributions of this work in subsections 7.3 and 7.4. The last part (subsection 7.5) of this chapter highlights the avenue for future research.

7.2 Why discerning plant species and estimating leaf water content from hyperspectral MIR – TIR

The discrimination of plant species and the estimation of leaf water content are vegetation parameters of great significance. Knowledge of plant species and their spatial distribution is necessary for sustainable management of an ecosystem and conserving biological diversity (Schmidt et al. 2004). Spatial distribution maps of vegetation species helps in biodiversity assessment, resource inventories and hold great economic values (e.g. in forestry, agriculture, medicinal plants) (Strachan et al. 2008; Cho et al. 2010; de Castro et al. 2012).

Leaf water content (second vegetation parameter covered) is a vital indicator of plant health and physiological condition (Datt 1999). Assessing the variability of vegetation water is essential for monitoring drought risk, predicting wildfire (Chuvieco et al. 2002), estimating crop yield (Peñuelas et al. 1993; Peñuelas et al. 1997) and irrigation scheduling (Bauer et al. 1986).

Plant species and leaf water content, besides their fundamental importance, are closely interlinked. Each plant species survives in an ecological niche and to cope with its environment comprises different amount of leaf water and other biochemicals. The spectral profile of plant species is affected by variation in biochemical constituents (e.g. nitrogen, lignin, cellulose, and leaf water content) and biophysical traits (e.g. leaf thickness, roughness, wax and hairs) (Curran 1989a). The primary absorption features associated with these compounds (particularly leaf water) and leaf structure (i.e. thickness, wax,

hairs) occur in the MIR and TIR domains (Ribeiro da Luz 2006; Fabre et al. 2011; Gerber et al. 2011). The variation in the MIR and TIR spectral profiles related to different plant species and leaf water content provides the opportunity to discern vegetation species (Ribeiro da Luz and Crowley 2010) and estimate leaf water content (Fabre et al. 2011).

7.3 Contribution for identifying plant species

Hyperspectral data (the spectral data composed of 100 or more contiguous narrow spectral bands) in the VNIR-SWIR have already proved that vegetation species can be identified from their spectral signature (Schmidt and Skidmore 2003; Adam and Mutanga 2009). However, the potential of MIR and TIR hyperspectral data is rarely explored and remain inconclusive for identifying plant species (Ribeiro da Luz and Crowley 2010).

The work reported in Chapter 2 & 3 on the potential of laboratory measured MIR and TIR emissivity spectra for identifying thirteen plant species. These studies found that different species have characterised spectral signatures (Figure 2.1) which are useful in the identification of plant species. The emissivity spectra (composed of 3024 spectral bands) acquired from thirteen plant species were tested for the discrimination of plant species at every spectral location using one way ANOVA (Chapter 2). The one way ANOVA coupled with Tukey HSD test identified a reduced number of wavebands that were most sensitive for the discrimination of thirteen plant species (Figure 7.1). The high value (≥ 1.94) of Jefferies Matusita (J-M) distance calculated between each pair of vegetation species confirmed that vegetation species are separable (Table 7.1) using the selected wavebands in the previous steps. The Jeffries–Matusita (J-M) distance is the average distance between two class density functions (Richards 1993; Schmidt and Skidmore 2003) and the square of the J-M distance values ranges between 0 and 2, with a larger J-M distance value indicating higher separability between group pairs (Richards 1993). In this study we used a J-M distance of ≥1.94 (≥ 97 percent of 2) as a threshold of spectral separablilty between group pairs, which is even stricter than the value of 1.90 that is commonly used in remote sensing practice (Thomas et al., 2003; ENVI software's user guide RSI Inc). As J-M distances only measures pairwise class distances, to test the discriminative power of the selected wavebands for many plant species a quadratic discriminant analysis (QDA) was used. The quadratic discriminant analysis (QDA) (Table 7.2) verified the performance of the selected wavebands for identifying multiple plants species. The primary findings of this study are: 1) vegetation species have characteristic emissivity signatures. 2) laboratory emissivity spectra of different vegetation species are statistically significantly different from other species and contain sufficient information to discriminate vegetation species at certain wavebands. 3) we now understand which part of

the electromagnetic spectrum has high potential for discriminating vegetation species and for floristic mapping. 4) this study results in a high accuracy (≥ 90 %) when classifying vegetation species.

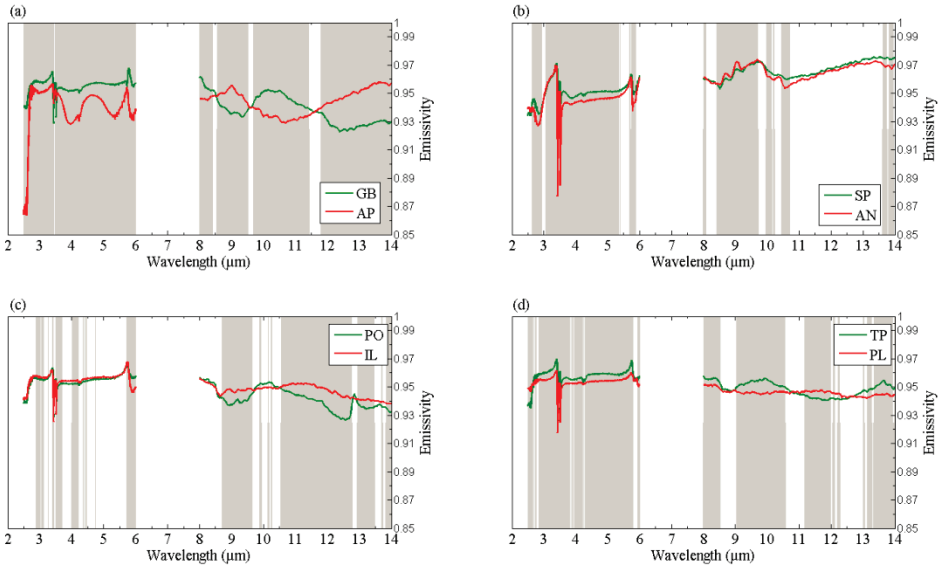

Figure 7.1: The results of a multiple comparison test for (a) *Ginkgo biloba* (GB) versus Acer platanoides (AP), (b) *Spathiphyllum cochlearispathum* (SP) versus *Asplenium nidus* (AN), (c) *Platanus orientalis* (PO) versus *Ilex opaca* (IL) and (d) *Tilia platyphyllos* (TP) versus *Prunus laurocerasus* (PL). The gray areas represent the wavebands where the species were statistically significantly different from each other. The wave wavebands 6 – 8 μm were removed from the analysis.

Table 7.1: The J-M distance between all 13 species using six bands (3.34, 4.19, 4.60, 9.44, 12.71, and 13.70 µm). The species pairs having a separability level below the defined threshold (J-M index of 1.94) are highlighted in gray.

	Acer platanoides	*Asplenium nidus*	*Cornus sericea*	*Fallopia japonica*	*Ginkgo biloba*	*Hedera helix*	*Ilex opaca*	*Liquidambar styraciflua*	*Prunus laurocerasus*	*Platanus orientalis*	*Rhododendron caucasicum*	*Spathiphyllum cochlearispathum*	*Tilia platyphyllos*
Acer platanoides	-	-	-	-	-	-	-	-	-	-	-	-	-
Asplenium nidus	2	-	-	-	-	-	-	-	-	-	-	-	-
Cornus sericea	2	2	-	-	-	-	-	-	-	-	-	-	-
Fallopia japonica	2	2	1.99	-	-	-	-	-	-	-	-	-	-
Ginkgo biloba	2	2	2	2	-	-	-	-	-	-	-	-	-
Hedera helix	2	2	2	2	2	-	-	-	-	-	-	-	-
Ilex opaca	2	2	2	2	2	2	-	-	-	-	-	-	-
Liquidambar styraciflua	2	2	2	2	2	2	2	-	-	-	-	-	-
Prunus laurocerasus	2	2	2	2	1.91	2	2	2	-	-	-	-	-
Platanus orientalis	2	2	2	2	2	2	2	2	2	-	-	-	-
Rhododendron caucasicum	2	2	2	2	2	2	2	2	2	2	-	-	-
Spathiphyllum cochlearispathum	2	2	1.99	2	2	2	2	0.92	2	2	2	-	-
Tilia platyphyllos	2	2	2	2	2	2	2	2	2	2	1.99	2	-

Table 7.2: The error matrix resulted from quadratic discriminant analysis using six bands (3.34, 4.19, 4.60, 9.44, 12.71, and 13.70 μm). The values along diagonal represent the truly classified cases.

	Acer platanoides	*Asplenium nidus*	*Cornus sericea*	*Fallopia japonica*	*Ginkgo biloba*	*Hedera helix*	*Ilex opaca*	*Liquidambar styraciflua*	*Prunus laurocerasus*	*Platanus orientalis*	*Rhododendron caucasicum*	*Spathiphyllum cochlearispathum*	*Tilia platyphyllos*	Row Total	User Accuracy
Acer platanoides	35	0	0	0	0	0	0	0	0	0	0	0	0	35	100
Asplenium nidus	0	35	0	0	0	0	0	0	0	0	0	0	0	35	100
Cornus sericea	0	0	34	1	0	0	0	0	0	0	0	0	0	35	97
Fallopia japonica	0	0	0	31	0	0	0	4	0	0	0	0	0	35	89
Ginkgo biloba	0	0	0	0	33	0	0	0	0	2	0	0	0	35	94
Hedera helix	0	0	0	0	0	31	0	0	0	0	2	0	2	35	89
Ilex opaca	0	0	0	0	0	1	30	0	4	0	0	0	0	35	86
Liquidambar styraciflua	0	0	0	0	0	0	1	31	0	0	3	0	0	35	89
Prunus laurocerasus	0	0	0	0	0	0	2	0	33	0	0	0	0	35	94
Platanus orientalis	0	0	0	0	0	0	2	0	1	32	0	0	0	35	91
Rhododendron caucasicum	0	0	0	0	0	0	0	0	0	0	34	0	1	35	97
Spathiphyllum cochlearispathum	0	0	4	0	0	0	0	0	0	0	0	31	0	35	89
Tilia platyphyllos	0	0	0	0	0	2	0	1	0	0	4	0	28	35	80
Column Total	35	35	38	32	33	34	35	36	38	34	43	31	31	455	
Producer Accuracy	100	100	89	97	100	91	86	86	87	94	79	100	90	**Total Accuracy = 92 %**	

Once the potential of MIR and TIR emissivity spectra for identifying different plant species was established in chapter 2 then in the second step (Chapter 3), an optimisation routine (i.e. genetic algorithm) coupled with spectral angle mapper (as an objective function) were combined to select wavebands containing the most relevant information for the identification of plant species. This study demonstrated the potential of genetic algorithms as band selectors using high resolution mid to thermal infrared emissivity spectra to differentiate between vegetation species at laboratory level. Based on the results obtained, it is concluded that the bands selected (detailed given in chapter 3) by genetic algorithms were more useful for discriminating vegetation species than randomly selected bands, when using laboratory emissivity spectra.

The selected bands in both these studies (chapter 2 &3) were different in number. The genetic algorithm selected five spectral bands (chapter 3) while using one way ANOVA and Tukey HSD, six spectral bands were chose (chapter 2). The overall classification accuracy (91%) based on genetic algorithms selected bands were nearly equal to the results obtained in chapter 2 (ANOVA and Tuckey HSD test). Unlike the manual criteria followed in chapter 2, the genetic algorithms (chapter 3) adopt a robust optimization procedure to select spectral bands. The improved classification accuracy with only five bands selected by genetic algorithms could be attributed to the fact that genetic algorithms provide several possible solutions, evaluate them on

the basis of an objective function and pick the best one for the next generation.

It is worth noting from the outcome of chapter 3 that selected bands are clustering at certain wavebands regions (Table 7.3) across the MIR and TIR domains. This finding may allow the most sensitive waveband positions to be exploited for discriminating vegetation species. The high dimensionality problem associated with hyperspectral data causes inaccurate class estimate in the feature space and as a result reduce the classification accuracy (Vaiphasa et al. 2007). In order to overcome this problem, either more samples are needed for the better class estimate (e.g. to enhance classification accuracy) or the number of bands (i.e. dimensionality) should be reduced. Using targeted waveband regions, will not only overcome the dimensionality problems associated with hyperspectral data but the demand of more training sample (to achieve high class accuracy) will also minimise (Vaiphasa et al. 2007), which in turn will reduce the cost incurred in field survey.

Table 7.3: Summary of the clustering of selected wavebands using genetic algorithms, the number of genes, spectral range, means wavelength location and standard deviation are detailed.

Group	Spectral region	No. of genes	Wavelength range (μm)	Mean wavelength (μm)	Standard deviation (μm)
A	Mid infrared	26	2.50 – 2.54	2.52	± 0.020
B	Mid infrared	12	2.84 – 3.03	2.94	± 0.097
C	Mid infrared	69	3. 40 – 3.48	3.44	± 0.041
D	Mid infrared	6	3.77 – 3.93	3.85	± 0.078
E	Mid infrared	30	5.70 – 5.90	5.80	± 0.099
F	Thermal infrared	16	9.27 – 9.48	9.36	± 0.107
G	Thermal infrared	35	9.74 – 10.00	9.87	± 0.121
H	Thermal infrared	7	11.46 – 11.58	11.52	± 0.064

Spectral discrimination of vegetation types in the MIR and TIR might be possible due to variation in the composition of the superficial epidermal layer of plant leaves producing unique emissivity features. The emissivity signature of plant leaves is dominated by a feature associated with major classes of cellulose of the epidermis (Ribeiro da Luz and Crowley 2007). The selected bands in the TIR atmospheric window (8 to14 μm) may be attributed to the surface or volume scattering of cellulose and cuticle (Ribeiro da Luz 2006; Ribeiro da Luz and Crowley 2007). The selection of features in the MIR atmospheric window (3 to 6 μm) may be attributed to the absorption features related to water molecules and cellulose in the plant leaves (Fabre et al.

2011; Gerber et al. 2011). Although, this study used spectral bands selected from laboratory measured emissivity spectra (reported in chapter 2 & 3) to discriminate vegetation species, the findings of this research (Chapter 2 & 3) helps to understand the portions of the electromagnetic spectrum that possess high potential for discriminating vegetation types. The possibility of distinguishing vegetation species based on laboratory measured emissivity spectra is an important prerequisite for future airborne and space borne floristic mapping. However, field conditions impose several challenges such as atmospheric condition, canopy structure, distance between the target and sensor, spatial and spectral resolution, and seasonal variation. This study can only be extended to field, airborne and space borne level if the sensing system has a high signal to noise ratio (SNR) thereby allow small spectral differences in plant canopies to be distinguished. The latest generation of airborne hyperspectral MIR and TIR sensors such as MASI600, TASI600, Telops Hyper-Cam and SEBASS have sufficiently high signal to noise ratios (SNR) to acquire data in numerous narrow spectral bands (Schlerf et al. 2012). The spatial distribution map of vegetation species may be anticipated in the future using these new generation airborne hyperspectral MIR and TIR sensors.

7.4 Contributions in estimating leaf water content

Estimation of leaf water content is essential in assessing plant physiological status (Datt 1999), predicting drought risk (Bauer et al. 1986), precision agriculture (Peñuelas et al. 1993; Peñuelas et al. 1997) and assessing the risk of forest fire (Chuvieco et al. 2002). Retrieving leaf water content using remote sensing data, is widely investigated from the VNIR-SWIR hyperspectral data (Thomas et al. 1971; Danson et al. 1992; Aldakheel and Danson 1997; Ceccato et al. 2001; Cheng et al. 2011), however the potential of MIR and TIR have been rarely studied despite the fact that the fundamental water absorption bands are located in the MIR (Fabre et al. 2011; Gerber et al. 2011). The technological advancement in MIR and TIR spectrometry offered the possibility to evaluate the potential of these spectral domains for the retrieval of leaf water content.

Chapter 4 of this thesis assessed the potential of hyperspectral MIR and TIR for the retrieval of leaf water content of nine plant species. In this chapter, continuous wavelet analysis was used to predict leaf water content using MIR and TIR spectra. The most interesting finding of this (Chapter 4) study was that with varying leaf water content, the variation in spectral response was more noticeable in the MIR compared to the TIR. As result of this strong relationship between leaf water content and the spectral response in the MIR (Figure7.2), the most sensitive wavebands (selected wavelet features that yielded high R2 in relation with leaf water content) lay in the MIR (Figure

7.3), thus MIR mid-wave infrared spectra contain sufficient information to retrieve leaf water content with high accuracy (Figure 7.4).

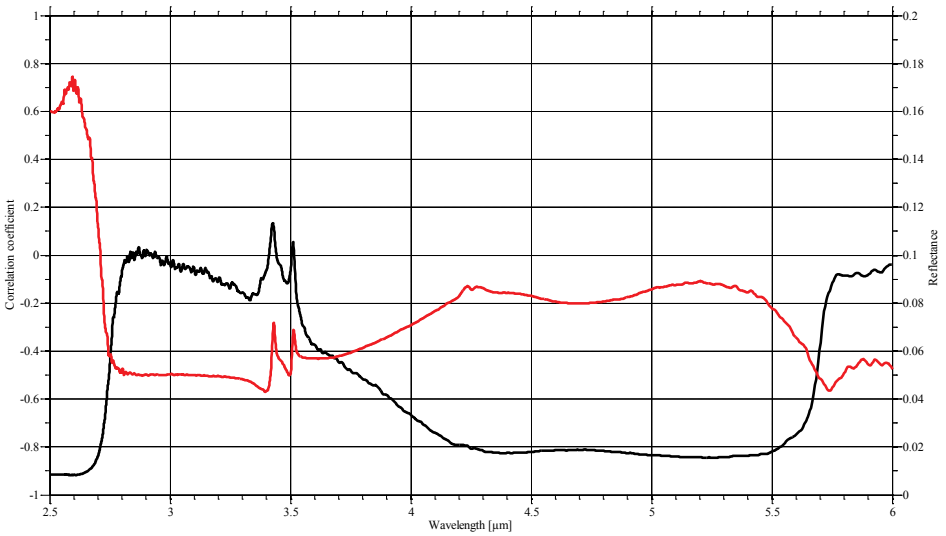

Figure 7.2: The correlation coefficients (black line) of leaf water content to the spectral response in the mid-wave infrared. The average DHR spectrum (red line) indicates typical vegetation reflectance features in the mid-wave infrared.

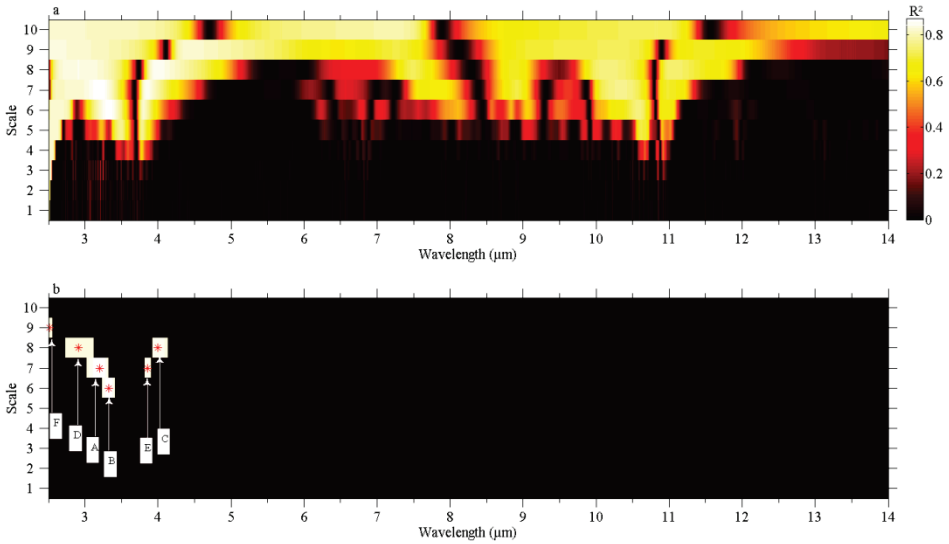

Figure 7.3: The correlation scalogram (a) and the selected wavelet features sensitive to leaf water content (b). The bright portion (a) represents the wavelet regions with high correlation (R2) with leaf water content and the dark region represents those that are less sensitive to variation in the leaf water content. The vertical axis represents the wavelet scale, while the horizontal axis displays the wavelength.

After the results obtained in chapter 4, the potential of MIR for the accurate retrieval of leaf water content was extended one step further in chapter 5. Three narrow spectral band indices were proposed for estimating leaf water content using laboratory measured MIR spectra. All possible two-band combinations were used to calculate the narrow band indices (chapter 5). The performances of these indices were also tested for the simulated spectra at airborne level. The main finding of chapter 5 was that leaf water content can be accurately (R^2 = 0.89, RMSE= 7.65 %) estimated from MIR spectra using narrow band indices. The most sensitive waveband combinations (with high R^2) were located at the absorption features related to water and dry matter (cellulose and lignin) content. Resampling laboratory measured data to airborne level (e.g. adopting only the band width and band positioning of the MASI600 airborne sensor) also predicted leaf water content with high accuracy (R^2 > 0.75), which suggesting that the retrieval of leaf water content may be explored from airborne mid-wave infrared sensors at canopy level.

Chapter 6 examined the strength the VNIR-SWIR, MIR and TIR for the retrieval of leaf water content. To the best of our knowledge, this study is the first of its kind to simultaneously use the entire spectra for the retrieval of leaf water from the visible to thermal infrared. Narrow-band spectral indices (calculated from all possible two band combinations) and a partial least square regression (PLSR) were used to assess the strength of each spectral region. The most interesting finding stems from the outcome of PLSR and narrowband indices (Figure 7.4 and Figure 7.5); namely that the SWIR and MIR domain are highly sensitive spectral regions and hold promise for the estimation of leaf water content (yielded high R^2 and low RMSE). The TIR was found the less sensitive compared to MIR and SWIR domains.

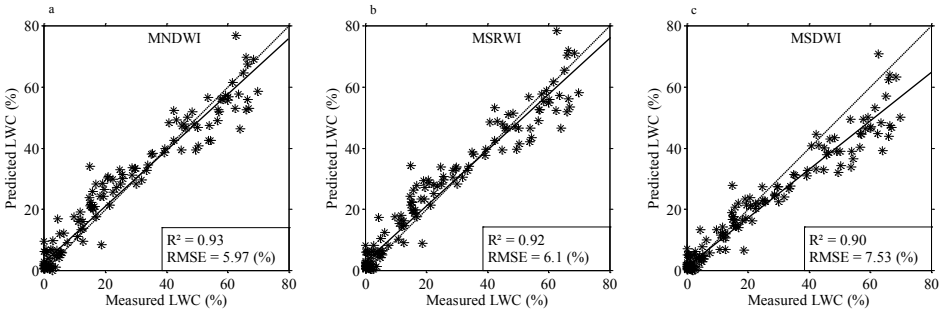

Figure 7.4: The scatterplot showing the relation between measured and predicted leaf water content (LWCf (%). The predicted leaf water content is based on the calibration models developed from MNDWI, MSRWI and MSDWI; the highest correlation shown produced using MNDWI.

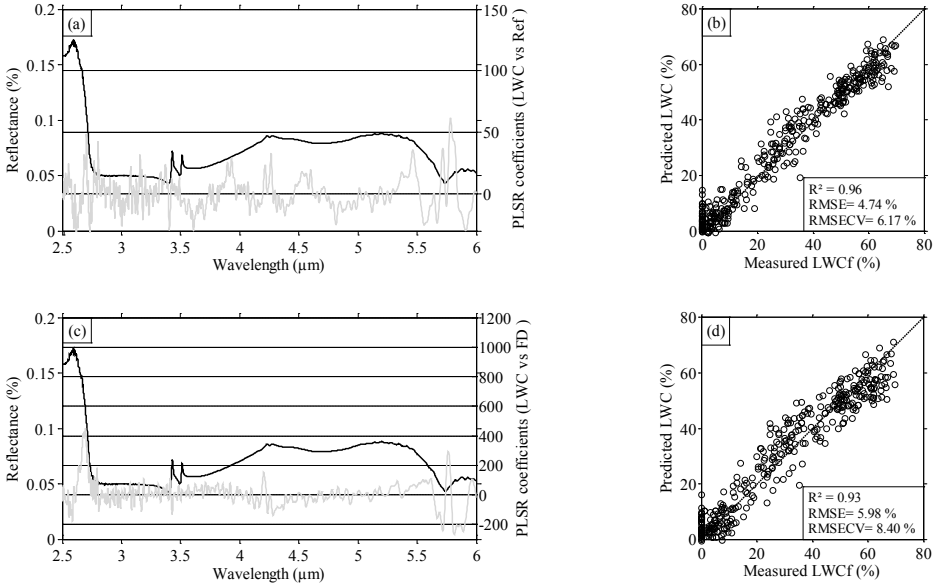

Figure 7.5: The PLSR coefficients (grey line) showing the importance of each waveband in developing the PLSR model for retrieving leaf water content from reflectance (a) and first derivative spectra (c) in the MIR. The average reflectance spectra (black line) are shown for reference purpose. The PLSR analysis using reflectance (b) predicted leaf water content more accurately (high R^2 and low RMSE and $RMSE_{CV}$) compared to PLSR model developed from first derivative spectra (d).

Although leaf water content has been widely estimated using the visible and shortwave infrared with varying degree of success, the mid-wave infrared has been seldom explored due to technical limitations. In this thesis, we quantified and accurately estimated leaf water content from mid-wave infrared spectra (2.5 – 6 μm) using various methodologies (e.g. narrow band indices, continuous wavelet analysis, PLSR). The finding of this research on the one hand complements knowledge from the VNIR-SWIR (0.4 – 2.5 μm) domain that leaf water content relates to remotely sensed spectra (Hunt and Rock 1989; Danson et al. 1992; Datt 1999; Ceccato et al. 2002a; Danson and Bowyer 2004; Claudio et al. 2006b; Colombo et al. 2008; Zygielbaum et al. 2009; Cheng et al. 2011) and on the other hand demonstrates that leaf water content can be more accurately retrieved from MIR (chapter 6). The hot spot of waveband combinations with the highest R2 occurred in the MIR (Chapter 4, 5 & 6). The outcome of this study supports the finding that the fundamental water absorption features in the mid-wave infrared have very high specific absorption coefficients (Figure 5.1) compared with the VNIR–SWIR, specifically showing strong absorption features at 2.90, 4.65, and 6.08 μm (Wieliczka et al. 1989; Fabre et al. 2011; Gerber et al. 2011). The potential of MIR for retrieving leaf water content encourages the future use of the MIR domain, and may have application in irrigation scheduling, as well as

assessing drought risk and predicting forest fire (Boyd and Petitcolin 2004; Gerber et al. 2011).

7.5 Future research avenues

The MIR and TIR hyperspectral sensors are new and their potential for characterising vegetation biophysical and biochemical parameters are not fully explored. In line with the parameters covered in this thesis, the prediction of other vegetation parameters (e.g. cellulose, lignin, protein, etc.) are important to be explored from MIR and TIR spectroscopy.

This thesis has investigated the potential of the MIR and TIR for identifying of plant species and the estimation of leaf water content at laboratory level. Future research is needed to investigate and extend these studies at canopy level using hyperspectal mid-wave and thermal infrared remote sensing at field and airborne platforms. The field and airborne MIR-TIR hyperspectral sensors such as MIDAC, Telops Hyper-Cam, MASI600, TASI600 and SEABAS are becoming popular in remote sensing community (Ribeiro da Luz and Crowley 2010; Schlerf et al. 2012) and spaceborne hyperspectral sensors covering MIR-TIR may also be anticipated in the future. The use of theses sensors for characterizing vegetation parameters will help to understand the strength of MIR and TIR in real world scenarios. The image acquired from these sensors providing information over a wide area and will thus help in management practices and decision making.

Under field conditions, it is difficult to calibrate remotely sensed signals in the MIR (3-6 µm) due to the overlap of the reflected and emitted energy from the surface. The MIR shows high potential for characterising vegetation but remains a little explored spectral domain. Further research is suggested to investigate how to mitigate the impact of overlap between emitted and reflected signals in the MIR. In addition to the optical properties of the target, its surface temperature plays an important role in the signal (when the temperature of a target is above absolute zero, it will emits energy). One possible way to overcome this difficulty is to acquire data during both the day and night, and consequently the reflectance may be separated from the emitted energy from the target.

The combined use of VNIR-SWIR, MIR and TIR hyperspectral data at airborne level is also recommended to benefit from the complimentary nature of various spectral domains and this might further improve the characterization of vegetation. Different sensors cover different spectral regions and no sensor alone can cover the entire range (VNIR-SWIR, MIR and TIR) but this could be achieved by simultaneously measuring spectra using various sensors mounted on the same platform.

In this thesis only experimental data (or observational data) are used to characterize vegetation parameters from MIR and TIR (2.5-14 µm) spectra. Generally, the estimation of vegetation parameters are limited to the VNIR-SWIR (0.4-2.5 µm) domain and there is a significant lack of experimental data and physical models (radiative transfer models) from wavelengths greater than 2.5 µm (MIR and TIR). In this thesis a robust experimental dataset was acquired and empirically tested for characterizing vegetation parameters. The outcome of the present work (i.e. experimental data, empirical models) may assist in selecting the appropriate initial parameters whenever inverting vegetation characteristic from physical models in the MIR and TIR. The physical models (which are based on certain physical laws) are universally applicable and do not needs extensive field work (unlike empirical models). The disadvantage mostly associated with physical models is the ill-posed problem (in which two or more different sets of parameters can have similar simulated spectra). In this thesis, the impact of water content on leaf spectra is demonstrated and that can help in minimizing the ill-posed problems associated with physical modelling. The integration of physical and empirical models in the MIR and TIR may be explored in the future and it can lead to a more accurate estimation of vegetation parameters which is crucial in disciplinea such as ecology, agriculture and forestry.

Bibliography

Achenbach, H., Lottes, M., Waibel, R., Karikas, G.A., Correa, M.D., & Gupta, M.P. (1995). Constituents of tropical medicinal-plants; alkaloids and other compounds from psychotria-correae. *Phytochemistry, 38*, 1537-1545

Adam, E., & Mutanga, O. (2009). Spectral discrimination of papyrus vegetation (Cyperus papyrus L.) in swamp wetlands using field spectrometry. *ISPRS Journal of Photogrammetry and Remote Sensing, 64*, 612-620

Aldakheel, Y.Y., & Danson, F.M. (1997). Spectral reflectance of dehydrating leaves: measurements and modelling. *International Journal of Remote Sensing, 18*, 3683-3690

Amolins, K., Zhang, Y., & Dare, P. (2007). Wavelet based image fusion techniques - an introduction, review and comparison. *ISPRS Journal of Photogrammetry and Remote Sensing, 62*, 249-263

Anderson, J.R., Hardy, E.E., Roach, J.T., & Witmer, R.E. (1976). *A land use and land cover classification system for use with remote sensor data*. Geological Survey, United States Government Printing Office, Washington

Asner, G.P. (1998). Biophysical and biochemical sources of variability in canopy reflectance. *Remote Sensing of Environment, 64*, 234-253

Asner, G.P., & Martin, R.E. (2008). Spectral and chemical analysis of tropical forests: Scaling from leaf to canopy levels. *Remote Sensing of Environment, 112*, 3958-3970

Banskota, A. (2006). Estimating leaf area index of salt marsh vegetation using airborne hyperspectral data. In (p. 39). Enschede: ITC

Banskota, A., Wynne, R.H., & Kayastha, N. (2011). Improving within-genus tree species discrimination using the discrete wavelet transform applied to airborne hyperspectral data. *International Journal of Remote Sensing, 32*, 3551-3563

Bauer, M.E., Daughtry, C.S.T., Biehl, L.L., Kanemasu, E.T., & Hall, F.G. (1986). Field spectroscopy of agricultural crops. *IEEE Transactions on Geoscience and Remote Sensing, 24*, 65-75

Belluco, E., Camuffo, M., Ferrari, S., Modenese, L., Silvestri, S., Marani, A., & Marani, M. (2006). Mapping salt-marsh vegetation by multispectral and hyperspectral remote sensing. *Remote Sensing of Environment, 105*, 54-67

Blackburn, G.A. (2007). Wavelet decomposition of hyperspectral data: a novel approach to quantifying pigment concentrations in vegetation. *International Journal of Remote Sensing, 28*, 2831-2855

Blackburn, G.A., & Ferwerda, J.G. (2008). Retrieval of chlorophyll concentration from leaf reflectance spectra using wavelet analysis. *Remote Sensing of Environment, 112*, 1614-1632

Bowman, W.D. (1989). The relationship between leaf water status, gas exchange, and spectral reflectance in cotton leaves. *Remote Sensing of Environment, 30*, 249-255

Boyd, D.S., & Petitcolin, F. (2004). Remote sensing of the terrestrial environment using middle infrared radiation (3.0–5.0 μm). *International Journal of Remote Sensing, 25*, 3343-3368

Broge, N.H., & Mortensen, J.V. (2002). Deriving green crop area index and canopy chlorophyll density of winter wheat from spectral reflectance data. *Remote Sensing of Environment, 81*, 45-57

Bruce, L.M., Morgan, C., & Larsen, S. (2001). Automated detection of subpixel hyperspectral targets with continuous and discrete wavelet transforms. *IEEE Transactions on Geoscience and Remote Sensing 39*, 2217-2226

Carlson, T.N., & Ripley, D.A. (1997). On the relation between NDVI, fractional vegetation cover, and leaf area index. *Remote Sensing of Environment, 62*, 241-252

Ceccato, P., Flasse, S., & Grégoire, J.-M. (2002a). Designing a spectral index to estimate vegetation water content from remote sensing data: Part 2. Validation and applications. *Remote Sensing of Environment, 82*, 198-207

Ceccato, P., Flasse, S., Tarantola, S., Jacquemoud, S., & Grégoire, J.-M. (2001). Detecting vegetation leaf water content using reflectance in the optical domain. *Remote Sensing of Environment, 77*, 22-33

Ceccato, P., Gobron, N., Flasse, S., Pinty, B., & Tarantola, S. (2002b). Designing a spectral index to estimate vegetation water content from remote sensing data: Part 1 - Theoretical approach. *Remote Sensing of Environment, 82*, 188-197

Champagne, C.M., Staenz, K., Bannari, A., McNairn, H., & Deguise, J.-C. (2003). Validation of a hyperspectral curve-fitting model for the estimation of plant water content of agricultural canopies. *Remote Sensing of Environment, 87*, 148-160

Chen, D., Hu, B., Shao, X., & Su, Q. (2004). Variable selection by modified IPW (iterative predictor weighting)-PLS (partial least squares) in continuous wavelet regression models. *Analyst, 129*, 664-669

Chen, G.Y., & Qian, S.E. (2011). Denoising of hyperspectral imagery using principal component analysis and wavelet shrinkage. *IEEE Transactions on Geoscience and Remote Sensing, 49*, 973-980

Chen, J., Itoh, S., & Hashimoto, T. (1993). ECG data-compression by using wavelet transform. *IEICE Transactions on Information and Systems, E76D*, 1454-1461

Cheng, J., Liang, S.L., Wang, J.D., & Li, X.W. (2010a). A stepwise refining algorithm of temperature and emissivity separation for hyperspectral thermal infrared data. *IEEE Transactions on Geoscience and Remote Sensing, 48*, 1588-1597

Cheng, T., Rivard, B., & Sánchez-Azofeifa, G.A. (2011). Spectroscopic determination of leaf water content using continuous wavelet analysis. *Remote Sensing of Environment, 115*, 659-670

Cheng, T., Rivard, B., Sánchez-Azofeifa, G.A., Feng, J., & Calvo-Polanco, M. (2010b). Continuous wavelet analysis for the detection of green attack damage due to mountain pine beetle infestation. *Remote Sensing of Environment, 114*, 899-910

Chmelka, L., & Kozumplik, J. (2005). Wavelet-based Wiener filter for electrocardiogram signal denoising. *Computers in Cardiology* (pp. 771-774). New York: IEEE

Cho, M.A., Debba, P., Mathieu, R., Naidoo, L., van Aardt, J., & Asner, G.P. (2010). Improving Discrimination of Savanna Tree Species Through a Multiple-Endmember Spectral Angle Mapper Approach: Canopy-Level Analysis. *Ieee Transactions on Geoscience and Remote Sensing, 48*, 4133-4142

Cho, M.A., Skidmore, A., Corsi, F., van Wieren, S.E., & Sobhan, I. (2007). Estimation of green grass/herb biomass from airborne hyperspectral imagery using spectral indices and partial least squares regression. *International Journal of Applied Earth Observation and Geoinformation, 9*, 414-424

Cho, M.A., & Skidmore, A.K. (2006). A new technique for extracting the red edge position from hyperspectral data: The linear extrapolation method. *Remote Sensing of Environment, 101*, 181-193

Chuvieco, E., Riano, D., Aguado, I., & Cocero, D. (2002). Estimation of fuel moisture content from multitemporal analysis of Landsat Thematic Mapper reflectance data: applications in fire danger assessment. *International Journal of Remote Sensing, 23*, 2145-2162

Clark, M.L., Roberts, D.A., & Clark, D.B. (2005). Hyperspectral discrimination of tropical rain forest tree species at leaf to crown scales. *Remote Sensing of Environment, 96*, 375-398

Claudio, H.C., Cheng, Y., Fuentes, D.A., Gamon, J.A., Luo, H., Oechel, W., Qiu, H.-L., Rahman, A.F., & Sims, D.A. (2006a). Monitoring drought effects on vegetation water content and fluxes in chaparral with the 970 nm water band index. *Remote Sensing of Environment, 103*, 304-311

Claudio, H.C., Cheng, Y.F., Fuentes, D.A., Gamon, J.A., Luo, H.Y., Oechel, W., Qiu, H.L., Rahman, A.F., & Sims, D.A. (2006b). Monitoring drought effects on vegetation water content and fluxes in chaparral with the 970 nm water band index. *Remote Sensing of Environment, 103*, 304-311

Clevers, J., De Jong, S.M., Epema, G.F., Van der Meer, F.D., Bakker, W.H., Skidmore, A.K., & Scholte, K.H. (2002). Derivation of the red edge index using the MERIS standard band setting. *International Journal of Remote Sensing, 23*, 3169-3184

Coblentz, W.W. (1913). The diffuse reflecting power of various substances. *Bulletin of the Bureau of standarads, 9(2)*, 283-325

Colombo, R., Merom, M., Marchesi, A., Busetto, L., Rossini, M., Giardino, C., & Panigada, C. (2008). Estimation of leaf and canopy water content in poplar plantations by means of hyperspectral indices and inverse modeling. *Remote Sensing of Environment, 112*, 1820-1834

Corso, G., Kuhn, P.S., Lucena, L.S., & Thome, Z.D. (2003). Seismic ground roll time-frequency filtering using the Gaussian wavelet transform. *Physica a-Statistical Mechanics and its Applications, 318*, 551-561

Crowe, J.A., Gibson, N.M., Woolfson, M.S., & Somekh, M.G. (1992). Wavelet transform as a potential tool for ECG analysis and compression. *Journal of Biomedical Engineering, 14*, 268-272

Curran, P.J. (1989a). Remote-sensing of foliar chemistry. *Remote Sensing of Environment, 30*, 271-278

Curran, P.J. (1989b). Remote sensing of foliar chemistry. *Remote Sensing of Environment, 30*, 271-278

Curran, P.J., Dungan, J.L., & Peterson, D.L. (2001). Estimating the foliar biochemical concentration of leaves with reflectance spectrometry testing the Kokaly and Clark methodologies. *Remote Sensing of Environment, 76*, 349-359

Danson, F.M., & Bowyer, P. (2004). Estimating live fuel moisture content from remotely sensed reflectance. *Remote Sensing of Environment, 92*, 309-321

Danson, F.M., Steven, M.D., Malthus, T.J., & Clark, J.A. (1992). High-spectral resolution data for determining leaf water-content. *International Journal of Remote Sensing, 13*, 461-470

Darvishzadeh, R., Skidmore, A., Schlerf, M., & Atzberger, C. (2008a). Inversion of a radiative transfer model for estimating vegetation LAI and chlorophyll in a heterogeneous grassland. *Remote Sensing of Environment, 112*, 2592-2604

Darvishzadeh, R., Skidmore, A.K., Schlerf, M., Atzberger, C.G., & Cho, M.A. (2008b). LAI and chlorophyll estimation for a heterogeneous grassland using hyperspectral measurements. *ISPRS Journal of Photogrammetry and Remote Sensing, 63*

Datt, B. (1999). Remote sensing of water content in Eucalyptus leaves. *Australian Journal of Botany, 47*, 909-923

de Castro, A.I., Jurado-Exposito, M., Pena-Barragan, J.M., & Lopez-Granados, F. (2012). Airborne multi-spectral imagery for mapping cruciferous weeds in cereal and legume crops. *Precision Agriculture, 13*, 302-321

Dong, J.R., Kaufmann, R.K., Myneni, R.B., Tucker, C.J., Kauppi, P.E., Liski, J., Buermann, W., Alexeyev, V., & Hughes, M.K. (2003). Remote sensing estimates of boreal and temperate forest woody biomass: carbon pools, sources, and sinks. *Remote Sensing of Environment, 84*, 393-410

Du, P., Kibbe, W.A., & Lin, S.M. (2006). Improved peak detection in mass spectrum by incorporating continuous wavelet transform-based pattern matching. *Bioinformatics, 22*, 2059-2065

Du, Q. (2004). Independent component analysis to hyperspectral image classification. In S.S. Shen, & P.E. Lewis (Eds.), *Imaging Spectrometry X* (pp. 366-373). Bellingham: Spie-Int Soc Optical Engineering

Duchemin, B. (1999). NOAA/AVHRR Bidirectional Reflectance: Modeling and Application for the Monitoring of a Temperate Forest. *Remote Sensing of Environment, 67*, 51-67

Elvidge, C.D. (1988). Thermal infrared reflectance of dry plant materials: 2.5-20.0 μm. *Remote Sensing of Environment, 26*, 265-285

Elvidge, C.D., & Chen, Z. (1995a). Comparison of broad-band and narrow-band red and near-infrared vegetation indices. *Remote Sensing of Environment, 54*, 38-48

Elvidge, C.D., & Chen, Z.K. (1995b). COMPARISON OF BROAD-BAND AND NARROW-BAND RED AND NEAR-INFRARED VEGETATION INDEXES. *Remote Sensing of Environment, 54*, 38-48

Fabre, S., Lesaignoux, A., Olioso, A., & Briottet, X. (2011). Influence of water content on spectral reflectance of leaves in the 3-15 μm domain. *IEEE Geoscience and Remote Sensing Letters, 8*, 143-147

Fang, H., Liang, S., & Kuusk, A. (2003). Retrieving leaf area index using a genetic algorithm with a canopy radiative transfer model. *Remote Sensing of Environment, 85*, 257-270

Ferwerda, J., & Jones, S. (2006). Continuous wavelet transformations for hyperspectral feature detection. *Progress in Spatial Data Handling* (pp. 167-178): Springer Berlin Heidelberg

Ferwerda, J.G., Skidmore, A.K., & Mutanga, O. (2005). Nitrogen detection with hyperspectral normalized ratio indices across multiple plant species. *International Journal of Remote Sensing, 26*, 4083-4095

Foody, G.M., & Cutler, M.E.J. (2003). Tree biodiversity in protected and logged Bornean tropical rain forests and its measurement by satellite remote sensing. *Journal of Biogeography, 30*, 1053-1066

French, A.N., Schmugge, T.J., & Kustas, W.P. (2000). Discrimination of senescent vegetation using thermal emissivity contrast. *Remote Sensing of Environment, 74*, 249-254

Fry, S.C. (2004). Primary cell wall metabolism: tracking the careers of wall polymers in living plant cells. *New Phytologist, 161*, 641-675

Gao, B.C. (1996). NDWI - A normalized difference water index for remote sensing of vegetation liquid water from space. *Remote Sensing of Environment, 58*, 257-266

Gao, X., Huete, A.R., Ni, W.G., & Miura, T. (2000). Optical-biophysical relationships of vegetation spectra without background contamination. *Remote Sensing of Environment, 74*, 609-620

Garnier, E., & Laurent, G. (1994). Leaf anatomy, specific mass and water-content in congeneric annual and perennial grass species. *New Phytologist, 128*, 725-736

Gates, D.M., & Tantraporn, W. (1952). The Reflectivity of Deciduous Trees and Herbaceous Plants in the Infrared to 25 Microns. *Science, 115*, 613-616

Geladi, P., & Kowalski, B.R. (1986). Partial least-squares regression: a tutorial. *Analytica Chimica Acta, 185*, 1-17

Gerber, F., Marion, R., Olioso, A., Jacquemoud, S., da Luz, B.R., & Fabre, S. (2011). Modeling directional-hemispherical reflectance and transmittance of fresh and dry leaves from 0.4 µm to 5.7 µm with the PROSPECT-VISIR model. *Remote Sensing of Environment, 115*, 404-414

Ghulam, A., Qin, Q., Teyip, T., & Li, Z.-L. (2007). Modified perpendicular drought index (MPDI): a real-time drought monitoring method. *ISPRS Journal of Photogrammetry and Remote Sensing, 62*, 150-164

Goetz, A.F.H., Vane, G., Solomon, J.E., & Rock, B.N. (1985). Imaging spectrometry for earth remote sensing. *Science, 228*, 1147-1153

Goldberg, D.E. (1989). *Genetic Algorithms in Search, Optimization and Machine Learning*. Addison-Wesley Longman Publishing Co., Inc. Boston, MA, USA

Hansen, P.M., & Schjoerring, J.K. (2003). Reflectance measurement of canopy biomass and nitrogen status in wheat crops using normalized difference vegetation indices and partial least squares regression. *Remote Sensing of Environment, 86*, 542-553

Hao, X., & Qu, J.J. (2009). Fast and highly accurate calculation of band averaged radiance. *International Journal of Remote Sensing, 30*, 1099-1108

Harry, V. (2006). Principles of soil and plant water relations *Geoderma, 133*, 478

Hecker, C., Hook, S., Meijde, M.v.d., Bakker, W., Werff, H.v.d., Wilbrink, H., Ruitenbeek, F.v., Smeth, B.d., & Meer, F.v.d. (2011). Thermal infrared spectrometer for earth science remote sensing applications: instrument modifications and measurement procedures. *Sensors, 11*, 10981-10999

Heredia, A. (2003). Biophysical and biochemical characteristics of cutin, a plant barrier biopolymer. *Biochimica et Biophysica Acta (BBA) - General Subjects, 1620*, 1-7

Holland, J. (1975). *Adaptation in Natural and Artificial Systems*. University of Michigan, Ann Arbor

Holloway, P.J. (1982). *Structure and histochemistry of plant cuticular membrane: an overview*. Cutler DF, Alvin kl, Price CE, London, UK Acadmic press

Huang, Z., Turner, B.J., Dury, S.J., Wallis, I.R., & Foley, W.J. (2004a). Estimating foliage nitrogen concentration from HYMAP data using continuum removal analysis. *Remote Sensing of Environment, 93*, 18-29

Huang, Z., Turner, B.J., Dury, S.J., Wallis, I.R., & Foley, W.J. (2004b). Estimating foliage nitrogen concentration from HYMAP data using continuum removal analysis. *Remote Sensing of Environment, 93*, 18-29

Huete, A.R. (1988). A soil-adjusted vegetation index (SAVI). *Remote Sensing of Environment, 25*, 295-309

Hughes, G. (1968). On the mean accuracy of statistical pattern recognizers. *Information Theory, IEEE Transactions on, 14*, 55-63

Hunt, E.R., & Rock, B.N. (1989). Detection of changes in leaf water-content using near-infrared and middle-infrared reflectances. *Remote Sensing of Environment, 30*, 43-54

Hunt, E.R., Rock, B.N., & Nobel, P.S. (1987). Measurement of leaf relative water-content by infrared reflectance. *Remote Sensing of Environment, 22*, 429-435

Ifarraguerri, A., & Chang, C.I. (2000). Unsupervised hyperspectral image analysis with projection pursuit. *Ieee Transactions on Geoscience and Remote Sensing, 38*, 2529-2538

Jackson, Q., & Landgrebe, D.A. (2002). An adaptive method for combined covariance estimation and classification. *Ieee Transactions on Geoscience and Remote Sensing, 40*, 1082-1087

Jago, R.A., Cutler, M.E.J., & Curran, P.J. (1999). Estimating canopy chlorophyll concentration from field and airborne spectra. *Remote Sensing of Environment, 68*, 217-224

Jones, H.G., & Tardieu, F. (1998). Modelling water relations of horticultural crops: a review. *Scientia Horticulturae, 74*, 21-46

Judd, C., Steinberg, S., Shaughnessy, F., & Crawford, G. (2007). Mapping salt marsh vegetation using aerial hyperspectral imagery and linear unmixing in Humboldt bay, California. *Wetlands, 27*, 1144-1152

Kacuráková, M., & Wilson, R.H. (2001). Developments in mid-infrared FT-IR spectroscopy of selected carbohydrates. *Carbohydrate Polymers, 44*, 291-303

Kaewpijit, S., Le moigne, J., & El-Ghazawi, T. (2003). Automatic reduction of hyperspectral imagery using wavelet spectral analysis. *IEEE Transactions on Geoscience and Remote Sensing, 41*, 863-871

Kalacska, M., Bohman, S., Sánchez-Azofeifa, G.A., Castro-Esau, K., & Caelli, T. (2007). Hyperspectral discrimination of tropical dry forest lianas and trees: comparative data reduction approaches at the leaf and canopy levels. *Remote Sensing of Environment, 109*, 406-415

Kawamura, K., Watanabe, N., Sakanoue, S., Lee, H.-J., Inoue, Y., & Odagawa, S. (2010). Testing genetic algorithm as a tool to select relevant wavebands from field hyperspectral data for estimating pasture mass and quality in a mixed sown pasture using partial least squares regression. *Grassland Science, 56*, 205-216

Kiema, J.B.K. (2000). Wavelet compression and the automatic classification of Landsat imagery. *Photogrammetric Record, 16*, 997-1006

Kirkland, L., Herr, K., Keim, E., Adams, P., Salisbury, J., Hackwell, J., & Treiman, A. (2002). First use of an airborne thermal infrared hyperspectral scanner for compositional mapping. *Remote Sensing of Environment, 80*, 447-459

Koger, C.H., Bruce, L.M., Shaw, D.R., & Reddy, K.N. (2003). Wavelet analysis of hyperspectral reflectance data for detecting pitted morningglory (Ipomoea lacunosa) in soybean (Glycine max). *Remote Sensing of Environment, 86*, 108-119

Kokaly, R.F. (2001). Investigating a physical basis for spectroscopic estimates of leaf nitrogen concentration. *Remote Sensing of Environment, 75*, 153-161

Kokaly, R.F., & Clark, R.N. (1999). Spectroscopic determination of leaf biochemistry using band-depth analysis of absorption features and stepwise multiple linear regression. *Remote Sensing of Environment, 67*, 267-287

Kokaly, R.F., Despain, D.G., Clark, R.N., & Livo, K.E. (2003). Mapping vegetation in Yellowstone National Park using spectral feature analysis of AVIRIS data. *Remote Sensing of Environment, 84*, 437-456

Kumar, L., Skidmore, A.K., & Mutanga, O. (2010). Leaf level experiments to discriminate between eucalyptus species using high spectral resolution

reflectance data: use of derivatives, ratios and vegetation indices. *Geocarto International, 25*, 327-344

Lamb, D.W., Steyn-Ross, M., Schaare, P., Hanna, M.M., Silvester, W., & Steyn-Ross, A. (2002). Estimating leaf nitrogen concentration in ryegrass (Lolium spp.) pasture using the chlorophyll red-edge: theoretical modelling and experimental observations. *International Journal of Remote Sensing, 23*, 3619-3648

Landgrebe, D.A. (2003). Signal Theory Methods in Multispectral Remote Sensing. (p. 528): John Wiley & Sons, Inc.

Leardi, R. (1994). Application of a genetic algorithm to feature selection under full validation conditions and to outlier detection. *Journal of Chemometrics, 8*, 65-79

Leardi, R., & Lupiáñez González, A. (1998). Genetic algorithms applied to feature selection in PLS regression: how and when to use them. *Chemometrics and Intelligent Laboratory Systems, 41*, 195-207

Lee, C.H., & Landgrebe, D.A. (1993). Feature-extraction based on decision boundaries. *Ieee Transactions on Pattern Analysis and Machine Intelligence, 15*, 388-400

Li, J. (2004). Wavelet-based feature extraction for improved endmember abundance estimation in linear unmixing of hyperspectral signals. *IEEE Transactions on Geoscience and Remote Sensing, 42*, 644-649

Li, S.T. (2008). Multisensor remote sensing image fusion using stationary wavelet transform: effects of basis and decomposition level. *International Journal of Wavelets Multiresolution and Information Processing, 6*, 37-50

Lillesand, T.M., Kiefer, R.W., & Chipman, J.W. (2004). *Remote sensing and image interpretation*. (5th ed.). John Wiley & Sons Ltd.

Lim, K., Treitz, P., Wulder, M., St-Onge, B., & Flood, M. (2003). LiDAR remote sensing of forest structure. *Progress in Physical Geography, 27*, 88-106

Lin, L., Ustin, S.L., & Riano, D. (2007). Retrieval of Fresh Leaf Fuel Moisture Content Using Genetic Algorithm Partial Least Squares (GA-PLS) Modeling. *Geoscience and Remote Sensing Letters, IEEE, 4*, 216-220

Lokupitiya, E., Lefsky, M., & Paustian, K. (2010). Use of AVHRR NDVI time series and ground-based surveys for estimating county-level crop biomass. *International Journal of Remote Sensing, 31*, 141-158

Ma, C.X., & Shao, X.G. (2004). Continuous wavelet transform applied to removing the fluctuating background in near-infrared spectra. *Journal of Chemical Information and Computer Sciences, 44*, 907-911

Mallat, S. (1991). Zero-crossings of a wavelet transform. *IEEE Transactions on Information Theory, 37*, 1019-1033

Maréchal, Y., & Chanzy, H. (2000). The hydrogen bond network in I[beta] cellulose as observed by infrared spectrometry. *Journal of Molecular Structure, 523*, 183-196

Miller, J.R., Hare, E.W., & Wu, J. (1990). Quantitative characterization of the vegetation red edge reflectance 1. An inverted-Gaussian reflectance model. *International Journal of Remote Sensing, 11*, 1755-1773

Mkhabela, M.S., Bullock, P., Raj, S., Wang, S., & Yang, Y. (2011). Crop yield forecasting on the Canadian Prairies using MODIS NDVI data. *Agricultural and Forest Meteorology, 151*, 385-393

Moleele, N., Ringrose, S., Arnberg, W., Lunden, B., & Vanderpost, C. (2001). Assessment of vegetation indexes useful for browse (forage) prediction in semi-arid rangelands. *International Journal of Remote Sensing, 22*, 741-756

Murwira, A., & Skidmore, A.K. (2005). The response of elephants to the spatial heterogeneity of vegetation in a Southern African agricultural landscape. *Landscape Ecology, 20*, 217-234

Murwira, A., & Skidmore, A.K. (2006). Monitoring change in the spatial heterogeneity of vegetation cover in an African savanna. *International Journal of Remote Sensing, 27*, 2255-2269

Murwira, A., & Skidmore, A.K. (2010). Comparing direct image and wavelet transform-based approaches to analysing remote sensing imagery for predicting wildlife distribution. *International Journal of Remote Sensing, 31*, 6425-6440

Mutanga, O., & Skidmore, A. (2007a). Red edge shift and biochemical content in grass canopies. *ISPRS Journal of Photogrammetry and Remote Sensing, 62*, 34-42

Mutanga, O., & Skidmore, A.K. (2004a). Hyperspectral band depth analysis for a better estimation of grass biomass (Cenchrus ciliaris) measured under controlled laboratory conditions. *International Journal of Applied Earth Observation and Geoinformation, 5*, 87-96

Mutanga, O., & Skidmore, A.K. (2004b). Integrating imaging spectroscopy and neural networks to map grass quality in the Kruger National Park, South Africa. *Remote Sensing of Environment, 90*, 104-115

Mutanga, O., & Skidmore, A.K. (2004c). Narrow band vegetation indices overcome the saturation problem in biomass estimation. *International Journal of Remote Sensing, 25*, 3999-4014

Mutanga, O., & Skidmore, A.K. (2007b). Red edge shift and biochemical content in grass canopies. *ISPRS Journal of Photogrammetry and Remote Sensing, 62*, 34-42

Mutanga, O., Skidmore, A.K., Kumar, L., & Ferwerda, J. (2005). Estimating tropical pasture quality at canopy level using band depth analysis with continuum removal in the visible domain. *International Journal of Remote Sensing, 26*, 1093-1108

Mutanga, O., Skidmore, A.K., & Prins, H.H.T. (2004). Predicting in situ pasture quality in the Kruger National Park, South Africa, using continuum-removed absorption features. *Remote Sensing of Environment, 89*, 393-408

Myint, S.W., & Mesev, V. (2012). A comparative analysis of spatial indices and wavelet-based classification. *Remote Sensing Letters, 3*, 141-150

Nicodemus, F.E. (1965). Directional Reflectance and Emissivity of an Opaque Surface. *Appl. Opt., 4*, 767-773

Pajares, G., & de la Cruz, J.M. (2004). A wavelet-based image fusion tutorial. *Pattern Recognition, 37*, 1855-1872

Pengra, B.W., Johnston, C.A., & Loveland, T.R. (2007). Mapping an invasive plant, Phragmites australis, in coastal wetlands using the EO-1 Hyperion hyperspectral sensor. *Remote Sensing of Environment, 108*, 74-81

Peñuelas, J., & Filella, I. (1998). Visible and near-infrared reflectance techniques for diagnosing plant physiological status. *Trends in Plant Science, 3*, 151-156

Peñuelas, J., Gamon, J.A., Griffin, K.L., & Field, C.B. (1993). Assessing community type, plant biomass, pigment composition, and photosynthetic efficiency of aquatic vegetation from spectral reflectance. *Remote Sensing of Environment, 46*, 110-118

Peñuelas, J., Pinol, J., Ogaya, R., & Filella, I. (1997). Estimation of plant water concentration by the reflectance water index WI (R900/R970). *International Journal of Remote Sensing, 18*, 2869-2875

Pu, R., & Gong, P. (2004). Wavelet transform applied to EO-1 hyperspectral data for forest LAI and crown closure mapping. *Remote Sensing of Environment, 91*, 212-224

Pu, R., Gong, P., & Biging, G.S. (2003). Simple calibration of AVIRIS data and LAI mapping of forest plantation in southern Argentina. *International Journal of Remote Sensing, 24*, 4699-4714

Pu, R.L. (2009). Broadleaf species recognition with in situ hyperspectral data. *International Journal of Remote Sensing, 30*, 2759-2779

Ramirez, F.J., Luque, P., Heredia, A., & Bukovac, M.J. (1992). Fourier-transform IR study of enzymatically isolated tomato fruit cuticular membrane. *Biopolymers, 32*, 1425-1429

Ramoelo, A., Skidmore, A.K., Schlerf, M., Mathieu, R., & Heitkönig, I.M.A. (2011). Water-removed spectra increase the retrieval accuracy when estimating savanna grass nitrogen and phosphorus concentrations. *ISPRS Journal of Photogrammetry and Remote Sensing, 66*, 408-417

Ribeiro da Luz, B. (2006). Attenuated total reflectance spectroscopy of plant leaves: a tool for ecological and botanical studies. *New Phytologist, 172*, 305-318

Ribeiro da Luz, B., & Crowley, J.K. (2007). Spectral reflectance and emissivity features of broad leaf plants: prospects for remote sensing in the thermal infrared (8.0-14.0 µm). *Remote Sensing of Environment, 109*, 393-405

Ribeiro da Luz, B., & Crowley, J.K. (2010). Identification of plant species by using high spatial and spectral resolution thermal infrared (8.0-13.5 µm) imagery. *Remote Sensing of Environment, 114*, 404-413

Richards, J.A. (1993). *Remote Sensing Digital Image Analysis: An Introduction*. Springer-Verlag New York, Inc.

Richards, J.A., & Jia, X. (2006). *Remote sensing digital image analysis: An introduction*. (4th ed.). Springer-Verlag Berlin Heidelberg

Rivard, B., Feng, J., Gallie, A., & Sánchez-Azofeifa, G.A. (2008). Continuous wavelets for the improved use of spectral libraries and hyperspectral data. *Remote Sensing of Environment, 112*, 2850-2862

Rosso, P.H., Ustin, S.L., & Hastings, A. (2005). Mapping marshland vegetation of San Francisco Bay, California, using hyperspectral data. *International Journal of Remote Sensing, 26*, 5169-5191

Rouse, J.W., Hass, R.H., & Schell, J.A. (1974). Monitoring the vernal advancement of retrogradiation of natural vegetation. In (pp. 1-371). MD, USA: NASA / GSFC

Rui, H., & Mingyi, H. (2005). Band selection based on feature weighting for classification of hyperspectral data. *Geoscience and Remote Sensing Letters, IEEE, 2*, 156-159

Salisbury, J.W. (1986). Preliminary measurements of leaf spectral reflectance in the 8-14 µm region. *International Journal of Remote Sensing, 7*, 1879 - 1886

Salisbury, J.W., & Milton, N.M. (1988). Thermal infrared (2.5 - 13.5 µm) directional hemispherical reflectance of leaves. *Photogrammetric Engineering and Remote Sensing, 54*, 1301-1304

Salisbury, J.W., Wald, A., & D'Aria, D.M. (1994). Thermal-infrared remote sensing and Kirchhoff's law 1. Laboratory measurements. *J. Geophys. Res., 99*, 11897-11911

Sankaran, S., & Ehsani, R. (2011). Visible-near infrared spectroscopy based citrus greening detection: Evaluation of spectral feature extraction techniques. *Crop Protection, 30*, 1508-1513

Savitzky, A., & Golay, M.J.E. (1964). Smoothing and Differentiation of Data by Simplified Least Squares Procedures. *Analytical Chemistry, 36*, 1627-1639

Schlerf, M., Atzberger, C., & Hill, J. (2005). Remote sensing of forest biophysical variables using HyMap imaging spectrometer data. *Remote Sensing of Environment, 95*, 177-194

Schlerf, M., Atzberger, C., Hill, J., Buddenbaum, H., Werner, W., & Schuler, G. (2010). Retrieval of chlorophyll and nitrogen in Norway spruce (Picea abies L. Karst.) using imaging spectroscopy. *International Journal of Applied Earth Observation and Geoinformation, 12*, 17-26

Schlerf, M., Rock, G., Lagueux, P., Ronellenfitsch, F., Gerhards, M., Hoffmann, L., & Udelhoven, T. (2012). A Hyperspectral Thermal Infrared Imaging Instrument for Natural Resources Applications. *Remote Sensing, 4*, 3995-4009

Schmidt, K.S., & Skidmore, A.K. (2003). Spectral discrimination of vegetation types in a coastal wetland. *Remote Sensing of Environment, 85*, 92-108

Schmidt, K.S., Skidmore, A.K., Kloosterman, E.H., Van Oosten, H., Kumar, L., & Janssen, J.A.M. (2004). Mapping coastal vegetation using an expert system and hyperspectral imagery. *Photogrammetric Engineering and Remote Sensing, 70*, 703-715

Sepulcre-Cantó, G., Zarco-Tejada, P.J., Jiménez-Muñoz, J.C., Sobrino, J.A., Miguel, E.d., & Villalobos, F.J. (2006). Detection of water stress in an olive orchard with thermal remote sensing imagery. *Agricultural and Forest Meteorology, 136*, 31-44

Shahshahani, B.M., & Landgrebe, D.A. (1994). The effect of unlabeled samples in reducing the small sample size problem and mitigating the Hughes phenomenon. *Geoscience and Remote Sensing, IEEE Transactions on, 32*, 1087-1095

Shi, T., Yu, B., Clothiaux, E.E., & Braverman, A.J. (2008). Daytime Arctic cloud detection based on multi-angle satellite data with case studies. *Journal of the American Statistical Association, 103*, 584-593

Siedlecki, W., & Sklansky, J. (1989). A note on genetic algorithms for large-scale feature selection. *Pattern Recognition Letters, 10*, 335-347

Silverstein, R.M., & Webster, F.X. (1998). *Spectrometric Identification of Organic Compounds*. (6 ed.). New York, NY, USA: John Wiley & Sons

Skidmore, A.K. (2002). Taxonomy of environmental models in the spatial sciences. *In: Environmental modelling with GIS and remote sensing / A. Skidmore (ed.). London etc. : Taylor & Francis, 2002. ISBN 0-415-24170-7 pp. 8-24*

Soulard, R., & Carré, P. (2011). Quaternionic wavelets for texture classification. *Pattern Recognition Letters, 32*, 1669-1678

Strachan, I.B., Pattey, E., Salustro, C., & Miller, J.R. (2008). Use of hyperspectral remote sensing to estimate the gross photosynthesis of agricultural fields. *Canadian Journal of Remote Sensing, 34*, 333-341

Suárez, L., Zarco-Tejada, P.J., Sepulcre-Cantó, G., Pérez-Priego, O., Miller, J.R., Jiménez-Muñoz, J.C., & Sobrino, J. (2008). Assessing canopy PRI for water stress detection with diurnal airborne imagery. *Remote Sensing of Environment, 112*, 560-575

Taylor, D., Kent, M., & Coker, P. (1993). Vegetation description and analysis: A practical approach

Geographical Journal, 159, 237-237

Thenkabail, P.S., Enclona, E.A., Ashton, M.S., Legg, C., & De Dieu, M.J. (2004). Hyperion, IKONOS, ALI, and ETM+ sensors in the study of African rainforests. *Remote Sensing of Environment, 90*, 23-43

Thenkabail, P.S., Smith, R.B., & De Pauw, E. (2000). Hyperspectral Vegetation Indices and Their Relationships with Agricultural Crop Characteristics. *Remote Sensing of Environment, 71*, 158-182

Thomas, E.V., & Haaland, D.M. (1990). COMPARISON OF MULTIVARIATE CALIBRATION METHODS FOR QUANTITATIVE SPECTRAL-ANALYSIS. *Analytical Chemistry, 62*, 1091-1099

Thomas, J.R., Namken, L.N., Oerther, G.F., & Brown, R.G. (1971). Estimating Leaf Water Content by Reflectance Measurements. *Agron. J., 63*, 845-847

Thomas, V., Treitz, P., Jelinski, D., Miller, J., Lafleur, P., & McCaughey, J.H. (2003). Image classification of a northern peatland complex using

spectral and plant community data. *Remote Sensing of Environment, 84*, 83-99

Todd, S.W., Hoffer, R.M., & Milchunas, D.G. (1998a). Biomass estimation on grazed and ungrazed rangelands using spectral indices. *International Journal of Remote Sensing, 19*, 427 - 438

Todd, S.W., Hoffer, R.M., & Milchunas, D.G. (1998b). Biomass estimation on grazed and ungrazed rangelands using spectral indices. *International Journal of Remote Sensing, 19*, 427-438

Torrence, C., & Compo, G.P. (1998). A practical guide to wavelet analysis. *Bulletin of the American Meteorological Society, 79*, 61-78

Ullah, S., Groen, T.A., Schlerf, M., Skidmore, A.K., Nieuwenhuis, W., & Vaiphasa, C. (2012a). Using a Genetic Algorithm as an Optimal Band Selector in the Mid and Thermal Infrared (2.5–14 μm) to Discriminate Vegetation Species. *Sensors, 12*, 8755-8769

Ullah, S., Schlerf, M., Skidmore, A.K., & Hecker, C. (2012b). Identifying plant species using mid-wave infrared (2.5–6μm) and thermal infrared (8–14μm) emissivity spectra. *Remote Sensing of Environment, 118*, 95-102

Ullah, S., Skidmore, A.K., Groen, T.A., & Schlerf, M. (2013). Evaluation of three proposed indices for the retrieval of leaf water content from the mid-wave infrared (2–6 μm) spectra. *Agricultural and Forest Meteorology, 171–172*, 65-71

Ullah, S., Skidmore, A.K., Naeem, M., & Schlerf, M. (2012c). An accurate retrieval of leaf water content from mid to thermal infrared spectra using continuous wavelet analysis. *Science of The Total Environment, 437*, 145-152

Underwood, E., Ustin, S., & DiPietro, D. (2003). Mapping nonnative plants using hyperspectral imagery. *Remote Sensing of Environment, 86*, 150-161

Ustin, S.L., Roberts, D.A., Pinzón, J., Jacquemoud, S., Gardner, M., Scheer, G., Castañeda, C.M., & Palacios-Orueta, A. (1998). Estimating Canopy Water Content of Chaparral Shrubs Using Optical Methods. *Remote Sensing of Environment, 65*, 280-291

Ustin, S.L., & Xiao, Q.F. (2001). Mapping successional boreal forests in interior central Alaska. *International Journal of Remote Sensing, 22*, 1779-1797

Vaiphasa, C., Ongsomwang, S., Vaiphasa, T., & Skidmore, A.K. (2005). Tropical mangrove species discrimination using hyperspectral data: A laboratory study. *Estuarine Coastal and Shelf Science, 65*, 371-379

Vaiphasa, C., Skidmore, A.K., de Boer, W.F., & Vaiphasa, T. (2007). A hyperspectral band selector for plant species discrimination. *ISPRS Journal of Photogrammetry and Remote Sensing, 62*, 225-235

van Leeuwen, W.J.D., & Huete, A.R. (1996). Effects of standing litter on the biophysical interpretation of plant canopies with spectral indices. *Remote Sensing of Environment, 55*, 123-138

Wan, H.S., Hsu, C.Y., & Ma, L.T. (2010). New approach for dynamic range compression of remote sensing image using wavelet fusion. *Journal of Applied Remote Sensing, 4*

Wang, A., Price, D.T., & Arora, V. (2006). Estimating changes in global vegetation cover (1850–2100) for use in climate models. *Global Biogeochem. Cycles, 20*, GB3028

Warner, T.A., Nellis, D.M., & Foody, G.M. (2009). The handbook of remote sensing. SAGE publications Ltd., 568 pp.

Wieliczka, D.M., Weng, S., & Querry, M.R. (1989). Wedge shaped cell for highly absorbent liquids: infrared optical constants of water. *Appl. Opt., 28*, 1714-1719

Wilson, R.H., Smith, A.C., Kacurakova, M., Saunders, P.K., Wellner, N., & Waldron, K.W. (2000). The mechanical properties and molecular dynamics of plant cell wall polysaccharides studied by Fourier-transform infrared spectroscopy. *Plant Physiology, 124*, 397-405

Wylie, B.K., Meyer, D.J., Tieszen, L.L., & Mannel, S. (2002). Satellite mapping of surface biophysical parameters at the biome scale over the North American grasslands - A case study. *Remote Sensing of Environment, 79*, 266-278

Yandell, B.S. (1997). *Practical data analysis for designed experiments*. New York: Chapman & Hall

Yang, Y.H., Xiao, Y., & Segal, M.R. (2005). Identifying differentially expressed genes from microarray experiments via statistic synthesis. *Bioinformatics, 21*, 1084-1093

Yu, S., De Backer, S., & Scheunders, P. (2002). Genetic feature selection combined with composite fuzzy nearest neighbor classifiers for hyperspectral satellite imagery. *Pattern Recognition Letters, 23*, 183-190

Zaini, N., van der Meer, F., & van der Werff, H. (2012). Effect of Grain Size and Mineral Mixing on Carbonate Absorption Features in the SWIR and TIR Wavelength Regions. *Remote Sensing, 4*, 987-1003

Zarrouk, N., & Bennaceur, R. (2009). A wavelet based analysis of cosmic rays modulation. *Acta Astronautica, 65*, 262-272

Zhang, L., Zhou, Z., Zhang, G., Meng, Y., Chen, B., & Wang, Y. (2012). Monitoring the leaf water content and specific leaf weight of cotton (Gossypium hirsutum L.) in saline soil using leaf spectral reflectance. *European Journal of Agronomy, 41*, 103-117

Zhang, M., Ustin, S.L., Rejmankova, E., & Sanderson, E.W. (1997). Monitoring pacific coast salt marshes using remote sensing. *Ecological Applications, 7*, 1039-1053

Zhao, D., Huang, L., Li, J., & Qi, J. (2007). A comparative analysis of broadband and narrowband derived vegetation indices in predicting LAI and CCD of a cotton canopy. *ISPRS Journal of Photogrammetry and Remote Sensing, 62*, 25-33

Zhou, M.D., Shu, J.O., & Chen, Z.G. (2010). Classification of Hyperspectral Remote Sensing Image Based on Genetic Algorithm and SVM. In W. Gao, T.J. Jackson, & J. Wang (Eds.), *Remote Sensing and Modeling of Ecosystems for Sustainability Vii*. Bellingham: Spie-Int Soc Optical Engineering

Zhu, C.Q., & Yang, X.M. (1998). Study of remote sensing image texture analysis and classification using wavelet. *International Journal of Remote Sensing, 19*, 3197-3203

Zygielbaum, A.I., Gitelson, A.A., Arkebauer, T.J., & Rundquist, D.C. (2009). Non-destructive detection of water stress and estimation of relative water content in maize. *Geophysical Research Letters, 36*

Summary

Information on vegetation characteristics (e.g. species type, canopy structure, leaf area index, leaf biochemical content) is critical in many applications, like precision agriculture, forage quality and availability assessments for wildlife and livestock, quantifying timber mass and monitoring species diversity. Hyperspectral remote sensing, unlike more conventional multispectral remote sensing, has a large number (usually more than 100) of contiguous narrow spectral bands. Being a cheap, non-destructive alternative to field based methods, and providing the possibility for repetitive observations it is regarded as an effective tool for characterizing vegetation parameters. This thesis investigates the potential of mid-wave to thermal infrared (2.5- 14 μm) hyperspectral data to characterize vegetation parameters at the leaf level. Since leaves constitute the bulk of plant canopies, we focused on leaf optical properties. In the past, the spectral characteristics of plant leaves in the mid-wave to thermal infrared were mostly overlooked due to low signal to noise ratios, the subtle and complex nature of the spectral features of vegetation in this domain and lack of equipment. The latest generation of sensors such as the Bruker FTIR spectrometer or the Midac FTIR spectrometer are now covering the mid-wave to thermal infrared part of the spectrum. Accordingly, this research aimed at extracting information for identifying plant species and estimating leaf water content using the mid-wave and thermal hyperspectral data.

The first two studies dealt with the identification of thirteen plant species from laboratory measured mid-wave to thermal infrared emissivity spectra. Using one way ANOVA coupled with a Tukey HSD test, it was concluded that plant species could be discriminated from mid-wave to thermal infrared emissivity spectra. The result of the statistical analysis provided a basis to use an optimization technique (genetic algorithms) to select the most important wave bands for the identification of plant species. The wavebands selected based on the genetic algorithm (means clustered at 2.52, 2.94, 3.44, 3.85, 5.80, 9.36, 9.87 and 11.52 μm), could indeed be used to differentiate between plant species.

The leaf water content was the second vegetation parameter addressed. This could be accurately predicted from mid-wave to thermal infrared spectra. The results of retrieving leaf water content from the newly proposed narrow band indices (MNDWI, MSDWI, MSRWI), continuous wavelet analysis and partial least square regression showed that variation in leaf water content can be accurately quantified using a few waveband features in the mid-wave infrared domain (2.5- 6 μm). Further down the thermal infrared spectrum (6- 14 μm) appeared less sensitive to the variation in leaf water content. The robustness and reliability of the proposed indices for the retrieval of leaf water content

across different plant species was also tested at the spectral band positions of an airborne sensor (MASI600). The proposed indices calculated from the resampled spectra demonstrated the effectiveness of the mid-wave infrared domain for retrieving leaf water content. Most of the selected wavebands were either related to the absorption of leaf water or to the absorption of dry matter and cellulose. Lastly, an evaluation of the entire spectrum (from visible to thermal infrared; 0.4 -14 µm) for retrieving leaf water content showed that mid-wave (2.5- 6 µm) and shortwave (1.1- 2.5 µm) are the most sensitive spectral regions that hold great potential for the estimation of leaf water content.

In a nutshell, this research has demonstrated the potential of mid-wave to thermal infrared hyperspectral remote sensing for charactering vegetation parameters such as plant species identification and leaf water content estimation. The finding of this thesis can be used to adjust band positions (in the mid-wave and thermal infrared) of air-borne and space-borne campaigns for the characterization of vegetation in the future.

Samenvatting

Informatie over vegetatie eigenschappen (b.v. plantensoort, bladerdakstructuur, bladoppervlakte index, of de biochemische samenstelling) is onontbeerlijk in veel toepassingen zoals de precisie landbouw, het inschatten van groenvoer kwaliteit en hoeveelheid voor wild en vee, het meten van houtvolumes in de bosbouw of het monitoren van soortsdiversiteit. Aardobservatie met behulp van hyper-spectrale sensoren levert informatie over elektromagnetische spectrale eigenschappen van objecten verdeeld over honderden spectrale banden, in tegenstelling tot meer conventionele multi-spectrale sensoren die deze informatie middelen over slechts enkele banden. Omdat deze observatietechniek over het algemeen een goedkoop, en niet-destructief alternatief biedt voor veldmethoden, en ook eenvoudig is toe te passen over uitgestrekte gebieden wordt het gezien als een effectieve manier om vegetatie eigenschappen waar te nemen. Dit proefschrift onderzoekt de mogelijkheden van hyper-spectraal gemeten midden- tot thermisch infrarode (2.5 – 14 μm) elektromagnetische emissie gegevens om vegetatie eigenschappen waar te nemen op het niveau van het blad. Omdat bladeren het merendeel van het bladerdak vormen, onderzochten we juist de optische eigenschappen van bladeren. In het verleden werd weinig aandacht geschonken aan dit deel van het elektromagnetische spectrum met betrekking tot bladeren, vanwege de lage signaal-tot-ruis verhouding, de subtiele en complexe spectrale eigenschappen van bladeren, en het ontbreken van geschikte apparatuur om hier metingen aan te doen. De nieuwste generatie spectrale sensoren in dit deel van het elektromagnetische spectrum zoals de Bruker FTIR spectrometer of de Midac FTIR spectrometer kunnen dit wel met hoge precisie. Dit onderzoek richtte zich daarom op het afleiden van informatie voor het identificeren van plantensoorten en het schatten van het vochtgehalte van bladeren in het midden- en thermisch infrarode deel van het elektromagnetische spectrum.

De eerste twee studies die zijn gedaan identificeerden dertien plantensoorten op basis van in het laboratorium gemeten midden –tot thermisch infrarode emissiviteitsspectra. Met gebruik van een variantie analyse (ANOVA) gekoppeld aan een Tukey HSD post-hoc test kon worden geconcludeerd dat soorten inderdaad onderscheiden konden worden met midden- tot thermisch infrarode spectra. Dit gaf aanwijzingen om verder te gaan met een optimalisatietechniek (een genetisch algoritme) om de belangrijkste golflengtes voor het identificeren van soorten te selecteren. De golflengtes de werden geselecteerd door dit algoritme (gemiddelden rondom 2.52, 2.94, 3.44, 3.85, 5.80, 9.36, 9.87 en 11.52 μm) konden inderdaad worden gebruikt om verschillende plantensoorten the herkennen.

Het watergehalte in het blad was een tweede eigenschap die werd onderzocht. Deze kon ook met precisie vastgesteld worden in het midden- tot thermisch infrarode gedeelte van het spectrum. Zowel nieuw ontwikkelde indices op basis van de hyper-spectraal gemeten emissiviteit (MNDWI, MSDWI en MSRWI), een wavelet analyse en een partiële kleinste kwadraten regressie lieten zien dat variaties in bladwatergehaltes met grote precisie konden worden geschat in het midden-infrarode deel (2.5 - 6 μm) van het spectrum, maar dat in het thermische gedeelte (6 – 14 μm) geen informatie over watergehaltes te vinden was. De betrouwbaarheid en robuustheid van de nieuw ontwikkelde indices om watergehaltes binnen verschillende plantensoorten te schatten werd ook getest voor golflengtes die door een operationele sensor (de MASI600) geregistreerd worden. De herschikking van de hyper-spectrale emissiviteiten naar deze golflengtes liet zien dat ook voor deze getransformeerde data, midden-infrarood gegevens goed gebruikt konden worden om watergehaltes te bepalen. De meeste geselecteerde golflengtes zijn in de vakliteratuur gerelateerd aan absorptie karakteristieken van water, droge stof en cellulose. Uiteindelijk is ook nog een analyse over een groter deel van het spectrum (van zichtbaar licht nabij 0.4 μm tot en met thermisch infrarood bij 14 μm) uitgevoerd om te kijken welk deel het meest geschikt was om watergehalte te meten. Hierbij bleken de midden-infrarode (2.5 - 6 μm) en kortgolvige infrarode (1.1 – 2.5 μm) gebieden het meest geschikt om watergehaltes vast te stellen.

In het kort kunnen we stellen dat dit onderzoek de potentie heeft aangetoond van midden-infrarood hyper-spectrale observaties om vegetatie eigenschappen, zoals plantentsoort of het bladwatergehalte, vast te stellen. Deze bevindingen kunnen gebruikt worden om aardobservatie systemen in de toekomst af te stellen op de juiste golflengtes om vegetatie eigenschappen waar te nemen.

Author's Biography

Saleem Ullah was born in Dir (lower), Pakistan, on 1st June 1980. He obtained his MSc degree in Environmental Sciences from the University of Peshawar, Pakistan, in 2004. After earning degree Environmental Sciences he join Environmental Protection Agency (EPA) and served there as technical officer. From September 2007 to March 2009, he followed an MSc degree course in Natural Resources Management (NRM) at ITC, the Netherlands. During his MSc at ITC, he estimated forage quality and quantity from remotely sensed data. Since March 2009, he pursued his PhD degree at the Faculty of Geo-Information Science and Earth Observation (ITC), University of Twente, which resulted in this thesis.

Scientific publications in peer reviewed journals

Ullah, S., Schlerf, M., Skidmore, A.K., & Hecker, C. (2012). Identifying plant species using mid-wave infrared (2.5–6μm) and thermal infrared (8–14μm) emissivity spectra. *Remote Sensing of Environment, 118*, 95-102

Ullah, S., Groen, T.A., Schlerf, M., Skidmore, A.K., Nieuwenhuis, W., & Vaiphasa, C. (2012). Using a Genetic Algorithm as an Optimal Band Selector in the Mid and Thermal Infrared (2.5–14 μm) to Discriminate Vegetation Species. *Sensors, 12*, 8755-8769

Ullah, S., Skidmore, A.K., Naeem, M., & Schlerf, M. (2012). An accurate retrieval of leaf water content from mid to thermal infrared spectra using continuous wavelet analysis. *Science of The Total Environment, 437*, 145-152

Ullah, S., Skidmore, A.K., Groen, T.A., & Schlerf, M. (2013). Evaluation of three proposed indices for the retrieval of leaf water content from the mid-wave infrared (2–6 μm) spectra. *Agricultural and Forest Meteorology, 171–172*, 65-71

Ullah, S., Si, Y., Schlerf, M., Skidmore, A.K., Shafique, M., & Iqbal, I.A. (2012). Estimation of grassland biomass and nitrogen using MERIS data. *International Journal of Applied Earth Observation and Geoinformation, 19*, 196-204

Ullah, S., Skidmore, A.K., Ramoelo, A., & Groen, T.A. (**In review**). Retrieval of leaf water content spanning the Visible to Thermal infrared spectra. *Remote Sensing of Environment*

Ullah, S., Skidmore, A.K., Naeem, M., & Schlerf, M. (2012). Estimation of leaf water content from far infrared (2.5 -14 µm) spectra using continuous wavelet analysis. In, *Geoscience and Remote Sensing Symposium (IGARSS), 2012 IEEE International* (pp. 4817-4820)

Iqbal, I.A., Dash, J., **Ullah, S.,** & Ahmad, G. (2013). A novel approach to estimate canopy height using ICESat/GLAS data: A case study in the New Forest National Park, UK. *International Journal of Applied Earth Observation and Geoinformation*

Shafique, M., van der Meijde, M., & **Ullah, S.** (2011). Regolith modeling and its relation to earthquake induced building damage: A remote sensing approach. *Journal of Asian Earth Sciences, 42*, 65-75

International symposia, workshop and conferences

Ullah, S. Estimation of forage biomass and nitrogen using MERIS data : abstract. In 2010 ESA living planet symposium, Bergen, Norway, 28 June-2July 2010**.**

Ullah, S., Si, Y. and Schlerf, M. Forage quantity estimation from MERIS using band depth parameters: In 38th COSPAR Scientific Assembly 2010, 18-25 July 2010, Bremen, Germany.

Ullah, S., Schlerf, M. and Skidmore, A.K. Spectral discrimination of vegetation species at laboratory level using far infrared, 2.5 - 14 um, emissivity spectra : In 7th EARSEL workshop of the Special Interest Group in imaging spectroscopy : 11-13 April 2011, Edinburgh, UK. pp. 76.

Ullah, S., Groen, T., Schlerf, M., Skidmore, A.K. Using a genetic Algorithm as an optimal Band Selector in the thermal Infrared to discriminate Vegetation Species: In 2nd TERRABITES Symposium, ESA ESRIN, Frascati, Italy 6-8 February 2012

Ullah, S., Schlerf, M., Skidmore, A.K., & Hecker, C. Identifying plant species using MIR and TIR (2 - 14 µm) emissivity spectra: In European Geosciences Union (EGU) general assembly, Vienna, Austria 22 – 27 April 2012

Ullah, S., Skidmore, A.K., Naeem, M. and Schlerf, M. (2012) Estimation of leaf water content from far infrared (2.5-14µm) spectra : In IEEE International Geoscience and Remote Sensing Symposium (IGARSS 2012) : Remote sensing for a dynamic earth, 22-27 July 2012, Munich, Germany.

Appendix 1: The winning genes at each run of genetic algorithms and their fitness score

Number of runs	The winning genes (bands in μm)					Fitness score (% Accuracy)
1	2.567	3.420	3.511	5.797	9.973	88.55
2	3.417	3.511	3.917	9.711	11.511	90.58
3	2.540	3.023	3.415	9.720	11.563	90.50
4	2.528	3.416	3.425	5.913	11.501	90.14
5	3.417	3.511	3.917	9.711	11.511	90.58
6	2.503	2.984	3.413	9.748	11.588	87.15
7	3.421	3.523	5.913	9.361	9.934	87.33
8	3.422	3.524	5.833	9.361	9.897	85.97
9	2.530	2.973	3.414	9.533	11.575	89.69
10	2.504	2.974	3.418	9.058	9.925	91.12
11	2.534	3.413	3.509	5.833	9.739	89.24
12	3.420	3.511	3.758	5.893	9.954	89.69
13	2.540	2.801	3.415	5.537	9.437	89.50
14	2.536	3.082	3.412	9.319	9.897	85.60
15	2.505	3.417	5.265	9.285	9.729	89.43
16	2.505	3.418	3.427	3.853	11.397	89.24
17	2.503	3.418	5.822	9.285	9.489	86.55
18	2.503	2.786	3.417	5.775	9.446	93.76
19	2.503	2.957	3.418	9.319	9.748	86.20
20	3.420	3.424	5.737	5.846	10.011	87.72
21	3.417	3.511	3.917	9.711	11.511	90.58
22	2.503	2.890	3.418	5.781	9.812	86.64
23	2.528	3.418	3.422	5.740	10.011	90.13
24	2.503	3.416	5.591	5.913	9.720	91.38
25	2.562	3.412	5.692	9.437	10.109	91.71
26	3.423	3.515	5.724	5.916	9.925	88.28
27	3.058	3.422	5.804	5.913	9.748	86.34
28	2.553	3.412	5.775	5.775	9.934	87.83
29	2.536	3.416	5.791	9.335	9.693	90.95
30	3.421	3.523	5.913	9.361	9.934	87.33
31	3.411	3.437	5.686	5.913	10.002	86.47
32	3.421	3.523	5.913	9.361	9.934	87.33
33	2.503	3.418	3.437	5.846	9.906	89.00
34	2.511	3.408	3.443	5.846	10.002	85.66
35	3.407	3.425	3.523	9.766	11.520	92.53
36	2.535	2.832	3.420	9.310	10.040	87.33
37	3.421	3.523	5.913	9.361	9.934	87.33
38	2.518	3.417	3.511	5.788	9.757	92.77
39	2.503	3.407	3.437	5.846	9.906	89.00
40	3.411	3.437	5.686	5.913	10.002	86.47

ITC Dissertation List

http://www.itc.nl/Pub/research/Graduate-programme/Graduate-programme-PhD_Graduates.html